# Two-Phase Electrophoresis of Biomolecules

Vom Fachbereich Maschinenbau
an der Technischen Universität Darmstadt
zur
Erlangung des Grades eines Doktor-Ingenieurs (Dr.-Ing.)
genehmigte

## Dissertation

vorgelegt von

**Dipl.-Ing. Götz Münchow**

aus Reinbek

Berichterstatter: Prof. Dr. Steffen Hardt (Technische Universität Darmstadt)
Mitberichterstatter: Prof. Dr. Jörg Peter Kutter (Technical University of Denmark)
Tag der Einreichung: 29. Mai 2009
Tag der mündlichen Prüfung: 17. Juli 2009

Darmstadt 2009
D17

# TWO-PHASE ELECTROPHORESIS OF BIOMOLECULES

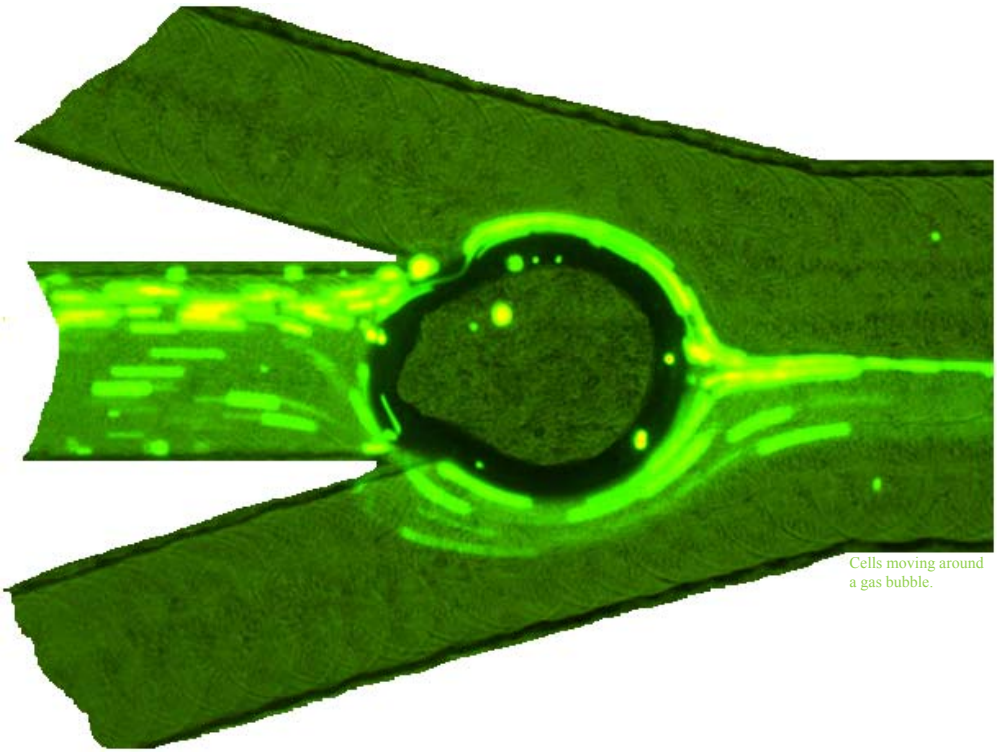

Cells moving around a gas bubble.

von
Götz Münchow

*För miene Familje.*

## Abstract

Existing microfluidic separation technologies for biomolecules commonly rely on single phase liquid systems as well as on electrophoresis. But microfluidics also facilitates the generation of stable, well-controlled and immiscible liquid-liquid two-phase arrangements, since interfacial forces usually dominate over volume forces. The present work combines these approaches and reports on protein and cell transport as well as on enrichment and separation phenomena discovered in various experiments with a novel microfluidic setup for continuous-flow two-phase electrophoresis. Therefore, phase boundaries of aqueous two-phase systems are formed within a microchannel in flow direction and the characteristic partition behavior of proteins and cells is manipulated and tuned by applying an electric field perpendicular to the phase boundary.

The two immiscible phases which separately are injected into a microchannel are taken from aqueous polyethylene glycol (PEG) - dextran systems. Different ways are possible to induce an electric field within a microchannel, but it was found out that electrodes have to be decoupled from the two-phase flow and especially hydrogels can be utilized as adequate ion conductors. Thus bubble generation inside the microchannel is prevented and a stable two-phase flow is guaranteed.

In contrast to macroscopic systems, microfluidic setups allow detailed investigations of local effects at the phase boundary. The results of the experiments show that the diffusive as well as the electrophoretic transport behavior of proteins between the laminated liquid phases is strongly influenced by their partition coefficients. Furthermore, effects of the phase boundary itself, like electric double layers, are negligible in this case. This derived knowledge helps to design specific two-phase partition and enrichment procedures combined with electric fields for future studies.

Besides a detailed examination of the transport behavior of proteins a continuous separation of proteins from cells is presented. While proteins in presence of an external electric field pass the boundary and leave the phase they have been initially dissolved in almost completely, lymphoblastoid cells can be retained, thus allowing a stable and continuous separation of these two kinds of biomolecules.

And finally, further kinds of fluid combinations such as water and propylene carbonate are presented, supporting an enrichment of proteins at the phase boundary.

## *Zusammenfassung*

Bestehende mikrofluidische Techniken zur Separation von Biomolekülen basieren üblicherweise auf einphasigen Flüssigkeitssystemen sowie auf Elektrophorese. Da die Grenzflächenkräfte in der Regel die Volumenkräfte dominieren, ermöglichen die Gesetzmäßigkeiten der Mikrofluidik aber auch die Erzeugung von stabilen, gut kontrollierbaren Anordnungen von nicht mischbaren flüssig-flüssig Zweiphasensystemen. Die vorliegende Arbeit kombiniert die oben genannten Ansätze und beschreibt den Transport von Proteinen und Zellen sowie Anreicherungs- und Separationsphänomene, die während unterschiedlichster Experimente in einem neuartigen, mikrofluidischen Aufbau für kontinuierliche Zweiphasenelektrophorese ermittelt worden sind. Dafür werden Grenzflächen wässriger Zweiphasensysteme innerhalb eines Mikrokanals in Flussrichtung erzeugt und das charakteristische Partitionierungsverhalten von Proteinen und Zellen durch ein zusätzliches elektrisches Feld senkrecht zur Phasengrenze manipuliert bzw. neu eingestellt.

Die zwei nicht mischbaren Flüssigkeitsphasen, jede für sich in den Mikrokanal injiziert, werden wässrigen Zweiphasensystemen entnommen, die aus Polyethylenglykol (PEG) und Dextran bestehen. Es bestehen unterschiedliche Möglichkeiten, ein elektrisches Feld im Mikrokanal zu erzeugen. Es wurde aber ermittelt, dass die Elektroden von dem Zweiphasensystem entkoppelt werden müssen und besonders Hydrogel als adäquater Ionenleiter verwendet werden kann. Dadurch ist es möglich, die Bildung von Gasblasen innerhalb des Mikrokanals zu unterbinden und einen stabilen Zweiphasenfluss zu garantieren.

Im Gegensatz zu makroskopischen Systemen, erlauben mikroskopische Systeme eine detaillierte Untersuchung von lokalen Effekten direkt an der Phasengrenze. Dabei zeigen die Ergebnisse der Experimente, dass das diffusive als auch das elektrophoretische Transportverhalten von Proteinen zwischen den Flüssigkeitslamellen maßgeblich durch deren Partitionierungskoeffizienten beeinflusst wird. Außerdem sind Effekte, die durch die eigentliche Phasengrenze verursacht werden, wie z.B. durch eine elektrische Doppelschicht, in diesem Fall vernachlässigbar. Das durch die vorliegende Arbeit erlangte Wissen hilft dabei, für unterschiedliche Zielstellungen bestimmte Partitionierungs- und Anreicherungsprozeduren innerhalb von mit elektrischen Feldern gekoppelten Zweiphasensystemen zu designen.

Neben der detaillierten Untersuchung der Transporteigenschaften der Proteine wird außerdem eine kontinuierliche Separation von Proteinen und Zellen beschrieben. In diesem Fall passieren die Proteine bei Vorhandensein eines elektrischen Feldes die Phasengrenze und verlassen vollständig die Phase, in der sie ursprünglich gelöst waren. Im Gegensatz dazu werden lymphoblastoide Zellen an der Phasengrenze zurückgehalten, was eine stabile und kontinuierliche Separation dieser beiden Biomoleküle ermöglicht.

Schließlich werden noch weitere Fluidkombinationen, wie z.B. Wasser - Propylencarbonat, vorgestellt, die ebenso eine Anreicherung von Proteinen an der Phasengrenze ermöglichen.

## *Content*

# 1 Introduction

*Over the last decades, analytical chemistry and, in particular, separation technology encountered an intensive trend towards miniaturization. This section introduces those trends and provides insight into the opportunities for microfluidics. Moreover, some governing scaling laws are discussed and an overview of realized microfluidic systems belonging to this field of research is given. The section closes with an outline of the aim and structure of this thesis.*

## 1.1 Microfluidic Technologies

Similar to the very miniaturization that has revolutionized the world of electronics with the invention of the transistor, over the last two decades the development of microfluidics has led to novel and innovative devices for analytical and bioanalytical chemistry with great advantages in terms of analysis speed and automation of processes [1-3].

The use of microfluidic devices allows for techniques and experiments, which are impossible with conventional techniques, thus yielding new functionality. Beginning from the 1980s, microfluidics is applied to different fields of technology, such as inkjet printheads or miniaturized pumping systems. Especially inkjet printheads are commercially one of the most successful applications. But also in the field of bioanalytical chemistry the advances of microfluidic technology have revolutionized operational procedures for DNA analysis, e.g., high-throughput screening and polymerase chain reaction [4], or proteomics [5-7]. Such systems are often called lab-on-chip systems and their main idea is to integrate assay operations such as sample preparation, biochemical reactions or amplifications and final detection. The main application area for such lab-on-chip systems is in clinical pathology and especially in point-of-care diagnosis of diseases. Since the microfluidic system presented in this work can be used for the extraction or enrichment of biological macromolecules or cells the main application areas can be found in the field of biotechnology.

One of the key elements of bioanalytical chemistry is the separation and enrichment of molecules in a continuous way [8,9]. Common separation processes include filtration and centrifugation steps or are based on chromatography or electrophoresis. They can be classified as batch processing, i.e., only a specific amount of sample volume is separated. By contrast, during a continuous flow separation or enrichment the sample solution is introduced into a separation channel continuously. The separation force acting on the sample components is not primarily applied in flow direction, like in conventional electrophoresis systems, but mostly perpendicular to it [8,10-14]. The main advantages of continuous flow separation and enrichment systems are the continuous introduction of the sample and, consequently, a continuous collection of desired sample components. Such a technology also allows for further downstream processing of specific sample components or, once the right process parameters have been elaborated, a label-free processing leaving the biomolecules in their original state.

On its own, two-phase and electrophoretic separation techniques belong to the most well established methods for the separation and analysis of complex mixtures of biomolecules, such as proteins or nucleic acids. Especially the principle of electrophoretic separation has been transferred numerous times to lab-on-chip systems in the past decade [1,2,6,9,15-19]. Two of the most prominent separation methods which have been miniaturized and implemented in a chip format are isoelectric focusing (IEF) [20] and capillary electrophoresis (CE) [15,17,21,22], where the latter one is already commercially available [23,24]. Besides the advantages of a continuous flow system the execution of biochemical processes in chip format bears several advantages, for example, small sample amounts, a high level of

automation and the direct coupling with subsequent analysis steps [1,2]. Current developments aim at fully integrated microsystems that combine various analytical steps on one chip, since a conventional genetic analysis including different process steps can last up to 12 hours [25,26]. Using appropriate microsystems, this time can be reduced to 20 to 70 minutes. This leads to the advantages of reduced analysis times, sample and reagents volumes and the elimination of manual transfer steps between individual analysis steps [4].

In parallel, there is another field of research achieving protein separation and partitioning by utilizing the properties of aqueous two-phase systems (ATPSs). The easiest way to carry out separation is to create a dispersed two-phase system and to dissolve a protein sample into one of the two phases [27,28]. Afterwards, and according to their chemical affinity, the proteins get distributed diffusively over the different phases. A final separation of the dispersed phases can be achieved easily due to gravitational forces since the two liquid phases usually differ in their densities. Since Albertsson rediscovered the aqueous two phase systems in the 1950s and used them for the partitioning of different kinds of biomolecules there is only a small number of studies where this separation method is applied in the context of microfluidic systems [27,29-33].

## 1.2 Downscaling Effects

In general, miniaturized bioanalytical procedures need a precise and well-controlled handling of very small liquid volumes. To this end, microfluidics offer great opportunities since not only the sample volume can be reduced but, it is also possible to untilize that fluids may behave differently on very small length scales compared to the familiar macroscopic world. Factors like surface tension, energy dissipation and fluidic resistance start to dominate the system.

With respect to the present study primarily the flow behavior in microfluidic systems is of high importance. In macroscopic systems a turbulent flow is mainly present that is characterized by random fluctuations in velocity of individual flow “particles” superimposed on the mean bulk fluid motion. In turbulent flows there is an enhanced mass transfer improving mixing processes or heat transfer. In contrast to those macroscopic systems, in microfluidics the flow is usually laminar and characterized by a steady, unidirectional flow with smooth and parallel streamlines. An important parameter that can give information about the characteristics of the flow in a channel is the Reynolds number, *Re*, which is defined as:

$$Re = \frac{L_c\, u\, \rho}{\eta} \qquad (1.1)$$

where $\eta$ denotes the dynamic viscosity of the fluid, $\rho$ is the density of the fluid, $u$ is the average velocity of the flow and $L_c$ is a characteristic length, in this case the hydraulic diameter [34]. Due to the small channel dimensions in microfluidic systems, *Re* is usually much less than 100, and often even less than one. In smooth, straight ducts, the transition to turbulent flow generally occurs at a Reynolds number of about 2,000. Accordingly, at such small Reynolds numbers inertial effects become irrelevant in contrast to viscous forces leading to robust laminar flow conditions. Hence, microfluidic flows are predominantly uniaxial, which means that the entire fluid moves parallel to the local orientation of the walls.

Since any mixing of liquids provided by turbulences is eliminated, two laminar flow streams meeting inside a microchannel are only mixed due to molecular diffusion. Diffusion in one

dimension can be described by the Einstein-Smoluchowski equation, where $\sigma_v$, $D$, and $t$ are the variance, diffusion coefficient, and time assuming a Gaussian diffusion profile:

$$\sigma_v^2 = 2\,D\,t \qquad (1.2)$$

Here, $\sigma_v$ can be considered as a typical distance that a biomolecule moves within the time $t$. Relating to Eq. (1.2) and in consideration of the squared dependence of the spatial motion the diffusion of a molecule, for example bovine serum albumin (BSA, $D = 6.3\ 10^{-11}\ m^2\ s^{-1}$), over a length of 10 µm is a million times faster than the diffusion over 1 cm [35]. Consequently, in microchannels diffusion becomes a very important issue. Laminating different kinds of liquids in multiple thin layers can dramatically accelerate the diffusive transport between the layers and contribute to very efficient mixing and reaction properties on the microscale [36-38]. But also the extraction of specific molecules from samples can be easily realized due to different diffusion coefficients [39,40].

In case of pressure driven microfluidic systems the pressure drop $\Delta p$ for laminar flow is given by

$$\Delta p = Q\,R_f \qquad (1.3)$$

where $Q$ is the flow rate and $R_f$ the fluidic resistance. For circular cross sections the resulting fluidic resistance is given by

$$R_f = \frac{8\,\eta\,L_{cl}}{\pi\,r^4} \qquad (1.4)$$

where $L_{cl}$ is the channel length and $r$ is the channel radius. In microfluidic devices the channel cross sections are often rather rectangular than circular. For high aspect ratios, i.e. $w >> h$, with $w$ and $h$ being the channel width and height, the resistance is given by

$$R_f = \frac{12\,\eta\,L_{cl}}{w\,h^3} \qquad (1.5)$$

Accordingly, $\Delta p$ scales with the cross sectional dimension to the power of minus four, i.e. $r^{-4}$ or $w^{-1}\,h^{-3}$, which imposes a severe limitation on flow rates in practical pressure-driven microfluidic systems.

By decreasing the lateral dimensions of fluidic systems a strong increase of the surface-to-volume ratio is the consequence elevating the significance of liquid interactions with the channel wall. One consequence and actually advantage of the high surface-to-volume ratio is the greatly accelerated heating and cooling of samples at low power consumption due to the increased contact surface and short characteristic length for temperature diffusion, i.e. heat conduction, between the liquid and the (temperature controlled) wall. This allows rapid thermal cycling of samples and can be utilized for, e.g., the acceleration of biochemical amplification procedures such as the polymerase chain reaction (PCR) [4,26]. Another point arising from the miniaturization and the increased surface-to-volume ratio in microsystems is the low diffusion distance for molecules compared to a large reactive surface. Because of that unspecific adsorption of molecules to surfaces becomes a very important issue since, e.g. in case of a PCR, it can lead to decreased yields or no amplification products at all [4,26]. Hence, controlling the physical and chemical properties of the surface is one central challenge during miniaturization.

## 1.3 Microfluidic Devices for Chemical Analysis and Separation

In contrast to conventional electrophoresis chips, where a small amount of sample is injected into a separation column, separated and detected afterwards, in typical continuous flow separation systems the sample together with a carrier liquid is injected continuously into a separation channel. The separation is induced by additional forces acting at an angle to the flow direction which leads to a diversion of the sample components perpendicular to the flow direction. Such forces can be induced by, e.g., electric [14,41,42] and magnetic fields [43] as well as pH gradients [44] or optical forces [45]. The main advantage of continuous systems is that the separation efficiency can be monitored in real-time and separation parameters can be adjusted at once [8]. Two microfluidic systems utilizing such additional forces for separation are closely related to the system presented in this study: the free-flow electrophoresis (FFE) and the split flow thin (SPLITT) fractionation.

Initially developed on larger scale [9,46], miniaturized FFE devices have been reported working in different modes like zone electrophoretic mode [14,47,48], isoelectric focusing mode [44,47,49-52] and isotachophoretic mode [53]. In general, the sample solution and the carrier liquid are continuously pumped into the shallow chamber of a FFE device through numerous inlet channels and collected *via* outlet channels on the opposite side, cf. Fig. 1-1.

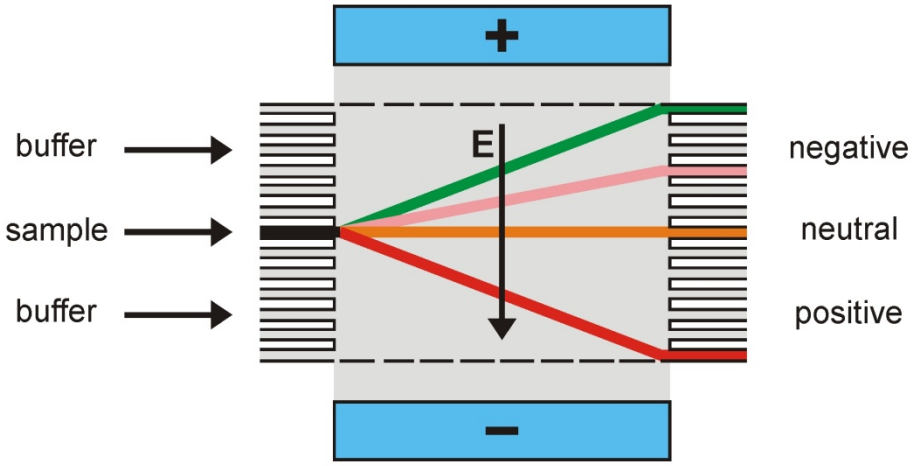


*Fig. 1-1: Typical setup of a free-flow separation device consisting of a shallow separation chamber and reservoirs. The buffer, also called carrier liquid, and the sample are pumped from left to right. Perpendicular to the flow direction a homogeneous electric field is applied deflecting charged sample components.*

Perpendicular to the hydrodynamic flow a homogeneous electric field is applied driving the charged molecules either to the one or other side depending on their charge. This leads to an inclined flow path arising from the longitudinal movement within the carrier liquid and the transverse movement due to the electric field. The distance of the transverse movement depends on the net charge to size ratio. The greatest challenge in the fabrication of µ-FFE devices is a practical voltage transfer to form an electric field inside the separation channel. This is also an important issue in this study and will be discussed in chapter 6 and 7.

First presented by Giddings [54] the SPLITT fractionation is capable of high-resolution separation of colloids and nanoparticles suspended in a solution. By applying an electric field across a long, thin channel, specific sample components are forced out of the sample stream into a neighboring buffer stream [55-59]. It was also shown that this driving force, for

example, can be replaced by gravity [60]. In general, SPLITT devices consist of a long channel with usually a flow splitter at the inlet and at the outlet, cf. Fig. 1-2. Due to a higher flow rate of the carrier stream the sample stream is focused into a relatively narrow band. Without any applied force all sample components leave the separation channel through the outlet on the same side as the sample inlet is located. But during a separation the applied force pulls one kind of the sample components beyond a so-called splitting plane leading to a collection of different molecules types at different outlets. Also for this kind of separation method where the molecules are driven electrophoretically, the transfer of an electric field into the separation channel is critical. Normally, electrolysis starts to take place at a voltage of 1.6 V [61]. If the electrodes are in direct contact to the sample and carrier liquid the applied voltage usually has to stay below this critical value in order to avoid any bubble generation. Since gas bubbles can lead to a clogging of the separation channel [57]. This limitation brings about that the majority of the electric field is shielded by an electric double layer which in turn leads to a weak influence on the transversal movement of the molecules.

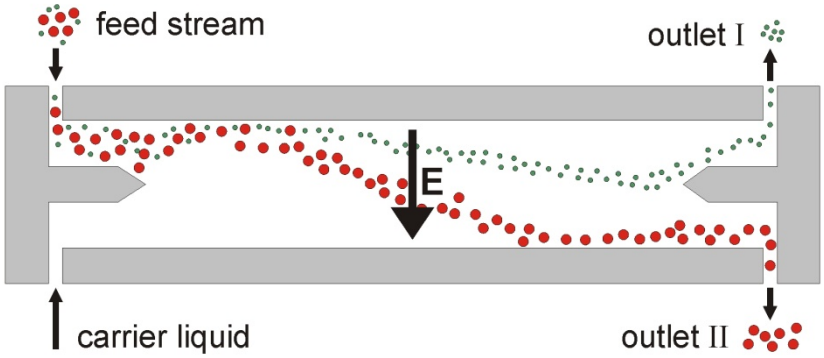


*Fig. 1-2: Principle of SPLITT fractionation. A feed stream including samples and a carrier liquid are pumped into a separation chamber. Splitters between the inlets and outlets and an additional electric field perpendicular to the flow direction accomplish a separation of the particles.*

In contrast to FFE and SPLITT system where an additional force is applied, most presented liquid-liquid extraction systems on chips are based on one aqueous and one organic phase. They are developed for the partitioning of small molecules [62-65] and due to the high interfacial tension between the phases these systems often require the addition of surfactants [66,67] or patterned surface treatments [68-71] to achieve a stable and laminated two-phase flow. Alternatively, a stable two-phase flow can be created by the integration of solvent-permeable [72] or sample-permeable membranes [73].

But aqueous-organic two-phase systems tend to disrupt, e.g., the three dimensional structure of proteins. Thus, they are generally not suitable for the partitioning of biomolecules such as proteins or living cells. In case of aqueous two phase systems both resulting phases largely consist of water (80-90% (w/w)) and under the condition there is no denaturing agent added, biocompatibility is essentially ensured within the bulk fluid. Additionally, due to the low interfacial tension between these phases and a resulting high capillary number even at low flow rates a stable, side-by-side two-phase flow can easily be established in microfluidic channels without any surfactants or special surface treatments. Besides a huge application area of aqueous two phase extraction in macroscopic environments [27,28,74,75] only a few applications can be found on chip. Starting with a simple protein fractionation inside a meander-shaped, long channel [76] ATPSs have been applied for the fractionation of live and

dead cells [30], the partitioning of *E. Coli* bacteria [77] and plant cells [29] or the isolation of specific proteins from sub-microliter volumes of *E. Coli* cell lysate [33]. All these demonstrations of aqueous two phase extraction systems are simply based on diffusion and the physico-chemical properties of the biomolecules leading to such a selective partitioning or purification. Although it seems to be obvious, so far only in macroscopic systems the molecule transport across the interface of ATPSs has been influenced by additional forces like electric fields [78-85].

## 1.4 Aim and Structure of the Thesis

This study aims at the exploration of a new class of methods of electrophoretic separation and enrichment of biomolecules and is embedded in the priority program "Nano- and Microfluidics" (SPP 1164) of the German Research Foundation (DFG). In contrast to the standard techniques, electrophoresis is not conducted in a single-phase fluid, but in a system of stratified layers. It is shown that besides chemical modifications of the used liquids of an ATPS an additional electric field perpendicular to the liquid-liquid phase boundary can be utilized in order to influence and to control the migration and partitioning of proteins. The technique is also known as electroextraction [78]. By utilizing the unique characteristics of microfluidic systems, the aim is to especially examine the interactions of biomolecules with liquid-liquid interfaces which may cause influences on the transport behavior between the two phases. Such influences can be potential-energy minima induced by electric double layers or interfacial tensions.

For this purpose, the main foci of this thesis are the investigation of useful two-phase systems and the development of a suitable microfluidic flow cell. This is followed by a detailed examination of the transport behavior of biomolecules in such a two-phase electrophoresis system, especially in the vicinity of the phase boundary. The flow cell should allow the creation of an arrangement of stratified layers of immiscible liquids and additionally the imposition of an external electric field allowing an electrophoretic transport of biomolecules perpendicular to the phase boundary. The main objective will be to explore the diffusive and electrophoretic behavior of biomolecules in stratified layers of immiscible liquids. It should be possible to study a number of effects which have not yet been accessible with macroscopic systems due to the reduced control over two phase arrangements and the unfavorable surface-to-volume ratio.

After this introduction part this thesis provides the fundamentals and introduces the used biological samples, see chapter 2. In chapter 3 and 4, the two separation methods, partitioning in aqueous two phase systems and electrophoresis, which are combined in one microfluidic system, will be presented separately in detail. In order to gain a fundamental understanding of the hydrodynamic flow in microchannels and two-phase flow regimes the governing equations and non-dimensional numbers are introduced in chapter 5

A premise using capable microfluidic chips for this purpose is the development of different manufacturing process steps enabling the integration of electrodes for applying an additional electric field within microfluidic channels. Furthermore, a suitable experimental setup is important for creating a stable two-phase flow and for analyzing the transport behavior of the biomolecules in detail. The setup including the fluid and electric connections as well as the fluorescence detection is discussed in chapter 6. Chapter 7, where the manufacturing of the

microfluidic chip is presented, deals mainly with the integration of electrodes, sealing of the channels, and phase separation at the outlet.

The final part of this thesis comprises the experimental results. Starting with the flow patterns and flow stability of the two-phase flow, see chapter 8, primarily the passive and active transport of biomolecules towards and across the phase boundary will be presented and discussed, chapters 9 to 11. Utilizing high partitioning coefficients of proteins a continuous enrichment can be achieved, see chapter 11. Additionally, the system under investigation also allows the separation of proteins and cells that can be used for purification processes, chapter 12. The thesis closes with a short presentation of a further two-phase system based on oil and water, see chapter 13, and a final conclusion and outlook, chapter 14.

# 2 Biological Samples

*Separation of molecules is applied in many fields as, for example, analytical chemistry, biotechnology or just biological research. But still the separation and analysis of biomolecules represents one of the biggest challenges. In this work the main focus is on two main types of biomolecules, proteins and cells. This chapter gives a brief overview of the structure and properties of these biomolecules and corresponding separation methods which are mainly applied at present. It also includes the fluorescence labeling procedures that allow a visualization of the samples and, accordingly, an evaluation of the experiments.*

## 2.1 Proteins

The word protein comes from the Greek word proteios, meaning "of first importance", and was coined by the Dutch chemist G.J. Mulder in 1839 after scientists realized that nitrogenous food components are essential for the survival of animals. Proteins are macromolecules and consist of a large number of standard amino acids which are arranged in linear chains. They appear in a three-dimensional shape (folding) which is well defined and essential for their activity and function in a living organism.

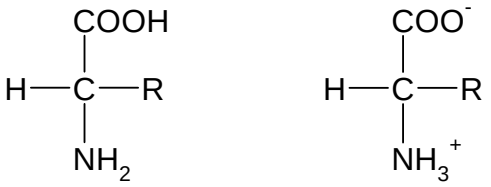


*Fig. 2-1: Chemical structure of standard amino acids. Right: The amine and the carboxyl group tend to ionize in solution, depending on the given pH value. At their pK value, the amino acids behave as a zwitterion, i.e. there is no net charge.*

The amino acids, the fundamental elements of a protein, are characterized by their amine and carboxyl functional groups. These groups are attached to the same carbon, which is called α-carbon, and completed by an additional side chain (R), cf. Fig. 2-1. All proteins in any living creature are constructed from the same set of twenty amino acids. They only differ in their side chains which are bonded to the α-carbon. The only exception is represented by Prolin, which has a secondary amine group instead of a primary one. The simplest amino acids, for example, are called Glycine, which has a single hydrogen atom as its side chain, and Alanine, which possesses a methyl (-CH3) group instead. The unique characteristics of each amino acid, like ionic charge, chemical reactivity and hydrophobicity, are given by the composition of the different side chains. Due to the folding process and the complex structure of proteins, four levels of organization are distinguished: primary, secondary, tertiary and quaternary structures. The simple linear sequence of amino acids, joined head-to-tail via peptide bonds, determines the primary structure of a protein. The sequence itself is essential for the activity and the function of the resulting protein. Already small changes in the sequence in a critical area can lead to a reduced activity or loss of function. The secondary structure is represented by alpha helices and beta sheets, higher regular sub-structures which are locally defined, meaning that many regions of different secondary structures can be present in the same protein. This regular kind of structure is formed by hydrogen bonds between the atoms of the amino acid backbones of the peptide chain. The tertiary structure refers to a complete three-dimensional structure and is initiated by bending and twisting of the peptide chain. This specific folding is kept by hydrogen bonding, electrostatic interaction and sulfide bridges and

depends on the environmental parameters, e.g. pH value, ionic strength and temperature. Outside of specific values the protein could change its structure, unfold and finally lose its activity irreparably. This process is called denaturation. Some proteins can consist of more than one peptide chain. This kind of association is described by the quaternary structure of a protein, where each peptide chain is called a subunit. These subunits work as a part of a larger assembly or protein complex.

However, proteins can be characterized by different properties:

- size - molecular weight (Daltons)
- shape
- amino acid composition and sequence
- isoelectric point (pI)
- hydrophobicity
- biological affinity

In the same way, the surface charge of a protein is also given by the incorporated amino acids. Amino acids are ampholytes which have, as a minimum, two ionizable groups, the amino group of the N-terminal residue, and the carboxyl group of the C-terminal residue. Additionally there may also be ionizable side groups which are located in the side chains of some amino acids. Since all these charged groups are titratable the overall charge of a protein, the sum of the charges of every ionizable group in the protein, is dependent on the pH value, cf. Fig. 2-2. At the isoelectric point (pI) the positive and negative charges are balanced with the result that the protein shows no net charge and will not move within an electric field. Most proteins are fragile biomolecules and have to be stored at suitable conditions maintaining the normal structure and function of the protein.

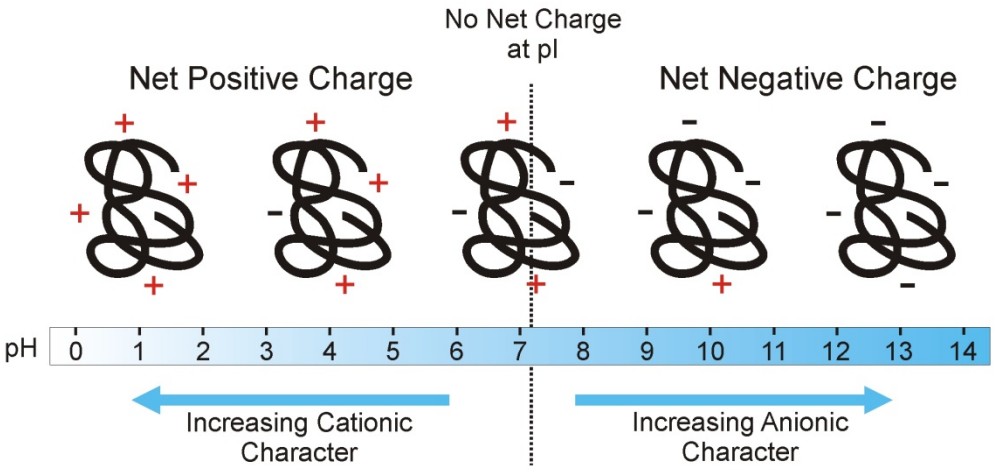


*Fig. 2-2: Charge of a protein depending on the pH value of the surrounding solution. For hemoglobin from human erythrocytes, for example, the isoelectric point is pH 7.1, i.e., at this pH value the protein has an equal number of positive and negative charges resulting in no net charge [86,87].*

Due to its weak interactions the three dimensional structure of a protein is sensitive to various environmental factors. A low or high pH, high ionic strength or high temperature, for example, can cause a denaturation or an unfolding, whereas the primary structure of the protein remains intact as a random coil. Proteins can also re-fold but in most cases a denaturation is not reversible.

All proteins used in this study have been obtained from Sigma-Aldrich (Germany) and are summarized in Table 2-1.

| Protein | Size | Isoelectric point | Order number |
|---|---|---|---|
| Bovine serum albumin | 66 kDa | 4.7 | 05480 |
| Carbonic Anhydrase | 29 kDa | 6.2 | C3934 |
| Conalbumin (chicken egg) | 77 kDa | 5.9 | 27695 |
| Hemoglobin (bovine) | 65 kDa | 7.1 | H2500 |
| Ovalbumin (chicken egg) | 45 kDa | 4.6 | A5503 |
| α-Chymotrypsinogen A (bovine) | 25 kDa | 9.5 | C4879 |
| β-Galactosidase | 116 kDa | 6.1 | G1875 |
| β-Lactoglobulin (bovine) | 35 kDa | 5.3 | L3908 |

*Table 2-1: List of proteins used in this study including their size, isoelectric points [86,87] and order numbers at Sigma-Aldrich.*

### 2.1.1 Protein Separation Methods

The manifold properties of proteins allow a separation in various ways. The most popular methods are based on electrophoresis (e.g. SDS-PAGE – separation by size) and on different affinities to fluid phases (e.g. aqueous two-phase partitioning - separation by physico-chemical affinities), cf. Table 2-2. The aim of protein separation is either analysis or purification. The former one helps to identify the ingredients and their quantities of given samples. The latter one describes the separation of specific proteins from contaminants in order to gain useful and specific end products. In contrast to the industry, where proteins are purified on a larger scale, for products as drugs or food additives the research usually requires purified proteins to determine their structure and study their biochemical properties. Starting at a cell as a sample, protein purification proves to be a big challenge since a typical cell contains several thousand different protein types and other ingredients like nucleic acids, lipids, and polysaccharides. The purification is evaluated in reasonable efficiency, yield and purity and the purification procedure is composed of a series of separation methods and steps and is unique to the individual protein type. Apart from a huge variety of macroscopic separation and analysis systems, over the last decades proteomics has found its way onto chips, for example, in the form of 2D electrophoresis (2DE) chips [88]. Typical 2DE chips consist of a chamber for isoelectric focusing and a large number of parallel microchannels for a subsequent electrophoretic separation. Other microfluidic systems perform free-flow electrophoresis [14,47,48], free-flow isoelectric focusing [44,47,49-52] or consist of a chip in combination with mass spectrometry [6]. Due to the connection with this study, only the principle of electrophoresis and the two-phase separation will be discussed in chapter 4 and 5 in more detail.

| Protein characteristic | Separation method |
|---|---|
| Charge | Ion exchange chromatography<br>Electrophoresis<br>Isoelectric focusing |
| Polarity | Hydrophobic interaction chromatography |
| Size | Gel filtration chromatography |
| Binding affinities | Aqueous two-phase partitioning<br>Affinity chromatography |
| Solubility | Salting out |
| Density | Ultracentrifugation |

*Table 2-2: Protein separation methods based on different protein characteristics.*

### 2.1.2 Protein Enrichment

Typically biological analytes are only available in very low concentrations or loaded into microchip systems in small sample volumes. But for a successful detection of specific ingredients either a high concentration of the target molecule or very sensitive detectors are required. Laser-induced fluorescence methods are often applied to the analysis of biological samples and can significantly help to decrease the detection limit. But their capabilities are restricted and for an adequate analysis as well as for a subsequent processing an enrichment of specific molecules often becomes essential.

Famous microfluidic applications for sample enrichment are field-amplified sample stacking (FASS) or isotachophoretic preconcentration (ITP) [89]. FASS utilized a gradient in electrolyte conductivity in order to expose sample molecules to non-uniform electric fields. The sample is dissolved in a buffer of relatively low conductivity leading to a high electrical resistance in comparison to the rest of the system. This leads to higher electric field strengths as soon as a voltage is applied. Accordingly, the sample molecules show an increased velocity within the low conductivity buffer. At the interface to the surrounding low-field buffer the molecules decelerate abruptly and stack into a narrow sample band leading to high concentration factors [90,91]. In contrast, ITP is based on buffers, leading and terminating buffer, with ions of different mobilities, where the sample components arrange themselves into discrete bands between these two buffers inside a capillary [89]. This principle was also realized in free-flow benefiting from the advantages of continuous flow devices [53].

### 2.1.3 Protein Labeling

Proteins are usually in size of a few nanometers. Accordingly, the labeling of proteins becomes an important role in biology science and allows researchers to study a protein's location, movement and, e.g., the interaction with a living cell. A most common way is the use of fluorescence labels which bind to primary amines forming stable dye-protein conjugates and enabling the study of proteins with fluorescence microscopy systems. In this study all used proteins were generally labeled with an Alexa Fluor® 488 protein labeling kit (A10235, Invitrogen, Germany). In experiments where proteins and cells are examined simultaneously the Alexa Fluor® 488 fluorescence dye is replaced by Alexa Fluor® 568 dye (A10238, Invitrogen, Germany) since the emission maximum of the cell labeling dye is similar to that of the Alexa Fluor® 488 dye. Related to the spectrum the Alexa Fluor® 488 dye is similar to

fluorescein but Alexa Fluor® 488 brings about protein conjugates with higher quantum yields which are more photostable than fluorescein conjugates. Another advantage of the Alexa Fluor® 488 dye is the insensitivity to pH between pH 4 and 10 [92]. In case of Alexa Fluor® 488 dye the labeled proteins have absorption and fluorescence emission maxima of approximately 498 nm and 519 nm, respectively. The maxima of Alexa Fluor® 568 dye are at approximately 577 nm and 603 nm for the absorption and fluorescence emission, respectively.

In preparation for the labeling, the proteins were dissolved in a 1x PBS buffer (phosphate-buffered saline, component of the labeling kit) leading to a final concentration of 2 mg $ml^{-1}$. The following labeling procedure was performed according to the given protocol which is identical for both the Alexa Fluor® 488 and 568 dye except for the applied reactive dyes [92]. The final protein concentration was approximately calculated from the initial protein amount and the final yield after labeling.

## 2.2 Cells

A biological cell represents the structural and functional unit of a living organism. While a human consists of about $10^{14}$ cells (multi-cellular), other organisms, such as bacteria, only consist of one single cell (unicellular). The word cell was given by Robert Hooke in 1665 who compared cork cells with small rooms (lt. cellula) monks lived in. Each cell represents a well-defined, self-contained and self-preserving system. Cells can ingest nutrients, are able to perform energy conversion and reproduce themselves by cell division. The information for all its functions and activities are stored within the cell, more precisely in the DNA. Cells utilize enzymes and proteins and can respond to external and internal stimuli such as food supply, temperature changes or pH level. Cell types are distinguished between prokaryotic and eukaryotic cells. The first mentioned type is usually a singleton while the latter one is mainly found in multi-cellular organisms. In this work only eukaryotic cells have been separated or transported within an electric field, respectively. Since cells are generally a complex topic, in the following paragraphs only the essential properties of cells relating to this study are described.

The typical cell size of eukaryotic cells is about 10 to 100 µm and they hold a real nucleus with a double membrane. Cells also include organelles like ribosomes, cytoplasm, mitochondria and lysosomes. The cell membrane or plasma membrane protects the cell from the surroundings and is primarily made from a bilayer of lipids and a variety of proteins which are embedded within this membrane. Thus the cell membrane is the interface to the environment and holds important cell properties for applicable separation techniques. Parts of the membrane proteins are the entry and exit ports of a cell for different molecules and serve as channels or pumps. This semi-permeable character of the cell membrane enables an exchange of ions and molecules between the inner cell and the environment allowing a simple fluorescence labeling of the cells. Additionally, the flexible lipid bilayer is composed of lipid molecules, mostly phospholipids, which consist of a hydrophilic head and two hydrophobic hydrocarbon tails. These lipid molecules are arranged in two opposing layers with the hydrocarbon tails face one another to form a hydrophobic core, while their charged heads face the aqueous solution on either side of the membrane. Thus, cell membranes show the unique property of self-repair after they have been torn.

Cells show a negative surface charge in their normal environment and, accordingly, they can be transported within an electric field. The polar side of the phospholipids, which are a major component of the membrane, is partly formed of a negatively charged phosphate group. But also ionizable groups of the embedded proteins create a negatively charged surface. Additionally, it has to be mentioned that since most of the ionizable groups are organic acids

or bases, the surface charge depends on the pH of the surrounded electrolyte [93]. Cell characteristics associated with the separation in two-phase systems will be discussed in chapter 12.

### 2.2.1 Cell Separation Methods

Cell populations are often heterogeneous and the cells of interest are mixed with different types of chemicals, biomolecules or other cell types. Accordingly, one primary objective of cellular separation techniques is the generation of a sample of cells having a specific phenotype, the removing of unwanted ingredients and the providing of cells for cellular assays [94].

Cell sorting principles of macroscopic as well as of microscopic devices can be divided into immunological and non-immunological methods [95]. The most common and conventional immunological techniques for cell separation are fluorescence activated cell sorting (FACS) and magnetic cell sorting (MACS) [94-96]. These principles are generally based on flow cytometry. For the separation of a subpopulation the cells of interest are tagged with an antibody which is in turn linked to a fluorescence dye or a magnetic particle. The antibody is bound to a protein that is uniquely expressed in the desired cells. The final sorting of the cells is accomplished by electrical charge or magnetic properties. Non-immunological methods are frequently found in microfluidic systems and based on dielectrophoresis [97], hydrodynamic separation, ultrasound separation or ATPSs [29,30,95,98]. Differing from a pure cell-cell separation this study presents a two-phase electrophoresis which is applied for an improved separation of cells and proteins especially for purification purposes.

### 2.2.2 Cell Labeling

The lymphoblastoid cells (LCL-BX-W4 provided by GSF-Hämatologikum, work group of W. Hammerschmidt, München, Germany) used in this study were labeled with carboxyfluorescein diacetate succinimidyl ester, called CFSE or CFDA-SE. CFSE is a fluorescein derivative, which diffuses passively into cells. Outside of living cells the dye is colorless and non-fluorescent. Once introduced into cells the acetate groups are cleaved by cellular esterase transferring the dye into fluorescent and cell impermeant carboxyfluorescein succinimidyl ester. Additionally, the succinimidyl ester group binds to free intracellular amines resulting in fluorescent conjugates. Excess unconjugated reagent and by-products passively diffuse to the extracellular medium, where they can be washed away. CFSE is partitioned equally among daughter cells with each division and the dye is also useful for in vitro studies and for the analysis of cell behavior when transferred in vivo [99]. The approximate excitation and emission peaks of this product after hydrolysis are 492 nm and 517 nm, respectively [92]. Differing from the labeling protocol given by Invitrogen [92] the lymphoblastoid cells were labeled as follows.

Lyophilized powder of CFSE, 50 µg (MW = 557, C34554, Invitrogen, Germany), was dissolved in 18 µl dimethylsulfoxide (DMSO) leading to a 5 mM stock solution. After the cell suspension has been centrifugated at 300x g for 5 minutes at room temperature the cell pellet was resuspended in 1 ml 1x PBS buffer that was previously warmed up to 37 °C. In a subsequent step 2 µl of the 5 mM CFSE stock solution was added to the cell solution leading to a final concentration of 10 µM. Afterwards, the cell solution was incubated for 15 minutes at 37 °C and centrifugated again at 300x g for 5 minutes. The excess liquid was discarded and the cell pellet was again resuspended in 1 ml 1x PBS buffer. After a repeated incubation for 30 minutes at 37 °C the cell solution was centrifugated the last time at 300x g for 5 minutes and the excess liquid was again replaced by 1 ml 1x PBS buffer.

After the cell labeling procedure the cells were counted and inspected. In this context the cell viability was examined by a trypan blue exclusion test. This test is based on the principle that living cells possess intact cell membranes that exclude certain dyes such as trypan blue, whereas dead cells do not. Therefore 10 µl of the cell solution was mixed up with 10 µl of trypan blue solution (0.4%, T8154, Sigma-Aldrich, Germany) and examined. This examination shall ensure that most of the cells are intact and can be used for separation experiments.

# 3 Aqueous Two-Phase Systems

*The principle of aqueous two-phase partitioning was initially developed in Sweden during the mid-1950s and has been intensively used for the separation of macromolecules, proteins, viruses, cells, and organelles during the last decades. This chapter gives an introduction into ATPSs, how they are formed and used for the separation of cells and proteins.*

## 3.1 Fundamentals

ATPSs can help to characterize, separate and purify biomaterials. In 1896, Beijerinck first noted the formation of two phases utilizing the incompatibility of dissolved polymers [100]. Those systems were rediscovered and first employed in the 1950s by Albertsson for the partitioning of different kinds of biomolecules [27]. Generally, ATPSs are formed by mixing two incompatible polymers or one polymer and certain salts, e.g. alkali phosphates, with the polyethylene glycol (PEG) - dextran system being the most extensively studied. Above critical concentrations of the solution components, spontaneous phase separation takes place with each of the resulting phases enriched with one of the components. Since both of the resulting phases largely consist of water (80-90% (w/w)) and under the condition there is no denaturing agent added, biocompatibility is essentially ensured within the bulk fluid and ATPSs can provide a suitable milieu for different kinds of biological molecules, like cells or proteins.

In the case of proteins the partitioning takes place due to the different affinities of the protein species to the polymers. In turn, the affinity itself depends on physico-chemical properties of the protein such as surface hydrophobicity or net charge. By utilizing these molecular properties systematically a selective partitioning and purification of the target protein can be achieved [27].

## 3.2 Phase Separation and Diagrams

When a solution of polymer A is added to a solution of polymer B, three scenarios might happen. The two solutions will mix leading to a homogeneous solution. Or the mixture of the polymer solutions will result in phase instabilities, i.e., the solution will not mix and the system separates into two discrete phases. In case of incompatibility a phase separation occurs and the two polymers are collected in different phases. Alternatively, for complex coacervations also a phase separation occurs but the two polymers are collected in one phase while the other phase consists almost entirely of solvent [27]. These different possibilities can be described by the change of the Gibbs free energy of mixing, $\Delta G_{mix}$, which is given by

$$\Delta G_{mix} = \Delta H_{mix} - T\Delta S_{mix} \qquad (3.1)$$

where $\Delta H_{mix}$ and $\Delta S_{mix}$ are the enthalpy and entropy of mixing, respectively. $T$ denotes the absolute temperature. In case of $\Delta G_{mix} \leq 0$, the system will mix, whereas in the case of $\Delta G_{mix} > 0$, the system will separate into separate phases.

In order to describe the phase separation and also the partitioning in two-phase systems it was first shown by Walter et al. [28] that the so-called Flory-Huggins theory provides a useful framework. This theory describes a mean field model in which the distribution of molecules on a lattice is calculated. In the first version of the model only the distribution of a single polymer species in solution is described. This model was later extended to more than one polymer species in solution [101]. The assumptions made in this model can be summarized as follows:

- each lattice site is occupied by either a polymer segment or a solvent molecule
- the dissolved polymers are flexible
- the interactions are restricted to nearest-neighbor pair interaction on the lattice

A further assumption is that the polymer chain is unbranched and occupies $M \cdot n$ lattice sites, where $M$ is the degree of polymerization (number of segments on the chain) and $n$ is the number of molecules in the system [102,103]. This leads to the total number of lattice sites $N$ occupied by $m$ different components

$$N = \sum_{i=1}^{m} M_i \, n_i \tag{3.2}$$

Accordingly, this leads to a volume fraction $\psi_i$

$$\psi_i = \frac{M_i \, n_i}{N} \tag{3.3}$$

of each component $i$ in the system. Under the given assumptions the following general expression for the Gibbs free energy of mixing has been derived by Flory and Huggins

$$\Delta G_{mix} = N \, RT \sum_{i=1}^{m} \frac{\psi_i}{M_i} ln \, \psi_i + N \sum_{i=1}^{m-1} \sum_{j=i+1}^{m} \psi_i \psi_j \, W_{ij} \tag{3.4}$$

where $W_{ij}$ denotes the effective pair-wise interchange energy which is a function of the energies of the interaction between segments of component $i$ and $j$ when these occupy neighboring positions on the lattice. Here, the first term in the expression is the combinatorial entropy part whereas the second term is the interaction part [102].

However, this means that two factors determine the result of mixing two substances. One is the interaction between the molecules, the other one is the gain in entropy when mixing the molecules. The latter one is related to the number of molecules involved in the mixing process. If defined on a molar basis the entropy of mixing for small and large molecules is of the same order of magnitude [27]. In contrast, the interaction energy between molecules increases with their size since it is composed of the sum of interactions between each small molecule segment. For very large molecules the interaction energy per mole will tend to dominate over the entropy of mixing per mole. Generally, mainly the type of interaction between the molecules will determine the result of mixing two polymers.

Typical ATPSs consisting of PEG and dextran can be described by a phase diagram as sketched in Fig. 3-1. At low polymer concentrations the polymers are mutually miscible, denoted by the point O in the figure. But when the polymer concentration is increased, phase separation occurs and yields an upper PEG-rich phase and a lower dextran-rich phase where each of the phases usually consists of more than 80% (w/w) water. Those mixtures are represented by points above the curved line, like A or S. The curved line is called a binodial. It separates these two states and also describes the two-phase system in more detail. Suppose point A, cf. Fig. 3-1, represents the total composition of the system, the compositions of the top and bottom phases are described by point T (top phase) and B (bottom phase ) connected by the tie line [27]. The relation between the resulting weights of the phases is given by the ratio between the lines AT (top phase) and AB (bottom phase), provided that the composition is expressed in percent per weight (wt%). Furthermore, any total composition that is

represented by points on the same tie line will lead to phases of same compositions but different volumes.

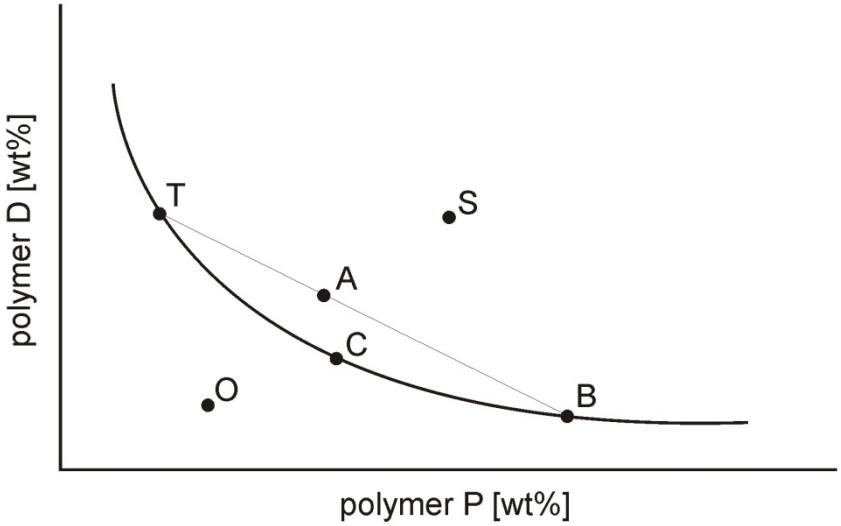


*Fig. 3-1: Sketch of a phase diagram: by mixing two polymers, D and P, in water or in a buffer solution, phase separation occurs above certain concentration thresholds. C is called the critical point.*

## 3.3 Preparation of Aqueous Tow-Phase Systems

ATPSs were prepared by dissolving a specific amount of dextran and PEG in a buffer solution. After stirring and settling overnight the phases separate with a sharp stable phase boundary. The upper phase mainly consists of PEG while the lower phase mainly consists of dextran, with both phases showing a high content of buffer solution [74]. After preparation, the two phases were separated by a pipette and stored in different vessels, cf. Fig. 3-2.

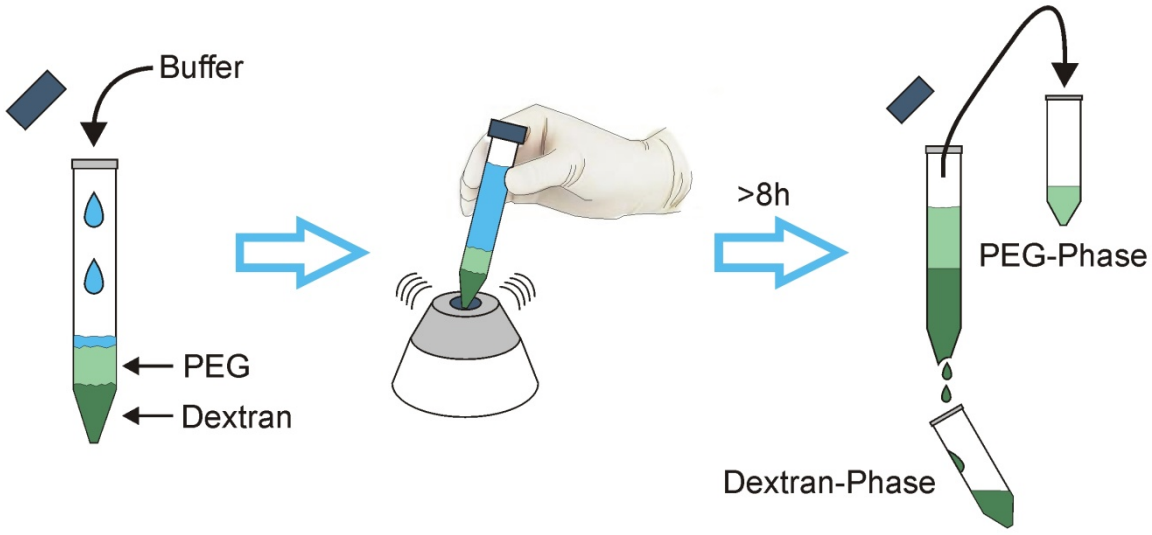


*Fig. 3-2: Exemplary preparation of a two-phase system. The desired buffer system is added to a specific amount of PEG and dextran. Subsequently, the solution is stirred and the arising phases are separated after more than 8 h of settling.*

In this study three compositions of ATPSs were mainly used and summarized in Table 3-1. The most experiments were performed in a system consisting of PEG 8000 and dextran 500,000, denoted as ‘standard system’. In case of hydrophobic affinity partitioning, PEG 8000 was replaced by PEG 6000 and PEG-palmitate (P-PEG) 6000, denoted as ‘P-PEG system’. For the third kind of ATPS dextran 500,000 was replaced by dextran 10,000 and PEG 8000 was partly replaced by PEG 35,000 in order to equalize the viscosities of both phases, denoted as the two-phase system of equal viscosity. All polymers are obtained from Sigma-Aldrich (Germany). Order number and additional information are given in Table 3-1.

| ATPS | dextran 500,000 | dextran 10,000 | PEG 35,000 | PEG 8000 | PEG 6000 | P-PEG 6000 |
|---|---|---|---|---|---|---|
| A - Standard system | 5.50% | - | | 3.80% | - | - |
| B - P-PEG system 10% | 6.20% | - | - | - | 3.96% | 0.44% |
| C - Equal Viscosity | - | 12.50% | 2.28% | 7.72% | - | - |
| Order number | D5251 | D9260 | 94646 | P2139 | 81255 | - |
| Range [kDa] | n.s. | 9-11 | n.s. | 7-9 | 5-7 | - |

*Table 3-1: Compositions of ATPSs mainly used in this study. The quantities of the polymers are given in weight percent (wt%). Accordingly, a corresponding amount of buffer solution has to be added. Additionally, the order numbers and the molecular weight range of each polymer are given.*

After phase separation and in case of the standard system (A) the upper PEG-phase consists approximately of 5.7 wt% PEG, 1.0 wt% dextran and 88.6 wt% water. In contrast, the dextran-phase consists of 1.9 wt% PEG, 9.5 wt% dextran and 93.3 wt% water [27,82]. In case of the P-PEG system (B) the upper PEG-phase consists approximately of 7.1 wt% PEG, 0.2 wt% dextran and 92.7 wt% water, the lower dextran-phase consists of 0.9 wt% PEG, 13.2 wt% dextran and 85.9 wt% water [74].

The resulting densities of the upper PEG-phase and lower dextran-phase of the systems A to C are given in Table 3-2. They were separately determined with the density meter DE 45 (Mettler Toledo, Germany). The resulting viscosity values after phase separation are presented in chapter 8.2 where a viscosity adjustment of the phases is described.

| ATPS | Density PEG-phase [g $cm^{-3}$] | Density dextran-phase [g $cm^{-3}$] |
|---|---|---|
| A - Standard system | 1.00785 | 1.04125 |
| B - P-PEG system 10% | 1.01110 | 1.04311 |
| C - Equal Viscosity | 1.03716 | 1.11646 |

*Table 3-2: Densities of the upper PEG- and lower dextran-phase.*

## 3.4 Ion Distribution and Conductivity

The addition of a single electrolyte to an initially uncharged ATPS, like PEG-dextran, can lead to the formation of a Galvani-type potential difference $\Delta\phi$ across the interface with electric double layers formed on both sides. Precondition for such a potential difference are different affinities of the anions and cations of the dissociated salt for the two phases. The magnitude is typically in the mV range and the sign of $\Delta\phi$ are determined by the partition behavior of ions of the majority salt in the system [102,104-110]. It has also been demonstrated that electrolytes can have a dramatic effect on the partition behavior of charged species, like proteins, which has been attributed to the existence of electrostatic potential differences [27,28,105]. In this context different groups tried to measure this potential difference with different experimental setups [107,108,111]. Pfennig et al. [104] later showed that $\Delta\phi$ can currently not be determined experimentally but systems with different salts added can be compared, leading to a $\Delta(\Delta\phi)$ [104]. However, it is generally accepted that potential differences exist between coexisting phases and often salts with polyvalent anions induce high potential values [78,80,104,107,108]. For that reason in this study potassium phosphate buffer has been mainly applied. A detailed discussion about the influence of the electric double layer on the protein transport across the interface can be found in chapter 11.4.

## 3.5 Separation of Biomolecules

The distribution of a molecule type between the two phases can be described by the partition coefficient $k$ [27,28,112] which is defined by the ratio of the concentration in the top, $c_t$, and bottom phase, $c_b$:

$$k = \frac{c_t}{c_b} \tag{3.5}$$

The logarithm of the partition coefficient itself can be split again into several terms affecting on the overall coefficient [27]:

$$ln\, k = ln\, k_{el} + ln\, k_{hyfob} + ln\ k_{conf} + ln\, k^0 \tag{3.6}$$

where *el*, *hyfob* and *conf* stand for electrochemical, hydrophobic, and conformational contributions to the partition coefficient. Other factors like biospecific affinity, size-dependent partitioning and further influences are summarized in $ln\, k^0$. Factors determining the partitioning can be identified by specific partitioning experiments, whereas ATPSs only vary in one factor like salt concentration, polymer type or hydrophobicity of the used polymers [27]. The main factors influencing the partitioning in PEG-dextran systems are polymer concentration, molecular weight of used polymers, molecular weight of the partitioned substance and added salts [27]. However, by controlling these factors the partitioning behavior of specific biomolecules can be adjusted.

Besides a number of other two-phase systems such as polymer-polymer, polymer-salt or polymer-detergent systems [27,28] the most famous one is still represented by the PEG-dextran system, cf. Fig. 3-3a. After phase separation has occurred the resulting two-phases offer different physical and chemical environments which allow for the selective partitioning of solutes such as proteins, cf. Fig. 3-3b.

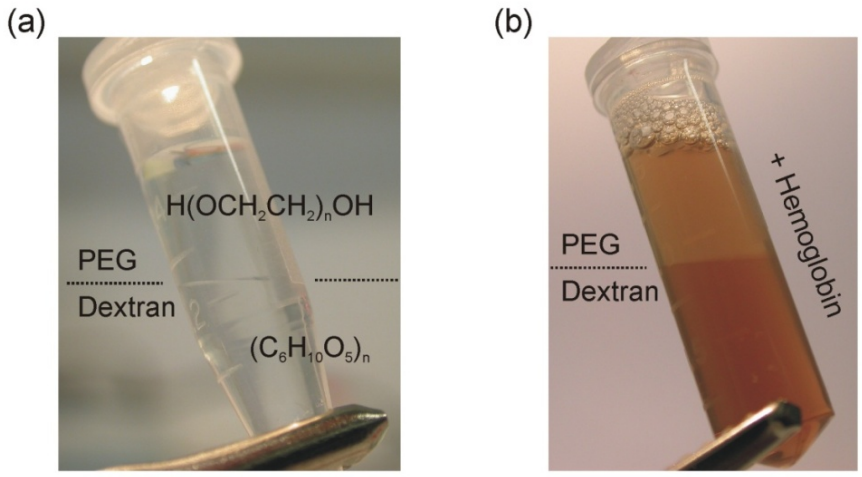


*Fig. 3-3: Exemplary preparation of a two-phase system; (a) before and (b) after adding the protein hemoglobin. In both examples a sharp interface between the PEG and dextran-phase is visible.*

Also in this study the PEG-dextran system is mainly used varying in molecular weight and attached ligands. The latter ones can be specifically used to increase the selectivity, also known as affinity two-phase partitioning. Therefore, a variety of bio-specific ligands can be attached to one of the phase polymers inducing a stronger biomolecule affinity to one of the phases. Typical ligands are, for example, attached antibodies or charged groups [75]. The main intention of such affinity partitioning is the reduction of extraction steps leading to a more efficient fractionation of the desired molecules.

### 3.5.1 Hydrophobic Affinity Partitioning

Another well-established affinity partition principle in ATPSs is the use of covalently bound hydrophobic groups [113-115]. This principle is also used in this study in order to achieve higher partition coefficients of different proteins. Therefore PEG has been partly replaced by P-PEG that is modified by additional hydrophobic side groups (fatty acids). In most cases These side groups strongly influence the protein partitioning between the two phases leading to increased partition coefficients. For example, without P-PEG the major part of bovine serum albumin (BSA) was found in the dextran-phase of a standard PEG-dextran ATPS while when a specific amount of PEG is replaced by P-PEG, the partition coefficient increases [113-115]. Due to the hydrophobic ligand, P-PEG now offers additional hydrophobic binding sites leading to a higher affinity to proteins exposing hydrophobic groups at their surface like BSA, cf. chapter 11.3.1.

P-PEG used in this study was synthesized by the method described by Shanbhag and Johansson [114] and others [113,115]. 100 g PEG 6000 was dissolved in 600 ml toluene. After complete mixing 100 ml toluene was distilled out of the solution at 65 °C at a pressure of 80 mbar in order to remove traces of moisture. After cooling down to 40 °C, 2 g (approx. 40 mM) of triethylamine was added. Maintaining the temperature at 40 °C, a solution of 5 g palmitoyl chloride in 50 ml toluene was added dropwise under continuous stirring leading to an amount of approximately 33 mM of palmitoyl chloride referring to the entire chemical preparation. The mixture was gently refluxed for 15 min at 112-113 °C and then filtered. After cooling to 4 °C the excess of palmitoyl chloride and toluene was removed by suction filtration and the filter cake was washed with absolute ethanol. The final P-PEG was obtained by drying the filter cake in a vacuum dryer at 40 °C for 24 hours. The degree of substitution can

be determined by saponification of the P-PEG and a subsequent titration. Typically over 50% of the terminal hydroxyl groups of PEG were esterified [115,116]. Accordingly a specific number of the linear PEG chains must have palmitoyl groups at both ends. In this study the degree of substitution was not analyzed since the goal was solely to achieve an increased partition coefficient for specific proteins.

PEG of 6000 Da average molecular weight was obtained from Sigma-Aldrich (Germany), cf. Table 3-1. For the synthesis of fatty acid esters of PEG, toluene (89682, purum, ≥ 99.0% (GC)), triethylamine (90340, puriss. p.a., ≥ 99.5% (GC)) and palmitoyl chloride (P78, 98%) were also obtained from Sigma-Aldrich (Germany). Ethanol (100971, 96%) was obtained from Merck (Germany). Water was deionized and further purified using a TKA GenPure UV water treatment unit (18.2 MΩ cm-1, 08.2205, TKA, Germany).

# 4 Electrophoresis

*Originally discovered by Reuss in 1809 [117] electrophoresis describes the movement of molecules in an electrolyte solution driven by electric fields. It has become a very popular utility in analytical chemistry or bioanalysis and electrophoretic separation techniques have been developed over decades and transferred to lab-on-chip systems in various ways. In this chapter the fundamentals of the electrophoretic motion are presented.*

## 4.1 Fundamentals

As soon as a charged object is immersed in an aqueous solvent it is surrounded by counter-ions until the global charge becomes zero (electroneutrality). The counter-ions are arranged in two layers. In the inner layer, called Stern layer, the attracted ions may be considered as permanently absorbed. In the outer layer, which is called the diffuse layer, the ions remain mobile. The combination of these two layers is called electric double layer, cf. Fig. 4-1.

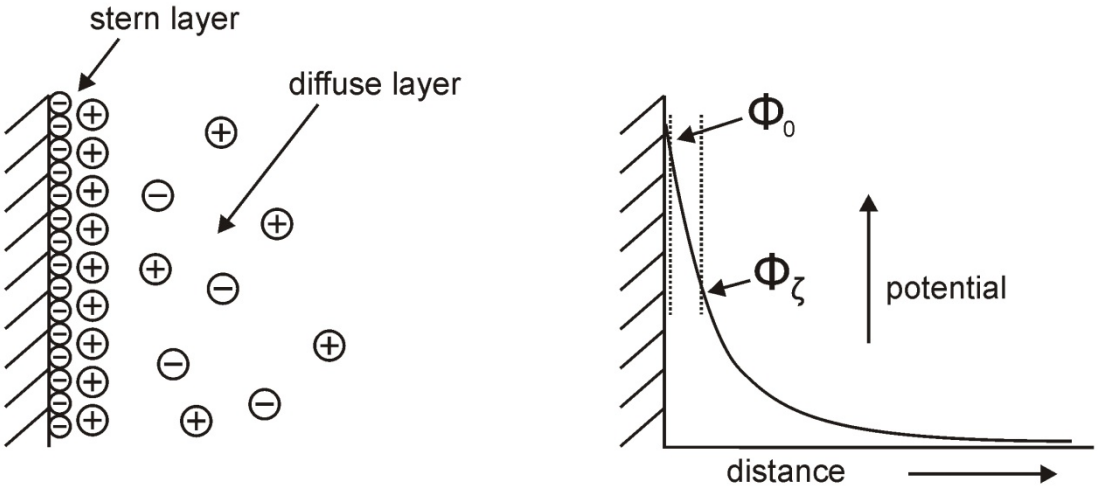


*Fig. 4-1: Double layer of a negatively charged surface. Counter-ions specifically adsorb near the surface and build an inner sub-layer, the so-called Stern layer. The outer part of the screening layer is called the diffuse layer. After a first potential drop within the Stern layer $\phi_0$ the potential at the beginning of the diffuse layer is called zeta potential $\phi_\zeta$.*

The thickness of the Stern layer is roughly given by the Bjerrum length, defined as

$$\lambda_B = \frac{e_0^2}{4\pi\ \varepsilon_r\ \varepsilon_0\ k_b\ T} \qquad (4.1)$$

where $e_0$ is the elementary charge, $\varepsilon_r$ is the vacuum permittivity, $\varepsilon_0$ is the dielectric constant of the fluid, $k_b$ is the Boltzmann constant and $T$ is the absolute temperature in Kelvin. In water and at room temperature $\lambda_B$ becomes normally thinner than 1 nm [19].

The diffuse layer can be described in a different way. Combining the Poisson equation, which relates the potential to the charge density, with the Boltzmann distribution the equilibrium distribution of mobile ions can be found. The Poisson-Boltzmann equation also serves as the basis for the one-dimensional Gouy-Chapman model. Furthermore, within the so-called Debye-Hückel approximation, i.e. in the case $\frac{e_0\phi(x)}{kT} \ll 1$, this model can be solved analytically and the electric potential is given by

$$\phi(x) = \phi_0 \, e^{-x/\lambda_D} \tag{4.2}$$

where $\phi_0$ is the surface potential, and $x$ is the distance from the surface. $\lambda_D$ is called the Debye length which describes the range of the electrostatic interactions and represents the distance from the surface at which the potential drops to 1/e of the original surface potential:

$$\lambda_D = \sqrt{\frac{\varepsilon_0 \, \varepsilon_r \, k_B T}{2 \, N_A \, I_{ion} \, e_0^2}} \tag{4.3}$$

$N_A$ is the Avogadro constant and $I_{ion}$ is the ionic strength of the buffer. Accordingly, the Debye length increases with increasing temperature and with decreasing ion concentration. The ionic strength of the solution $I_{ion}$ is defined by the concentrations $c_i$ of all ions in solution

$$I_{ion} = \frac{1}{2} \sum_i z_i^2 \; c_i \tag{4.4}$$

where $z$ is the charge number. The zeta potential $\phi_\zeta$ which is the potential drop across the charged cloud, cf. Fig. 4-1, is related to the surface charge density $q_0$ [34]. Considering a charged surface and an external electric field $E$ parallel to it, the non-zero charge density near the surface induces an electric body force, also parallel to the surface. The hydrated charges from the diffuse layer mediate the flow by viscous drag. After reaching a fully developed flow, the integration of the Stokes equation leads to

$$u = -\frac{\varepsilon_0 \, \varepsilon_r \, \phi_\zeta}{\eta} E \, (1 - e^{-x/\lambda_D}) \tag{4.5}$$

where $\eta$ denotes the dynamic viscosity of the fluid and $x$ the distance from the charged surface. The fluid velocity $u$ approaches exponentially the Smoluchowski's constant also denoted as 'slip viscosity'

$$u = -\frac{\varepsilon_0 \, \varepsilon_r \, \phi_\zeta}{\eta} E \tag{4.6}$$

outside of the diffuse layer [34]. If the charged surface with its solid/fluid interface is part of the microchannel system, the induced velocity leads to an electroosmotic flow (EOF), which varies linearly with the applied field, cf. Eq. (4.6). The ions of the diffuse layer of the electric double layer will migrate towards one electrode depending on their charge. Since these ions are solvated and clustered at the channel walls, they drag the rest of the solution with them. This electrokinetic effect becomes especially important in chapter 9.3.1, where the side walls of a microfluidic channel partly consist of dialysis membranes occupying small nanochannels.

In case of electrophoresis where the charged solid/fluid interface is part of a freely suspended particle, the electrophoretic movement of the particle is caused by the electroosmotic slip at the interface pushing the particle in the opposite direction [34]. The resulting velocity can be calculated in a similar way:

$$u = \frac{\varepsilon_0 \, \varepsilon_r \, \phi_\zeta}{\eta} E \equiv \mu_E E \tag{4.7}$$

where $\mu_E$ is the electrophoretic mobility of the particle. When the double layer is thin compared to the particle diameter and $\phi_\zeta$ is fixed, $\mu_E$ becomes independent of particle size and shape. But in case of proteins it has to be considered that their surfaces show generally a non-uniform charge distribution [118] and also the thickness of the double layer is in the same order of magnitude as the protein's dimensions. This characteristic could lead to significant variances in the electrophoretic mobility [119] and in the velocity, cf. Eq. (4.7). Accordingly, it has been observed that even for high zeta potential values the Helmholtz-Smoluchowski equation for the electrophoretic mobility can differ from measured values [120].

## 4.2 Proteins

Electrophoresis of proteins is often carried out in agarose or polyacrylamide gels. Thus, the protein separation is based on both the sieving effect and the differences in the electrophoretic mobilities of the proteins. In general, the pH of the buffer solution of the gel is usually about pH 9, so that nearly all proteins are negatively charged. The advantage of such high pH value is that after applying an electric field all proteins move towards the anode and all molecules, showing the same size and charge, will move within one band through the gel. Typically for macroscopic setups, each electrophoresis process is followed by a visualization procedure, e.g. a dye is added which binds to the proteins. A common and famous kind of protein electrophoresis is SDS-PAGE, the sodium dodecyl sulfate polyacrylamide gel electrophoresis, which has been also transferred onto microfluidic chips [5,7]. Here, the use of capillary electrophoresis for protein separation helps reducing separation times and allows a better automation and quantification. The typical diameter of the capillaries varies from 20 to 75 µm which allow high electric fields and good heat dissipation.

Proteins contain both acidic and basic groups. At a particular pH value the charges on the groups are balanced and the molecules behave as neutral, cf. Fig. 2-2. When a protein is placed in a pH gradient and moved in an applied electric field, it will pick up or lose protons. As it migrate towards its isoelectric point its net charge and its mobility will decrease and, accordingly, the velocity of the protein will slow down. Arriving at the point where pH is equal to pI the protein will stop migrating. In case of leaving this point the protein will pick up charges again and move back to the former position where it is neutral. This kind of separation method can also be combined with capillary electrophoresis to a two-dimensional, 2-D, gel electrophoresis allowing a global analysis of complex samples. In the first step the proteins are separated by their pI's and afterwards transferred into a channel network of parallel microchannels where a gel capillary electrophoresis is performed [88]. A big disadvantage of most electrophoretic separation principles is the irreparable denaturation of the proteins due to additives like SDS which can be avoided by alternative separation principles like aqueous two-phase partitioning.

## 4.3 Cells

In order to quantify the cell surface charge and study events at the level of cell membranes, cell electrophoresis has proven its capability. Already in the 1920's groups have described the movement of cells suspended in an electrolytic medium under the influence of an applied electric field. Over the last decades different groups have developed separation techniques allowing a characterization and analysis of cells due to their electrophoretic behavior, i.e. differences in electrophoretic mobilities [121]. Because of the cell membrane properties and numerous examinations it has been established that all cells of multi-cellular organisms have negatively charged surfaces - as long as they stay within their natural environment [121-123]. The surface charge is determined by ionogenic groups exposed on the plasma membrane.

Anionic charges associated with the cell surface charges are phosphate, sulfate, and carboxyl groups. In contrast, the cationic charge originates from the guanidium and ammonium groups. But the net surface charge is mainly determined by sialic acids, sulfated proteoglycans and phosphates which are responsible for the anionic behavior of cells [123,124]. The range of electrophoretic mobilities is narrow. If the electrophoretic mobility of erythrocytes of an adult individual were to serve as a standard, the majority of typical cells have mobilities ranging from 40% above to 50% below the electrophoretic mobility value of such erythrocytes, which typically migrate 1.1 $\mu m\ s^{-1}$ at 1 $V\ cm^{-1}$ [121,122].

One of the famous principles for cell separation bases on the differences in electrophoretic mobilities of cells is the continuous free-flow electrophoresis [9,121-123]. As already described in chapter 1.3, the charged particles, the cells, are injected into a thin carrier buffer film flowing between two parallel plates. A deflection of the charged sample components according to their mobility or isoelectric point is induced by electric fields, applied perpendicular to the flow direction.

Since cells are also polarizable in microfluidic systems cell manipulation by dielectrophoresis has been utilized for the separation of cell mixtures, cell enrichment or cell handling in general as well [97,125]. Aqueous two phase systems offer a good and gently alternative to cell electrophoresis. And, as shown in this study, the combination of electrophoresis and aqueous two-phase partitioning leads to alternative separation effects as well as continuous cell enrichment, cf. chapter 12.

# 5 Hydrodynamic Flow in Microchannels

*Microfluidic flow refers to liquid and gas flows in channels or geometries with at least one characteristic dimension being less than one millimeter and usually above one micrometer. Besides chemical micro process engineering, microfluidics is most commonly encountered in bioMEMSs (biological micro electromechanical system) and lab-on-chip devices. Due to the small dimensions viscous forces dominate and the flow is primarily laminar. Instead of the mixing, rotating and unsteady nature of turbulent flows, flow on the microscale is naturally smooth, regular and streamlined (irrotational flow). This characteristic property becomes especially important in multiphase flows, i.e. when two or more immiscible fluids are brought in contact within a microchannel.*

## 5.1 Governing Equations

According to Newton's second law, the conservation of momentum equation states that the change in momentum within the control volume is equal to the sum of forces acting on it. The general continuum description of fluid dynamics can be expressed in form of the a Navier-Stokes equation, here adapted for incompressible Newtonian fluids

$$\rho\left(\frac{\partial u_i}{\partial t}+u_j\frac{\partial u_i}{\partial x_j}\right)=-\frac{\partial p}{\partial x_i}+\eta\frac{\partial}{\partial x_j}\left(\frac{\partial}{\partial x_j}u_i\right)+f_i \qquad (5.1)$$

$$\frac{\partial u_i}{\partial x_i}=0 \qquad (5.2)$$

where $u_i$ is an instantaneous velocity component in the $i$th direction and $p$ is the pressure. $f_i$ represents body forces per unit mass. Eq. (5.2) is the continuity equation or conservation of mass, while (5.1) represents the conservation of momentum. The two terms on the left-hand side of (5.1) stand for the inertia subdivided in the unsteady and convective acceleration. The three terms on the right-hand side represent the force densities acting on a given volume element consisting of pressure drop, the viscous force and the body forces, such as gravity or centrifugal forces.

Since the continuum assumption is fulfilled, the Navier-Stokes equation, originally developed for macroscopic flows, remains still valid for microscopic flows. In contrast, on the nanoscale level the equation may become inapplicable. Since at this level the Knudsen number, the ratio of the molecular mean free path to the characteristic channel dimension, can become one.

## 5.2 Non-dimensional Numbers

As for macrofluidics, the flow behavior on the microscale can be quantified by dimensionless numbers. But compared to macrofluidic flow, the multiphase flow in microchannels is largely dominated by interfacial effects [126].

Considering multiphase flows on length scales smaller than one millimeter gravity usually becomes negligible. This is expressed by the Bond number

$$Bo=\frac{\rho\, a\, L_c^2}{\gamma} \qquad (5.3)$$

where $\rho$ is the density, or the density difference between fluids, $a$ is the acceleration, here gravity, and $\gamma$ is the surface tension. In regard to the present study the Bond number becomes less than 1 because of the small channel dimensions ($L_c$ ~ 100 µm). Therefore the flow is not significantly influenced by the three dimensional orientation of the channels. Also, a sessile

drop will take the shape of spherical cap in such dimension, which is the solution to the Young-Laplace equation with gravity completely absent.

The Reynolds number is the most famous dimensionless number in the field of fluid dynamics. In microscale, the Reynolds number, cf. Eq. (1.1), usually stays below 100 or less. Inertial effects become irrelevant in contrast to viscous forces that results in laminar flow conditions. Another important dimensionless number is the Weber number *We* which describes the ratio between the inertial effect and the surface tension $\gamma$:

$$We = \frac{\rho\, u^2\, L_c}{\gamma} \tag{5.4}$$

Due to the strong dependence on the velocity *We* can yield large values, for example in the field of inkjet printing where drops are ejected from a nozzle at high speed [127]. Due to the low flow velocities applied in this study the flow behavior is dominated by the surface tension and the Weber number becomes small. The capillary number *Ca* describes the ratio between viscous and capillary forces and is given by

$$Ca = \frac{u\,\eta}{\gamma} \tag{5.5}$$

[128]. In case of low capillary numbers capillary forces dominate the flow. The term capillarity denotes the rise or depression of a liquid, for instance, in a small tube or microchannel and occurs when the adhesive intermolecular forces between the liquid and the wall are stronger than the cohesive intermolecular forces within the liquid. The effect causes a concave meniscus to form where the liquid is wetting the solid surface. In microfluidics, capillary forces can be used for automated sample flow and flow control without any external pumps or valves [26,129]. In this study capillarity is combined with stop structures. They allow a selective filling of channels and are applied for coating processes and gel positioning, see chapter 7.2.2.

## 5.3 Two-Phase Flow

Two-phase flow denotes the flow of two immiscible phases, liquid-gas or liquid-liquid, through a channel. The resulting flow regimes depend on the fluids, the channel properties and the interactions between both. Especially in case of liquid-gas flow several different flow regimes occur which can be categorized by the flow rates [130], like bubbly flow or virtually dry flow. In this section, the main focus lies on liquid-liquid flow where the wetting properties are associated with both, liquids and microchannel walls and the viscosities of both phases are not negligible [131].

### 5.3.1 Liquid-Liquid Flow

Pushing two immiscible liquids through a channel, the flow pattern can be isolated drops, pearls necklaces, stratified flow or pears [66]. The resulting pattern does not only depend on the superficial velocities and the inlet geometry but especially on the wetting properties of the channel walls and its geometry. In particular, the latter two factors become increasingly important at low superficial velocities, as used in this study. Therefore, the wetting and surface tension effects in general have to be examined in more detail.

A liquid can be considered as a disordered phase where each molecule has its specific energy. This energy depends on the location of the molecule with respect to the surrounding fluid. In the bulk the potential energy of a molecule is minimal since the forces exerted by the

surrounding molecules are balanced out. In contrary, the energy reaches its maximum at the surface because of the unbalanced attractive forces towards the bulk of the medium. Accordingly, liquids tend to minimize their (free) surfaces since additional work is required to move a molecule from the bulk to the surface. The tendency to reduce the surface area can be quantified by the surface tension $\gamma$ which is defined as the energy needed to increase the surface area of a liquid by an amount $\Delta A$:

$$\Delta E_S = \gamma \, \Delta A \tag{5.6}$$

where $\Delta E_S$ is the surface energy. As an example, the surface tension of water in air is about $72 \cdot 10^{-3}$ N m$^{-1}$. However, surface tension is not only present between the liquid and the surrounding air but also between different kinds of liquids and between liquids and solids.

The ability of a liquid to wet surfaces becomes especially important in microfluidic systems and two-phase flow regimes. At the liquid-solid surface interface, wetting occurs when the adhesive forces are stronger than the cohesive forces. In such case, the molecules of the liquid have a stronger attraction to surface molecules of the solid than to each other. In contrast, if the cohesive forces between the liquid molecules are stronger than the adhesive forces the liquid wants to minimize the contact surface area to the solid. The wetting characteristics of a solid surface can be quantified by measuring the contact angle $\theta_0$ which is formed by the solid-liquid and the liquid-vapor interfaces. If $\theta_0$ is lower than 90° the surface is usually called hydrophilic. Contrariwise, if $\theta_0$ is larger than 90° the surface tends to repel the liquid and is called hydrophobic. The balance of the forces which act at the so-called three-phase contact line is given by Young's equation

$$\gamma_{LV} \cos\theta_0 = \gamma_{SV} - \gamma_{SL} \tag{5.7}$$

where $\gamma_{LV}$ is the liquid-vapor, $\gamma_{SV}$ the solid-vapor and $\gamma_{SL}$ the solid-liquid interfacial tensions, and $\theta_0$ denotes the contact angle at equilibrium. The Young equation assumes perfectly flat surfaces but in many cases surface roughness and impurities cause a deviation in the equilibrium contact angle from the contact angle predicted by Young's equation. Hence, even on smooth but not perfectly smooth surfaces a drop will assume a wide spectrum of contact angles ranging from the advancing contact angle $\theta_a$ to the receding contact angle $\theta_r$, cf. Fig. 5-1.

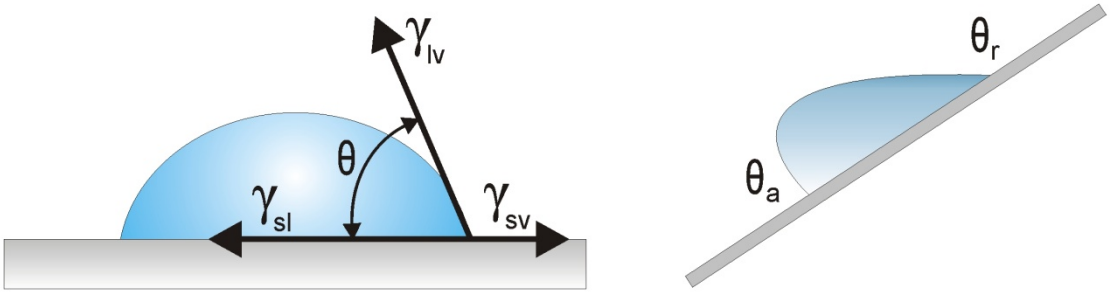


*Fig. 5-1: Left: Liquid drop on a surface and corresponding contact angle and surface tensions. Right: Pinned drop on an inclined plane and its resulting advancing and receding contact angle.*

Accordingly, when two liquids are present, the wetting properties of each liquid on the surface have to be considered resulting in two possible configurations. If one of the liquid is non-wetting it is separated from the wall by the other liquid. If both liquids are partially wetting an equilibrium contact angle can be found, cf. Fig. 5-2.

To characterize the behavior of two-phase flows, dimensionless numbers like the Weber number [132] as well as the Capillary number [66,133] are commonly used. But it is shown by different groups that such numbers are not the only relevant parameter describing, e.g., the transition point between stable parallel flows and parallel flows which break into droplets inside a microchannel [134-136]. Thus, the breakup mechanism is not simply a competition between shear stress and surface tension.

In summary, one can say that the flow behavior in microchannels of two immiscible fluids mainly depends on the interplay between the wetting behavior of each fluid, the interfacial tension between the fluids, the channel geometry and flow velocities. Accordingly, there exist different strategies reaching a stable two-phase flow with stratified layers.

In case of an organic-inorganic liquid pair, like oil and water, surfactants are very often used to influence the interfacial tension and to create stable and reproducible flow patterns like stratified flows [67]. Within a simplified picture, a typical surfactant molecule consists of a hydrophobic tail and a hydrophilic head. Since it is soluble in both organic phase and water phase it tends to reside mainly on the interface between both phases. This leads to a strong reduction of the interfacial tension. Without such surfactants no well-defined flow patterns may appear, as shown by Dreyfus et al. [66].

By shrinking the channel dimensions not only the liquid interface but also the interaction between the liquids and the solid wall surface becomes essentially important. This interaction leads to a further well-known technique inducing a stable and stratified two-phase flow of immiscible liquid pairs. By selectively and chemically modifying the channel surface in order to create different areas of wetting properties, liquid-liquid interfaces can be pinned and multiphase flows are decoupled into virtual single-phase subsystems [131]. Thus, even stable gas-liquid flows or counter flowing configurations are feasible [137].

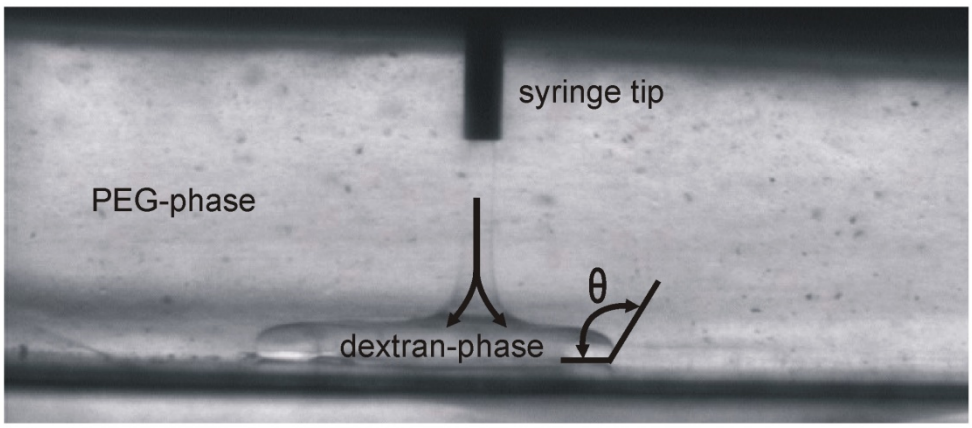


*Fig. 5-2: Droplet of dextran-phase immersed in a PEG-phase and placed on a polymer surface.*

Another strategy stabilizing the flow is to change the aspect ratio of the microchannel in order to minimize the interface area and by that the interaction between the immiscible liquids or to increase the area between each individual liquid and the channel walls. Related to the latter one, Guillot and Colin have shown that the transition to a stable parallel flow of oil and water can be reached at much lower flow rates compared to a square channel shape only by doubling the channel width [134]. By such a geometry change the interaction between the walls and the liquids becomes dominant. Even if a liquid-liquid interface inherently induces flow instabilities, the interface can also help to stabilize stratified flow patterns. Since systems tend to minimize their energy an increase of the interface surface would be generally counterproductive.

However, Fig. 5-3 shows the effect of changing the channel geometry. Here, not the channel width is increased but the channel depth leading to an increased interface area between water and propylene carbonate (PC) while the rather low flow velocity is kept constant. The parallel flow breaks into droplets as soon as the interfacial interaction becomes dominant. Since PC has a lower contact angle on PMMA compared to water, PC wets the whole circumference and forms the continuous phase. A similar liquid combination is also used in this study for protein enrichment at the liquid interface, see chapter 13.1.

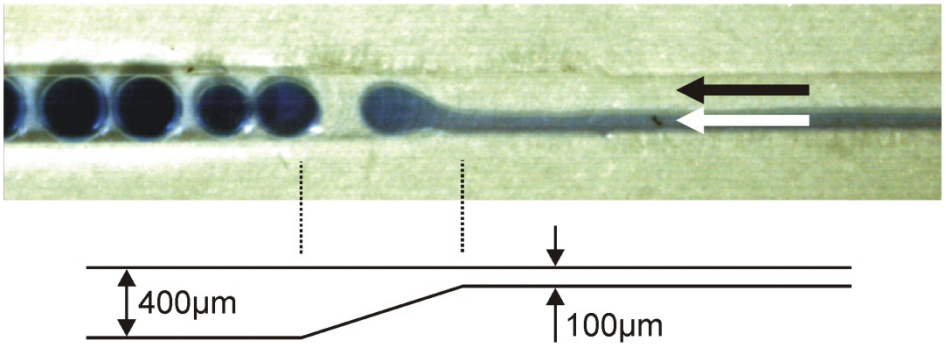


*Fig. 5-3: Two-phase flow of propylene carbonate and water colored by aniline blue in a microchannel (w x h: 600 x 100 µm). The flow is from right to left. As shown in the sketch below the channel depth is increased from 100 to 400 µm while the width remains unchanged. Due to the increased channel depth the parallel flow is forced to break up into droplets.*

A further approach to minimize the interfacial area is to create two separate channels with only a small overlap between them. Thus the ratio between the liquid-solid and liquid-liquid interface area is strongly increased and flow instabilities are largely suppressed [131,137-139]. This method is used to create a stable interface between oil and water described in chapter 13. Moreover, it has been shown that also high viscosities of the liquids or increased flow rates would lead to stabilized flow conditions [134].

# 6 Experimental Setup and Methods

*For experimental observations and the gaining of detailed information about flow patterns and movements of fluorescent biomolecules in microfluidic devices special instruments are essential. This chapter describes all components of the experimental setup including the macro-to-micro fluidic connections of the microfluidic chip, the syringe pumps, the power supply and the fluorescence unit adapted to a microscope.*

## 6.1 Measurement Setup

Microfluidic devices for analysis or manipulation of biomolecules generally require different external instrumentation for their operational reliability. Furthermore, for the observation of the transport behavior of biomolecules additional equipment is required making the fluidic chip to one of the smallest part of the whole setup. As shown in Fig. 6-1, the setup consists of the microfluidic test chip, syringe pumps to drive the liquids, a microscope system for observations inside the main channel and a voltage supply which is connected to the chip electrodes.

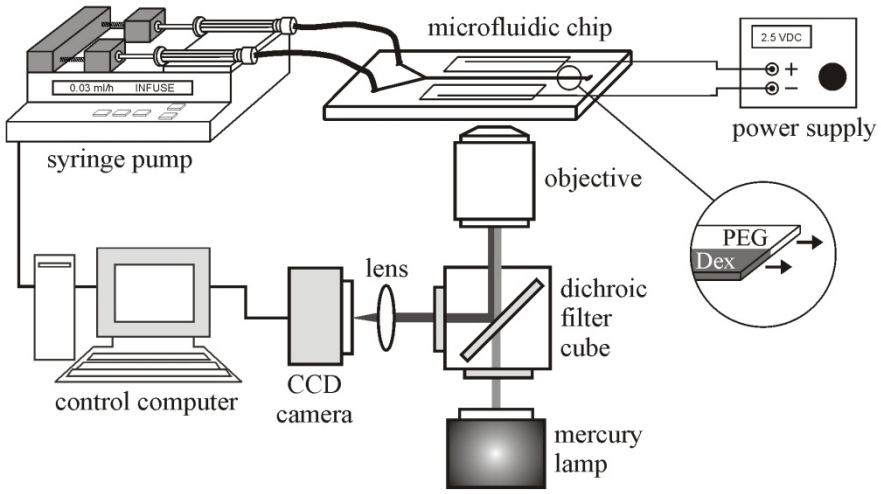


*Fig. 6-1: Schematic of the experimental setup for active two-phase transport measurements. The microfluidic chip is equipped with two reservoirs and electrodes. For optical analysis the setup also includes an inverse fluorescence microscopy system.*

During a typical experiment, the immiscible liquids are pumped into the test device at low flow rates such that a stable phase boundary is formed. Fluorescence labeled proteins or cells are used as a sample. The concentration distribution of the proteins or the position, in case of living cells, are recorded by mapping the fluorescence intensity using an inverse microscope (CKX 41, Olympus, Germany) equipped with a fluorescence unit and a CCD camera (Color View III, Olympus, Germany). Afterwards, the intensity profiles are plotted using the image analysis tool ImageJ, see Fig. 6-2 [140]. In case of active transport, the electrodes are driven by an additional precision power supply.

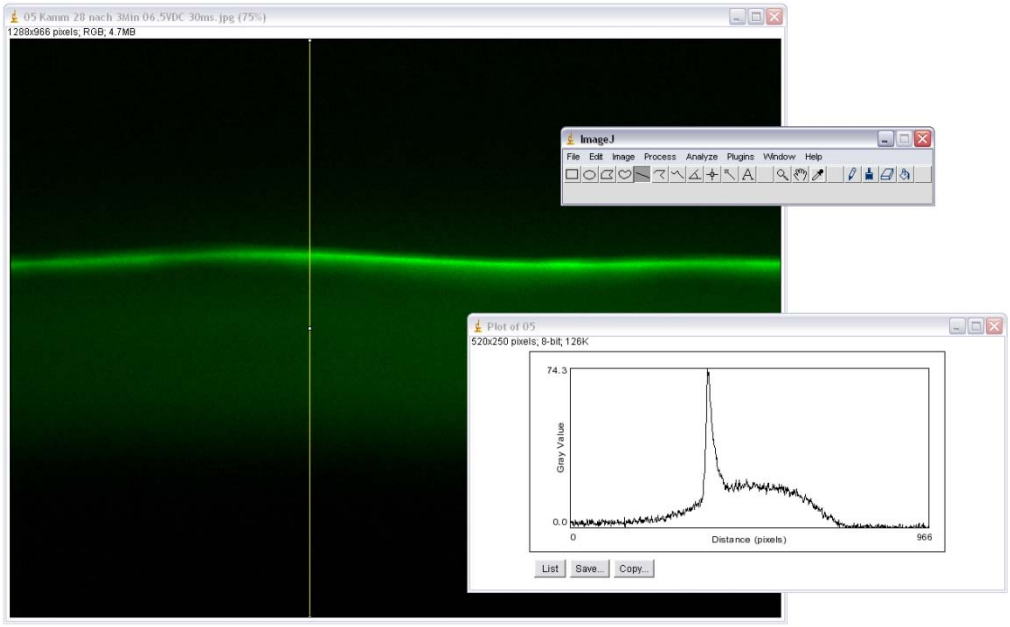


*Fig. 6-2: Analysis of the concentration distribution of the proteins using the image analysis tool ImageJ. The fluorescence picture shows protein enrichment directly at the phase boundary between the PEG- and dextran-phase.*

## 6.2 Fluidic Setup

Since the microchannels are empty before their first usage the fluids have to be injected into the channel network in a suitable manner. Distinct from capillary electrophoresis chips or fluidic systems based on liquids of limited volume [17,22] the requirements differ for continuous flow through systems. Especially when two different and immiscible liquids are injected into a microchannel and a stratified flow pattern is achieved, not only the geometry of the channel but also the feeding has to be adapted to such requirements. Accordingly, the syringe pumps, the supply tubes and the macro-to-micro chip interface deserve closer attention.

When pressure is applied to a microfluidic network the compliance causes walls, especially the walls of the tubes, to expand and store extra liquid volume, i.e. the walls act like fluidic ‘capacitors’ also showing typical transient responses known from electronic circuits. Oscillatory applied pressure at low frequency deforms the walls to a steady state whereas at high frequency the liquid is only pumped into and out the extra volume space created by deforming channel walls [34]. Hence, using syringe pumps for liquid transport, the instantaneous flow in microchannels usually differs from the pump settings due to connection compliance. Accordingly, the flow rate imposed by a syringe pump depends on the tubing and the microfluidic network characteristic. For systems with a high fluidic ‘capacity’ it can take a long time till a stable flow rate within the microchannel is achieved. And, furthermore, every change of the flow rate requires new time to equilibrium, especially in case of high fluid viscosities.

In order to meet the requirements of a stable two-phase flow and to reach short equilibrium times fluidic ‘capacities’ have to be minimized. In this study it has been observed that the material of the syringes and the connection tubes between syringe and chip hold a significant part of the overall capacity. Accordingly, polymeric syringes have been replaced by syringes made of glass (HA-81228, 1700 series, PTFE luer lock, 500 µl, Hamilton Bonaduz AG,

Switzerland) connected to DuPont Teflon® FEP (fluorinated ethylene propylene) tubes (1526, inner diameter 0.01´´, outer diameter 1/16´´, Upchurch Scientific Inc., USA) showing much higher tensile strength and stiffness compared to often used silicone tubes, cf. Fig. 6-3. For the connection between syringe and tube precision dispense tips made of stainless steel were placed in between (5130-B, EFD Inc., USA). Finally, the syringes were mounted on programmable infusion pumps (KDS210, KD Scientific Inc., MA, USA) which were controlled by a LabView program.

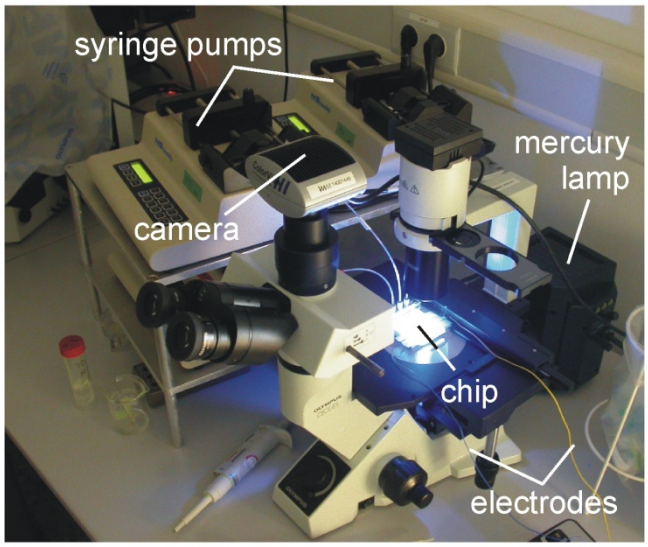


*Fig. 6-3: Experimental setup for active two-phase transport measurements. For optical analysis the setup includes an inverse fluorescence microscopy system. The electrodes are connected to a precision power supply and the chip is connected to up to four syringe pumps on the opposite side.*

## 6.3 Fluidic Connections

The interfacing between the macro- and microworld still remains as a main challenge for chip development. Depending on the application, fluids not only have to be injected into or/and removed from the microfluidic chip but also requirements like low dead volumes, operation over a wide pressure range, or chemical resistivity have to be addressed [141-143]. Since in this study the microfluidic chips are generally reused, an easy and non-permanent connection method has to be developed. Additionally, in order to prevent the risk of channel clogging the application of glue is not suitable.

One possibility is the integration of a plug-in connection directly into the chip material. Such a technique allows an easy and fast connection to the microfluidic network and the integration into injection molding manufacturing processes, cf. Fig. 6-4. Therefore the inner diameter of the tube is smaller than the outer diameter of the connection port. Depending on the desired pressure range inside the chip the tightness can thus be adjusted.

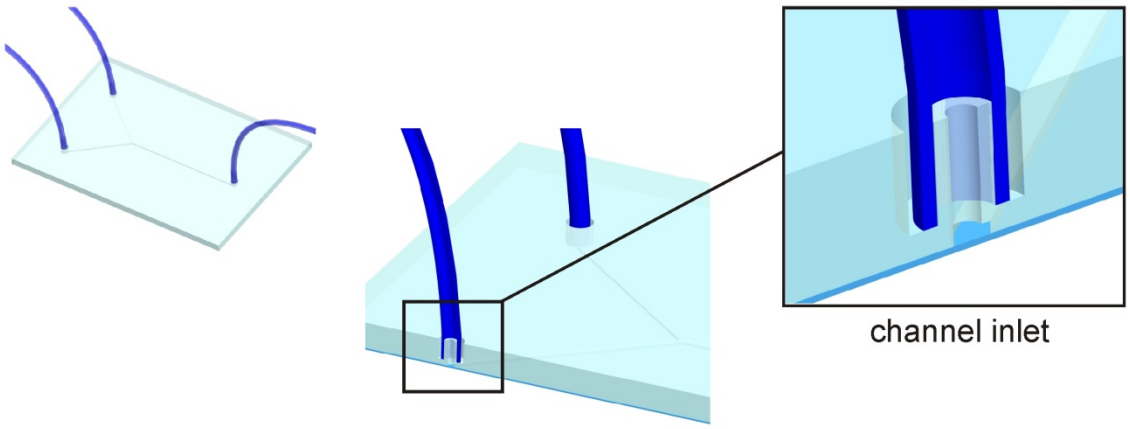


*Fig. 6-4: In-chip connection port. The fluidic socket is part of the chip itself allowing a fast and easy connection.*

During the manufacturing process by micro milling it is essential to ensure that the through hole has to be milled before the outer groove due to heat transmission purposes. Such kind of connection is very practical for easy and fast setups using elastic polymeric tubes, like silicone tubes. But for stiffer tubes with small inner diameters such a connection principle is not applicable. The reusable and quick-release fluidic connection system which was mainly used in this study was adopted from chromatography devices [144]. Here, one possibility to connect Teflon® tubing is the usage of flangeless fittings (P-283x and P-200x, Upchurch Scientific Inc., USA), cf. Fig. 6-5. Therefore the tubing is first cut with a square end. Next, the ferrule is slipped onto the tubing and the male nut tightened in a fitting. The special designed ferrule squeezes and holds the tubing.

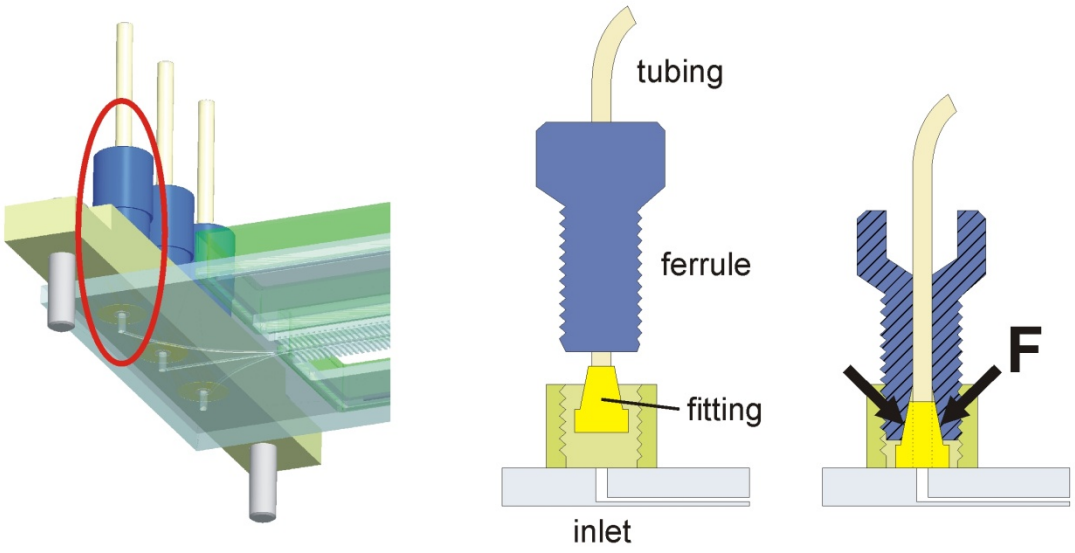


*Fig. 6-5: Reusable and quick-release fluidic connection system adapted from low pressure HPLC connection ports.*

For multiphase flow configurations the chips have up to four inlet ports and three outlet ports. Both, the numbers and positions of the ports as well as the fact that the main part of the chip, the main channel, has to be visible to a microscopic lens, become important for the design and configuration of the chip holder. Also relevant is the flexibility of the chip holder since chip designs often changes during different development steps. In Fig. 6-6, the developed chip holder is shown with a microfluidic chip placed in it. The chip can incorporate up to ten inlet and outlet ports. Here, the outlet is designed as an 'open' outlet port. The 4-nut holder can be replaced, for example, by a 3-nut or 5-nut holder and also the lateral position can be adjusted to different chip designs (three positions for the inlet and outlet nut holder). The connection ports don't require extra sealing gaskets and the chip has to be only equipped with one through hole per port, typically 0.8 mm in diameter. Due to its flexibility, the nut holder positions can also be used for additional fluid control components like microfluidic backpressure valves, as presented in chapter 8.3.

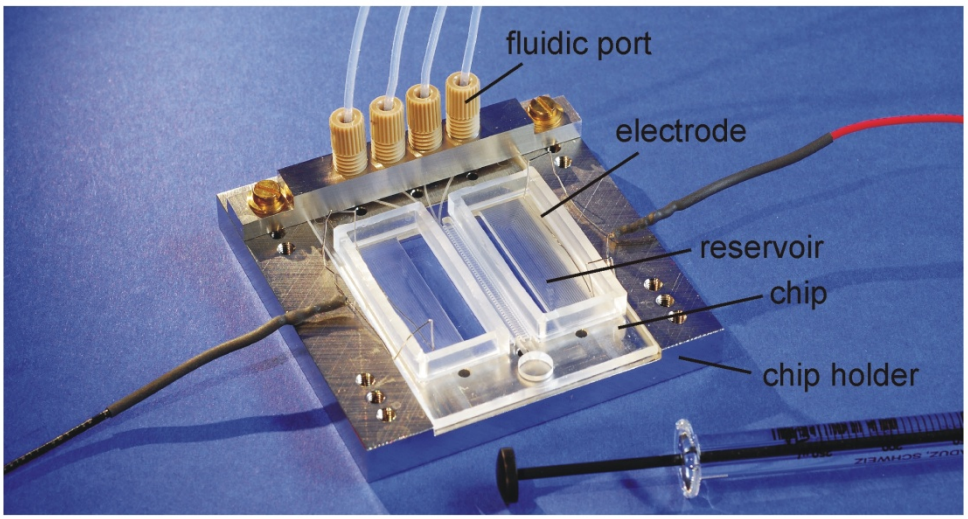


*Fig. 6-6: Components of the microfluidic setup. The chip is placed in a chip holder and the fluidic ports are pressed against it for sealing purposes.*

## 6.4 Fluorescence Detection

Fluorescence detection is one of the widest used detection method for microchip-based analysis devices. Not only its outstanding sensitivity but also the increasingly wide choice of fluorescent markers for non-fluorescent biomolecules makes this technique very attractive. As a non-contact detection technique, in most cases all detector instrumentation remains external and no extra components have to be integrated on-chip. These circumstances allow the use of disposable low-cost chips, as expensive detector components are reused. The principle of the fluorescence microscopy is based on the phenomenon that fluorescence markers emit energy detectable as visible light when irradiated with light of a specific wavelength. Therefore, the microscope system is equipped with different filters and mirrors allowing radiation with the desired wavelength to pass, cf. Fig. 6-1. After reaching the sample the radiation collides with the atoms in specimen and electrons are excited to a higher energy level. As soon as they relax to a lower level, light is emitted. The energy dissipation during the excited state is responsible for a Stokes shift, the difference between the absorption spectra and the emission spectra. This shift in wavelength allows the isolation of the emitted light from the much brighter excitation light using a second filter. Since here the emitted light is of lower energy a high-pass filter of

a longer wavelength is applied. Thus, the fluorescing molecules can be observed usually shining against the dark background with high contrast.

Different light sources may be used as excitation sources, including lasers, photodiodes, and lamps. The microscope system used in this study was equipped with a super high pressure mercury lamp (USH-102D, Ushio, Japan) combined with a fluorescence mirror unit (U-MNB2, excitation: bandpass filter 470 - 490 nm, emission: high-pass filter 520 nm, dichroic mirror: high-pass filter 500 nm, Olympus, Germany). During experiments, fluorescence images of the protein distribution and cell positions were taken at different positions along the main channel. In addition to that, each time images with transmitted light are taken shortly afterwards. These images allow to identify the channel walls unambiguously afterwards.

The fluorophores used in this study are based on fluorescein having their absorption and fluorescence emission maxima at approximately 495 nm and 518 nm, respectively. Before the diffusion and transport experiments, the linearity of the functional fluorescence intensity versus protein concentration was confirmed by taking fluorescence images of microchannels that are filled with solutions of different protein concentration, cf. Fig. 6-7.

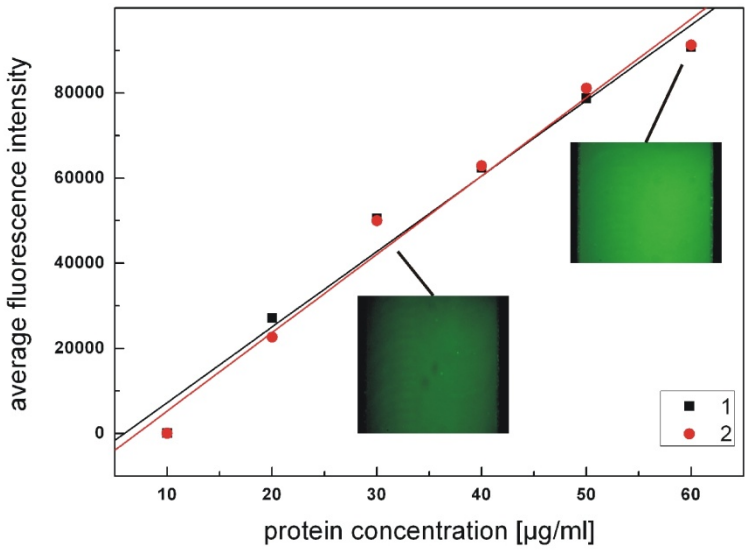


*Fig. 6-7: Fluorescence intensities of BSA samples (1 and 2) of different concentrations and at two different locations inside one microchannel. For low protein concentrations linearity of the functional fluorescence intensity is given.*

Related to protein fluorescence labeling the advantages of the used Alexa Fluor® 488 dye are higher quantum yields and photostability compared to other fluorescein conjugates. Additionally, the Alexa Fluor® 488 dye is insensitive to pH changes between pH 4 and 10 [92]. Although the Alexa Fluor® 488 dye shows minor bleaching effects [92], after each measurement all light sources were turned off, i.e. the proteins were only exposed during taking fluorescence images. In case of the cells only their spatial positions are important. Accordingly, bleaching or other effects on the fluorescence dye play only a minor part.

## 6.5 Electric Connections and Electrodes

To provide the driving electric fields for electrophoretic transport and separation, a reliable and precise power supply is essential. Since for dc mode the necessary voltage range lies between zero and thirty volts maximum, the requirements can be fulfilled by commercial power supplies. Therefore, a precision dc linear power supply (TTi-QL355TP, Thurlby Thandar Instruments Ltd., United Kingdom) was chosen allowing a stable and accurate output voltage. For applying ac voltage, an in-house developed LabView program in combination with a multifunction I/O board (AT-MIO-16XE-10, National Instruments, Germany) was used. The LabView program permits every desired waveform which can be specified by an equation.

To 'connect' the electric field with the chip or rather with the main channel, different options are conceivable. One requirement to create an electric field inside a liquid medium is that the electrodes have to be directly or indirectly in contact with the liquid itself. In this study two possible strategies have been examined to identify a suitable way for an active transport of biomolecules inside the chip.

For realizing the first strategy the electrodes have been placed inside the main channel and thus in direct contact to the test medium. This kind of electrode arrangement has been used for molecule transport and adopted from electrical field flow fractionation systems [145-152] as well as from SPLITT systems [55-58]. Since in aqueous solutions electrode potentials higher than 1.6 $V_{dc}$ may cause electrolysis and bubble generation which leads to a blockage of the small microchannels, the applied voltage has to stay below a critical value.

However, even if at low dc voltage the electrodes should be totally shielded by counter-ions, see chapter 4, there still exists an effective electric field which induces particle migration. The strength of the field strongly depends on the used buffer system as well as on the flow velocity. Due to the capacitance the electric field is effectively reduced to less than 3% of the applied field value [151,153]. But assuming that only two percent of applied two volts are left within an 800 µm wide channel there still remains an electric field of 50 V $m^{-1}$. As an alternative and in order to provide sufficiently large field strength while preventing bubble formation from electrolysis, an ac voltage could be applied to the electrodes. Thereby increased transport velocities compared to dc voltages are possible [154]. The results of both, the application of ac and dc voltage, are discussed in chapter 9 in more detail.

Also in order to avoid a blockage of the microchannel by bubbles, the electrodes can be decoupled and placed outside of the main flow path, i.e. bubbles are generated outside the channel network. The electric field is applied to the main channel through narrow liquid bridges. In order to ensure that the main flow is still guided through the main channel the 'bridges' must have either a high flow resistance or enable a fluidic decoupling. But they also need a low electrical resistance to guarantee electric field strength high enough for an adequate electrophoretic transport of biomolecules inside the main channel. To meet these demands, ion bridges can be used that are distinguished between nanochannels [14], ion exchange or dialysis membranes [155,156], and different kinds of gels [47,49,157,158]. They are often applied for electroosmotic pumps [157,159-161] and free-flow electrophoresis [14]. In this thesis two possible ion bridges have been examined, dialysis membranes and hydrogels. The fabrication steps and their application will be presented in chapter 7 and 9, respectively.

# 7 Fabrication of Microfluidic Chips

*During the last decades a broad spectrum of microfabrication techniques has been developed offering the processing of a variety of materials. Initially started with silicon, materials like glass and polymers are now widely used in the field of microfluidics. Especially polymer-based microchips have a high potential as low-cost and disposable devices. For polymer prototyping different fabrication procedures are available enabling short fabrication times and fast design changes. All microfluidic devices presented in this thesis are either based on cyclo olefin copolymer (COC) or polymethylmethacrylate (PMMA). In this chapter the basic fabrication procedures are presented including the milling of the channel network, the sealing and the integration of electrodes.*

## 7.1 Construction and Manufacturing

Complex tasks in today's lab-on-a-chip systems often require a number of development cycles until the final design of the chip is reached. Thus, short periods from the design idea to a testable chip are necessary to obtain microfluidic solutions within a reasonable time. With regard to these requirements a concept for rapid prototyping was initiated. Starting with the transformation of the sketched concept to a CAD drawing with Pro/ENGINEER (ProE, Wildfire 2.0, Parametric Technology Corporation (PTC), Germany) the resulting CAD data was semi-automatically transferred to machine codes. Standard blank chips (dimension: 64x43x2 $mm^3$) were manufactured before by injection molding and were available in COC (5013, TOPAS Advanced Polymers GmbH, Germany) and PMMA (7N, Röhm GmbH, Germany). Before milling, the curvature of the chip in x and y direction was controlled by an optical scanning profilometer (µScan AF-2000, Nanofocus, Germany). In contrast to other manufacturing methods, during the milling process the milling cutter is first reset at one position on the chip surface. Every further cutting is related to this point. Accordingly, surface curvature can lead to strong deviations in channel depths. The curvature measurement results are summarized in Table 7-1.

| Material | Max. curvature x-direction | Max. curvature y-direction | Max. curvature x-direction (sect.) | Max. curvature y-direction (sect.) |
|---|---|---|---|---|
| PMMA | 12.1 µm | -8.1 µm | 5.8 µm | < -1 µm |
| COC | 42.2 µm | -16.0 µm | 16.8 µm | < -1 µm |

*Table 7-1: Maximum curvature of the chip surface in x- and y-direction ($x_{max}$ = 64 mm, $y_{max}$ = 43 mm). Since the applied channel structure under investigation is only located in parts of the chip area (sect.), also the expected maximum curvature of the channel within this area itself was calculated.*

During the following manufacturing steps these blanks were transformed to working fluidic chips using a CNC micro milling machine (Evo4 3D, Hochbach GmbH, Germany) and, in special needs (additional gold electrodes), by laser treatment (eximer laser Exitech 700, 193 nm, 200 mW, formerly Exitech, United Kingdom). The milling machine allows structures down to 100 µm in lateral and a few µm in vertical direction. Related to the latter mentioned dimension it is essential to ensure that the operating temperature of the machine is reached before milling since the spindle mounting shows a thermal expansion of approximately 2.5 µm $°K^{-1}$ and a maximum extension of approximately 50 µm until a final position is reached at constant operating temperature. Chips used in this study were mainly milled by a

milling cutter of 300 µm in diameter (HM-FS-030 D, Horbach GmbH, Germany) combined with an air cooling. With a number of revolutions per minute of 12,000 RPM and a feed speed of 20 mm $s^{-1}$ best milling results have been observed. In order to realize steps of 20 µm and smooth inclined planes, the maximum increment chosen for the vertical dimensions was 20 µm. Additionally, the milling results have been optimized by an adjusted milling strategy, cf. Fig. 7-1. Although micro milling forms rough surfaces this fabrication technique is less time-consuming and cheaper compared to injection molding or hot embossing during development procedures. The average roughness height and mean waviness height of the milled channel bottom was 0.41 µm and 4.87 µm, respectively. The depth of the main channel was also measured with a profilometer and the deviation from the desired value is approximately 8%. All values were measured at different positions of the channel.

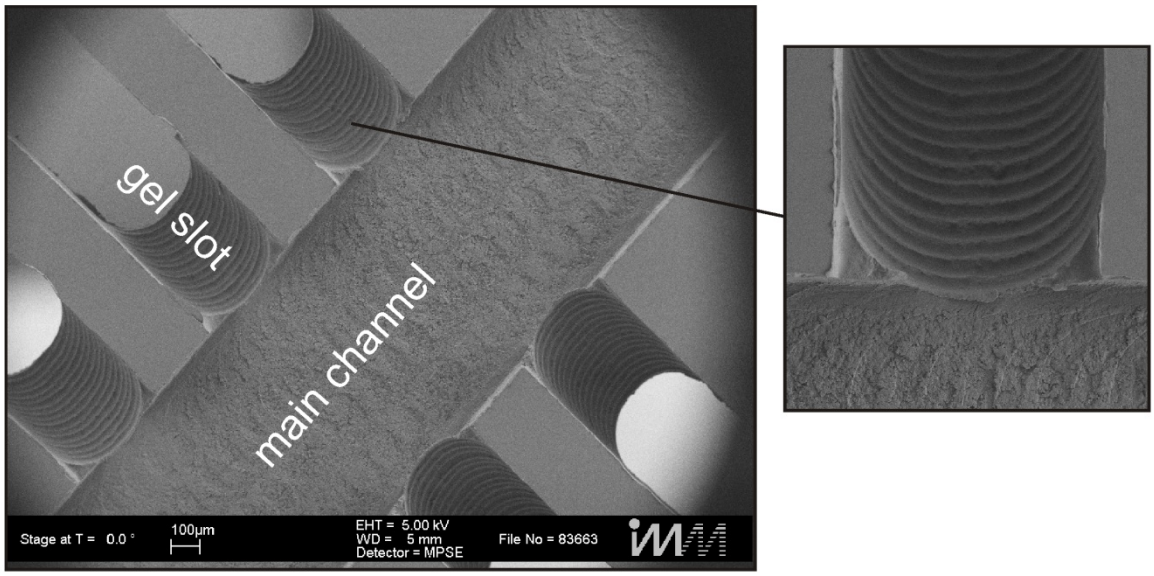


*Fig. 7-1: REM picture of the milled channel structure. The main channel is connected to gel slots which are later filled with agarose gel. The steps (right) are in the range of 20 µm.*

Rough surfaces can cause different disadvantages related to lab-on-a-chip devices consisting of various small channels [162]. Since the overall surface area is intensively increased offering much more binding sites for biomolecules, surface coating becomes very important. Without any coating agent BSA molecules preferably adhere to the channel walls after a short period of time. For checking purposes, a PMMA channel was flushed with BSA dissolved in pure water not containing any PEG. When removing the BSA solution after 30 minutes, the channel surface showed strong adsorption of BSA molecules visualized by fluorescence emission, cf. Fig. 7-2. This leads to a non-wanted background fluorescence which may corrupt the analysis of the experimental data. But fortunately due to the high PEG concentration in the used ATPSs the adsorption of BSA to the PMMA surface is strongly suppressed. For these reasons PEG is, for example, also used for dynamic wall coatings to prevent protein adsorption during polymerase chain reaction [4,26]. Nevertheless, to quantify the amount of protein adsorbed to the channel walls, the channel was flushed with pure water after each experiment and a fluorescence image with the same camera setting was taken. These images showed no significant fluorescence emission at all.

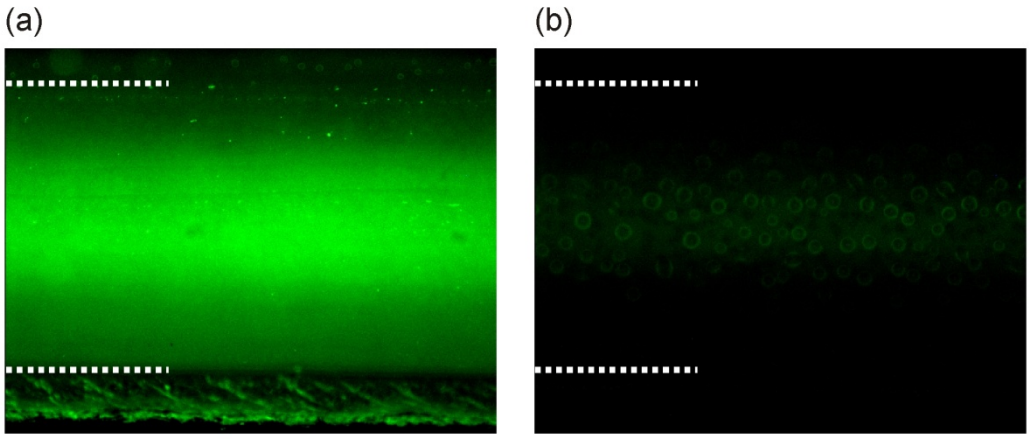


*Fig. 7-2: (a) Adsorption of BSA dissolved in pure water on a PMMA surface after a residence time of 30 min. Before taking this image the solution was already removed. Only after flushing the channel with a 0.5 M NaOH solution most of the molecules were removed (b). The image, which was taken after the flushing, also includes some left water droplets.*

Additionally and since the chips were reused, the channel network was flushed with a 0.5 M NaOH solution and placed into an ultrasonic bath for at least two minutes after each usage in order to remove possible adherent proteins. To remove further organic residua the channel network was flushed with pure water and placed again into an ultrasonic bath containing isopropanol for two minutes. Cleaning experiments using, for example, proteinase K or other kinds of solvents did not lead to satisfying results. As an explanation, proteinase K is an enzyme which is commonly used in molecular biology to digest proteins and to remove contamination from preparations of nucleic acid. As PEG almost suppressed protein adsorption the possibility of surface reduction by channel smoothing has not been considered. But it has been shown by Pinzón Caballero that milled polymeric surfaces can be smoothed by solvents in a simple way [162].

## 7.2 Electrodes

As described in chapter 6.5, two possibilities for integrating the electric field into the chip have been examined. Hence, in the following sections the manufacturing and assembly of two different chip designs are described in more detail. In the first case the electrodes have direct contact to the analyzed liquid. Accordingly, two plane electrodes have to be integrated into the microfluidic chip. They need to be placed, disconnected from each other, on opposite channel walls. For the second design the electrodes are decoupled from the main channel in order to prevent bubble generation inside the channel network. Here, the manufacturing can be divided into two sub-strategies since two different materials, dialysis membranes and hydrogels, have been used as ion bridges.

### 7.2.1 Integrated Electrodes

Since not all metals are resistant to corrosion or oxidation only noble metals come into consideration. Thus, mainly gold has been used as electrode material. The main challenges of realization can be divided into the selective deposition of two electrodes onto two opposite narrow channel walls and the separate contacting of the wall electrodes, cf. Fig. 7-3.

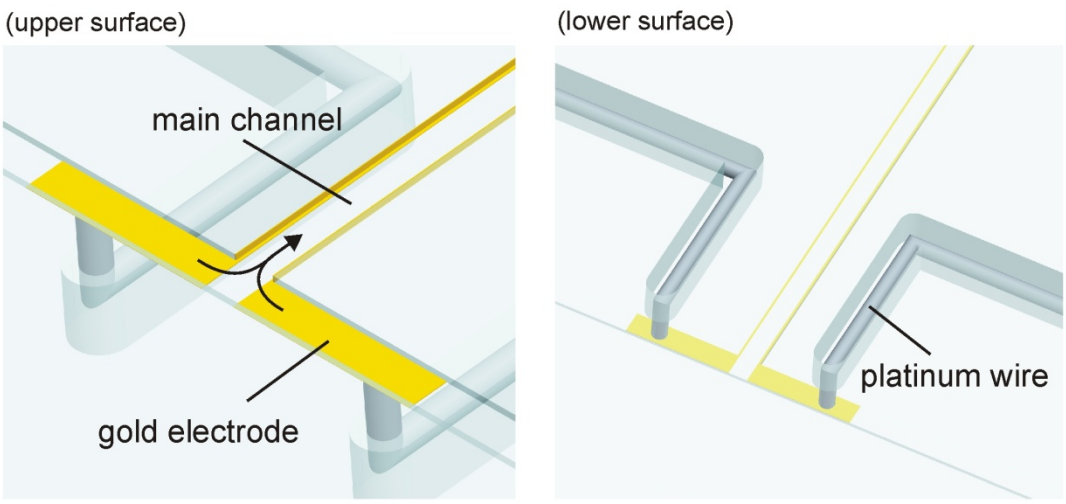


*Fig. 7-3: Drawing of gold electrodes integrated into a microchannel. The two inlets join each other passing into the main channel. The gold electrodes are connected from outside by two platinum wires from the opposite site of the chip.*

#### 7.2.1.1 Fabrication Process

Although gold can be easily deposited onto PMMA or COC surface by physical vapor deposition, only the gold layer deposited by sputtering on COC has passed the scotch test whereas no interface layers are necessary. The fabrications steps are schematically shown in Fig. 7-4. In the first step the chip was mounted on a 5' Si wafer and a small layer of photoresist (Clariant, Germany) was deposited on the chip surface. The protocols for different types of photoresist are summarized in Table 7-2. In all cases a final hard bake has been omitted. Subsequently, only those parts of the main channel have been milled which were intended to be sputtered with gold. In this process also the previously integrated wires were cut, now being part of the channel walls.

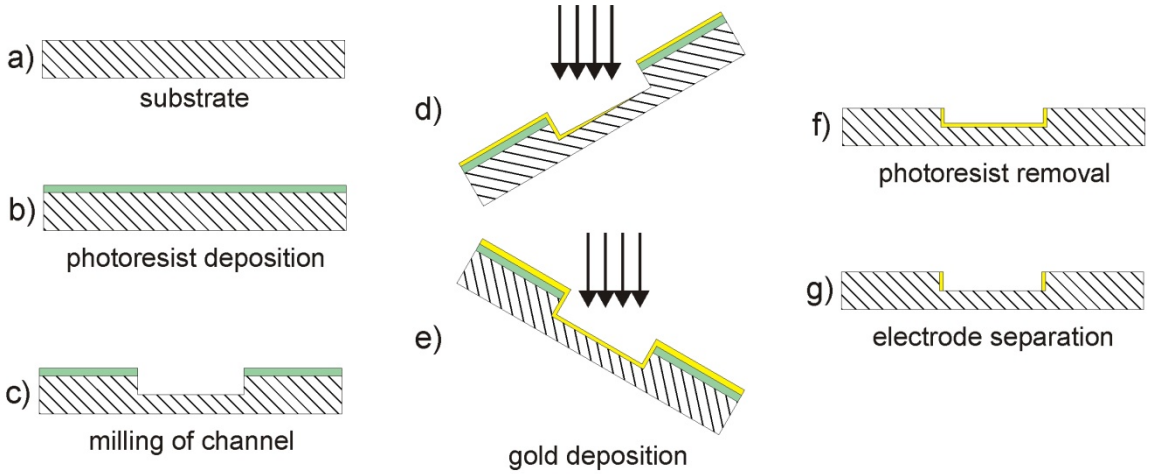


*Fig. 7-4: Fabrication steps of integrated gold electrodes.*

| | AZ 1512 HS | AZ 6632 | AZ 4562 |
|---|---|---|---|
| Layer Thickness | 1.2 µm | 5.8 µm | 12.5 µm |
| Parameters | 4600 RPM /25 s | 1200 RPM /25 s | 1500 RPM /25 s |
| Softbake (Hotplate) | 100 °C / 1 min | 100 °C / 1 min | 100 °C / 1 min |
| Gold Removal | < 3 min acetone bath | < 25 min acetone bath and 1 min US-bath | experiment abort |
| Results | ++ | + | – |

*Table 7-2: Process parameters and resulting layer thickness of different used photoresist. The use of AZ 1512 HS photoresist allows a very good gold removal with sharp edges.*

The sputtering was done by a mini deposition system (MED 010, Oerlikon Balzers, Lichtenstein). On a flat surface a sputtering rate of $r_{0°}$ = 0.47 nm $s^{-1}$ for gold was determined (process parameters: gold target, 50 mA, 6-8·$10^{-2}$ mbar). To ensure that the whole surface of the vertical walls gets covered with gold, the chip was first rotated $\alpha$ = 45° around the longitudinal direction of the main channel and sputtered for 300 s. Then the chip was rotated 90° in the opposite direction and sputtered again for the same period of time. Due to the angled position, the surface area of the vertical wall with regard to the position of the sputter target is increased by *cos α*. Accordingly, the sputtering rate of a flat surface is reduced by the same value leading to $r_{45°} = \cos\alpha \cdot r_{0°}$ , and the sputtering rate finally becomes $r_{45°}$ = 0.33 nm $s^{-1}$. The calculated layer thickness is about 100 nm. But undirected coating methods, such as sputtering, have the effect that the regions under the undercut are also covered with gold. This often leads to layers thicker than calculated. After sputtering the photoresist was removed in an acetone bath partially supported by ultrasonic. The best results were obtained by the thinnest photoresist layer which enables a complete removal of unwanted gold layers and sharp edges, cf. Fig. 7-5 and Table 7-2.

During the sputtering process also the channel bottom is covered with gold which was subsequently removed by laser ablation. In a final structuring process the missing channels and through holes were milled. A closed channel network was obtained by sealing the substrate as described in chapter 7.3.

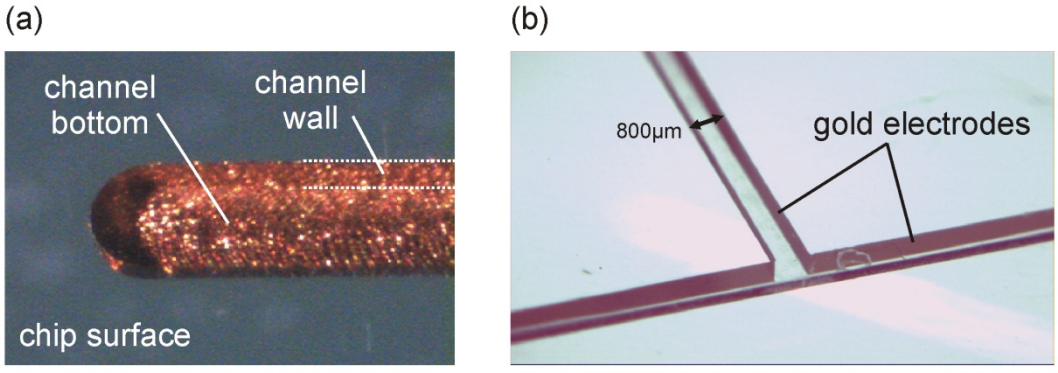


*Fig. 7-5: (a) Gold surface after photoresist removal with sharp edges with regard to the COC chip surface. (b) Test channel structure after electrode separation by laser ablation.*

As mentioned above, for electrical connection also interlayer connections have been integrated into the polymer chip. These connections are small wires which pass the chip in vertical direction. Another possibility are electrode structures at the same side of the chip as the main channel, like conducted passes known from printed circuit boards. But this latter solution has at least disadvantages. To connect the electrodes, which are deposited on the vertical channel walls, the conducted pass has to overcome sharp corners of ninety degrees. Additionally, contact durability can not be guaranteed after the application of pressure during the channel sealing process, since the gold layer thickness is only a few hundred nanometers thick. Furthermore, for the sealing process specific solvents are used. In this context it has been observed that the solvents used for bonding itself affect the gold layer leading to numerous small cracks, cf. Fig. 7-6. Hence, contact durability can not be ensured again.

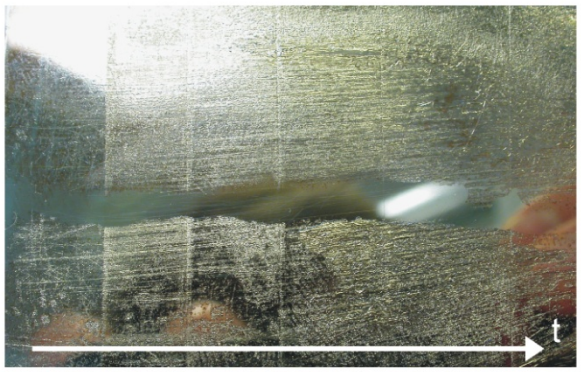


*Fig. 7-6: Gold surface on COC after treatment by bonding solvent. With increasing residence time (up to 60 sec.) the number and intensity of small cracks increases. The centre of the chip remains untreated.*

The interlayer connections have been realized in three different but comparable ways. And their manufacturing has been integrated into the gold layer deposition process. After drilling a hole, a platinum was positioned and fixed in this hole by glue, cf. Fig. 7-7a and Fig. 7-7b, or dissolved COC material, cf. Fig. 7-7c. During the following milling step, parts of the wiring got cut and thereby the bare surface was also subsequently covered with gold which led to an electrical connection through the chip.

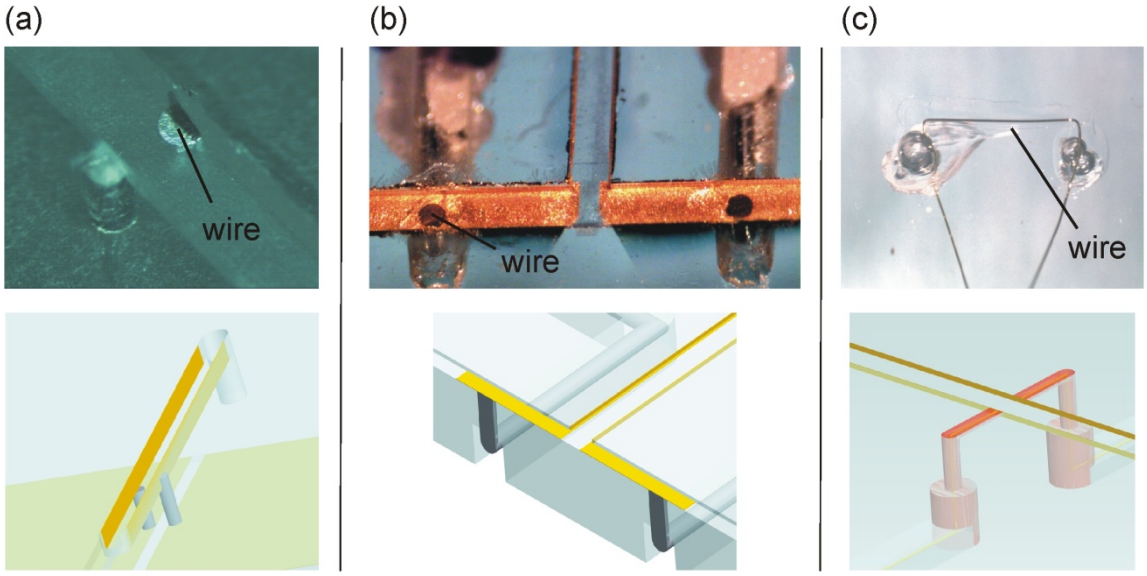


*Fig. 7-7: Possible connection solutions. In all cases a through hole including a wire helps connecting the chip from the opposite side. The wires are cut during the milling of the channels and covered with gold afterwards.*

For most experiments the chip connection type (b) was applied. The channel dimension of the main channel is 600 x 100 µm (w x h) and the complete chip is shown in Fig. 7-8.

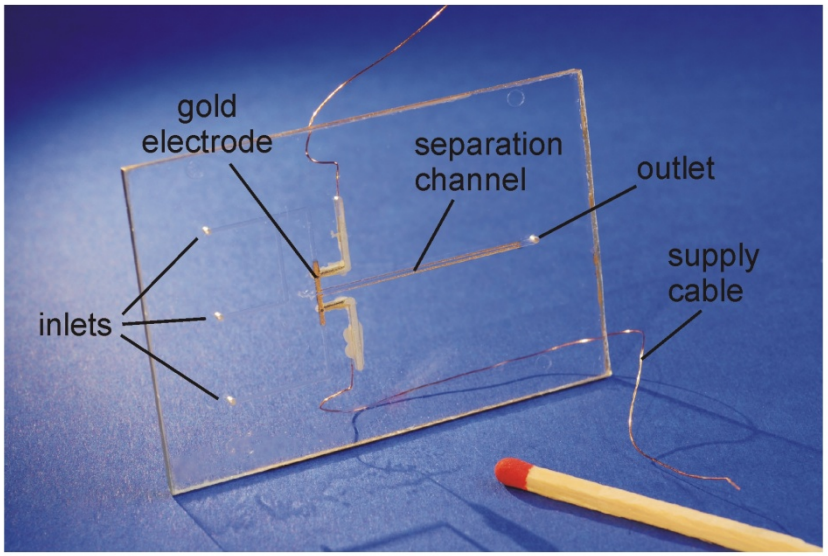


*Fig. 7-8: Test chip with integrated gold electrodes.*

### 7.2.2 Decoupled Electrodes

All experiments using electrodes in direct contact to the test medium, i.e. the electrodes are deposited on inner wall surfaces, are restricted as the maximum voltage that can be applied to such electrodes is limited by the threshold value of electrolysis. By crossing this value, bubbles are generated which block the microchannel and interrupt the experiment. As described in chapter 9.2.1, this problem can be resolved by using the fact that the

electrochemical reactions at the electrodes and the corresponding transport processes are characterized by certain time constants. For a voltage pulse above the threshold voltage but for a shorter time period the electrode reactions are largely suppressed. Thus, a pulsed electric field allows a larger driving force for electrophoresis than possible in dc mode. But besides the increasing of the electrophoretic transport of the molecules this proceeding has further effects like phase instabilities and mixing processes [163-169].

The electric field strength can also be effectively increased by a fluidic decoupling of the main channel and the electrodes. When applying a dc voltage above the threshold value of electrolysis, still bubbles are created, but these can simply escape from the system. The principle for such a decoupled system is sketched in Fig. 7-9. The side walls of the main channel are made from a material, like a dialysis membrane or gel, e.g. agarose or polyacrylamide, which serves as an ion conductor, but decouples the channel from the electrodes.

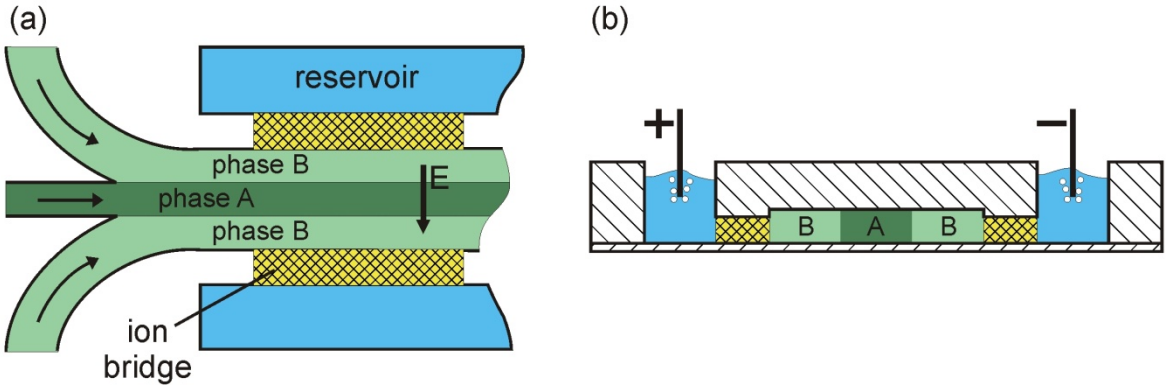


*Fig. 7-9: (a) Schematic of the chip design with decoupled electrodes. Here, the microfluidic chip comprises a main channel with three inlets. Phase A is sandwiched between phase B. The electric field is oriented perpendicularly to the lamellae. (b) Cut perpendicular through the microchannel showing the reservoirs and the main channel in the center.*

On both sides of the channel the electrodes are placed in large buffer reservoirs which are open to the environment. The ions in the buffer reservoirs can diffuse into the gel matrix, thus ensuring that the electric field is guided from the electrode in the buffer reservoir through the ion bridge, further across the microchannel, through the ion bridge on the opposite site to the second reservoir and electrode. In that way an electric field perpendicular to the interface between two immiscible aqueous phases can be applied. Bubbles which are created by electrolysis can escape from the system and do not interfere with biomolecule enrichment or separation processes. Since the depth and the volume of the buffer reservoirs are much larger than the main channel, most of the voltage drop should occur in the channel and in the ion bridge network. Decoupled electrodes allow very high electric field strengths which can be applied perpendicular to fluid interfaces. As discussed later in chapter 11, in a number of experiments, the bilaminated PEG-dextran system could typically withstand voltages of about 10 to 15 $V_{dc}$ (>800 V $m^{-1}$) depending on the concentration and molecular weights of the used polymers. Furthermore, it was observed that undulations of the phase boundary occur for voltages and field strengths above the stated values, see chapter 9.3.3. However, this poses no severe limitations to most of the experiments performed, because at these voltages already a considerable electrophoretic motion of the biomolecules is observed. Hence, the setup with decoupled electrodes turns out to be a major improvement over the system with electrodes

integrated inside the channel. With such an increase of the driving force for electrophoretic transport a thorough study of biomolecule motion in a broader parameter range was finally enabled.

#### 7.2.2.1 Membrane

One possibility, which was also investigated in this study, is to decouple the flow inside the main channel from the electrodes by membranes that are permeable for the buffer ions but not for small biomolecules, like proteins. Therefore, dialysis membranes have been integrated into the polymeric chip acting as a part of the channel wall, cf. Fig. 7-10. Beginning inside the main channel, ions are guided through the dialysis membranes on both sides into intermediate reservoirs which are again connected to the main reservoirs where the electrodes are placed in.

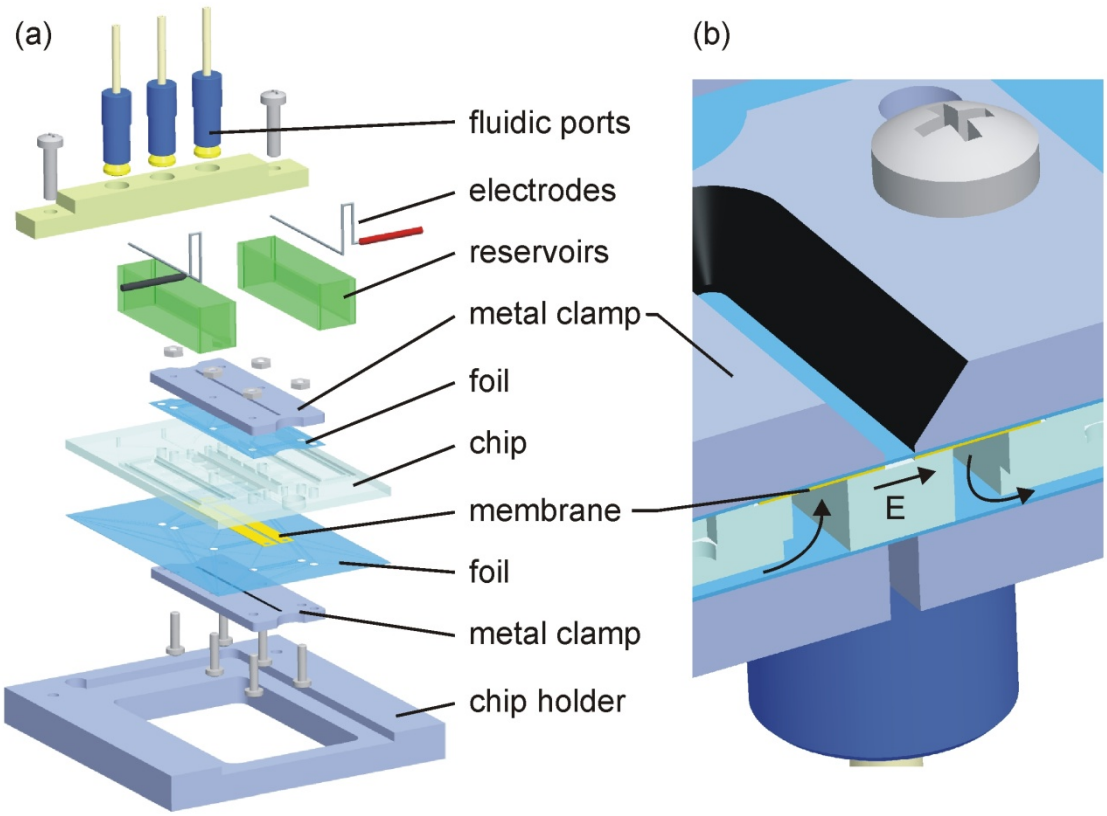


*Fig. 7-10: (a) Components of the membrane setup. (b) The dialysis membrane is pressed onto the chip by a metal clamp. The electric field is guided from the one reservoir through the dialysis membrane, perpendicular to the main channel and back through the membrane towards the opposite reservoir. The frame of the metal clamp is painted black in order to reduce reflections.*

The dialysis membranes have been manufactured by laser treatment as well as by micro milling. In case of the latter one, the untreated membrane has been completely sandwiched between two polymeric chips for stability purposes. The silhouette of the membrane was first milled into the upper chip. Afterwards, the milling was stepwise continued until the depth of the membrane was nearly reached. During the next milling increment not only the membrane was cut but also the chip below allowing a clean cut of the membrane itself. Fig. 7-11 shows the milling results of a Nadir® membrane (cellulose hydrate, MWCO 10-20 kDa, 5101.01,

Carl Roth GmbH & Co. KG, Germany). By comparing the cutting edges of the two manufacturing principles, the edges of the milled membrane are generally smeared due to the rotating milling cutter. Oppositely, in case of laser treatment the membrane edges with its containing pores are largely intact. Both types of membranes show a working ion transport but the laser treated membranes have been preferably used.

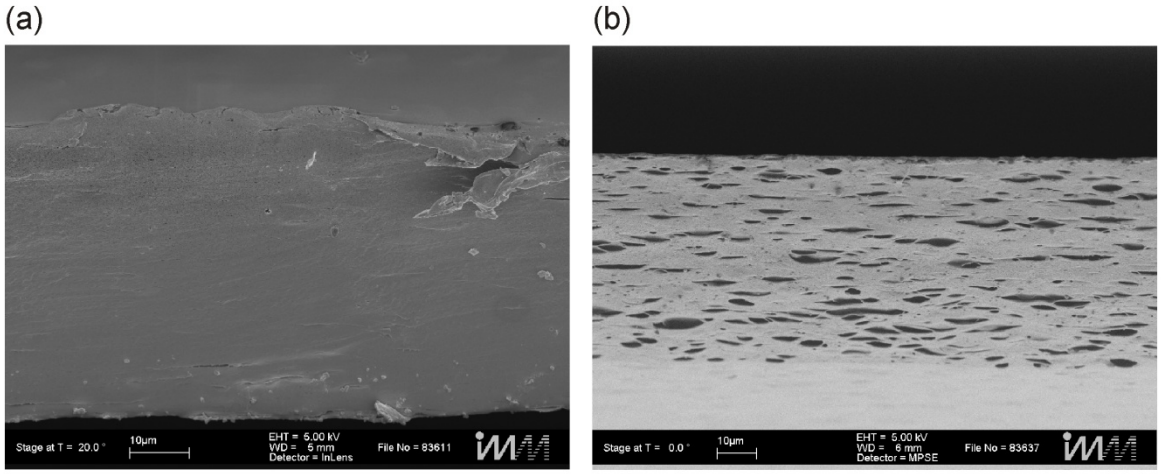


*Fig. 7-11: (a) Milled Nadir® dialysis membrane of 45 µm thickness. (2) The same dialysis membrane, but instead of milling laser ablation was applied for shape forming. The outer pores are still intact.*

The assembly of the chip incorporating membranes is illustrated in Fig. 7-12. In order to reach a high positional accuracy of the membranes, the chip was initially equipped with dowel pins ensuring a fixed position. Subsequently, the position of the membranes is set by an adhesive tape comprising microcapsules, cf. chapter 7.3, and the pins are removed piece by piece. Since there is still a small gap between the membrane and the chip, the membrane itself is now used for the sealing of the main channel since it is pressed onto the chip surface by an additional metal clamp, cf. Fig. 7-10.

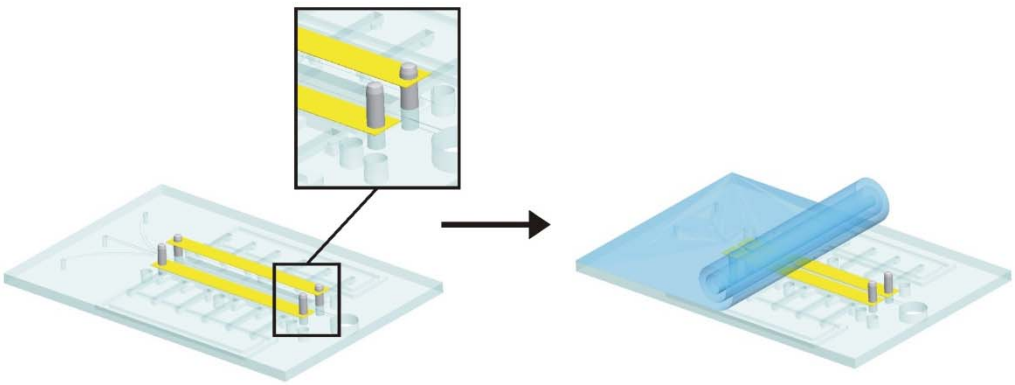

*Fig. 7-12: Assembly of dialysis membrane chip with the help of dowel pins leading to high positional accuracy.*

During the next step the chip is prepared for the final transport experiments. Therefore the intermediate and main reservoirs are filled with the desired buffer. Once the buffer has reached the membrane surface the buffer liquid penetrates spontaneously into the membrane due to capillary forces. The membrane swells inducing an additional sealing effect, cf. Fig. 7-13. Because of the small nanopores most of the applied electric field is expected to be dropped over the membrane. Unfortunately, it was also observed that the small pores lead to a strong electroosmotic flow disturbing the lamellae arrangement of the two-phase system (discussed in chapter 9.3.1). For that reason most of the transport experiments were carried out with decoupled electrodes made of gel.

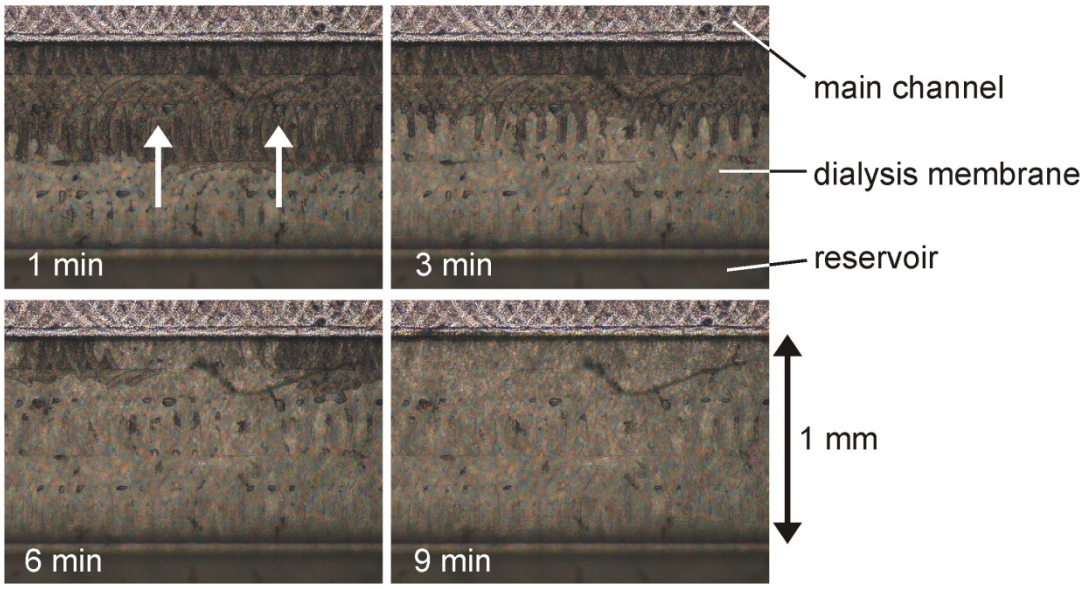


*Fig. 7-13: Penetration of buffer solution into the matrix of a Nadir® dialysis membrane. Within approximately 9 minutes the matrix is completely filled and due to additional swelling the gap between reservoir and main channel is definitely sealed. Here, for better visibility the metal clamps are replaced by polymer clamps.*

#### 7.2.2.2 Gel Bridge

Instead of a membrane the electrodes and the main channel can also be fluidically decoupled by hydrogels. For this purpose the channel was equipped with perforated walls where the gaps are filled with a gel matrix. The final design of the microfluidic chip is shown in Fig. 7-14 and Fig. 7-15. With such type of chip most of the active transport experiments have been performed. The chip comprises a main channel with up to five inlets, two buffer reservoirs on both sides of the channel and comb-structured side walls with gaps, which allow a fluidic decoupling of the buffer reservoirs from the channel. Before an experiment is performed, the wall gaps are filled with an agarose gel matrix (05068, Sigma-Aldrich, Germany). Capillary forces are utilized to prevent the gel precursor from penetrating into the main channel.

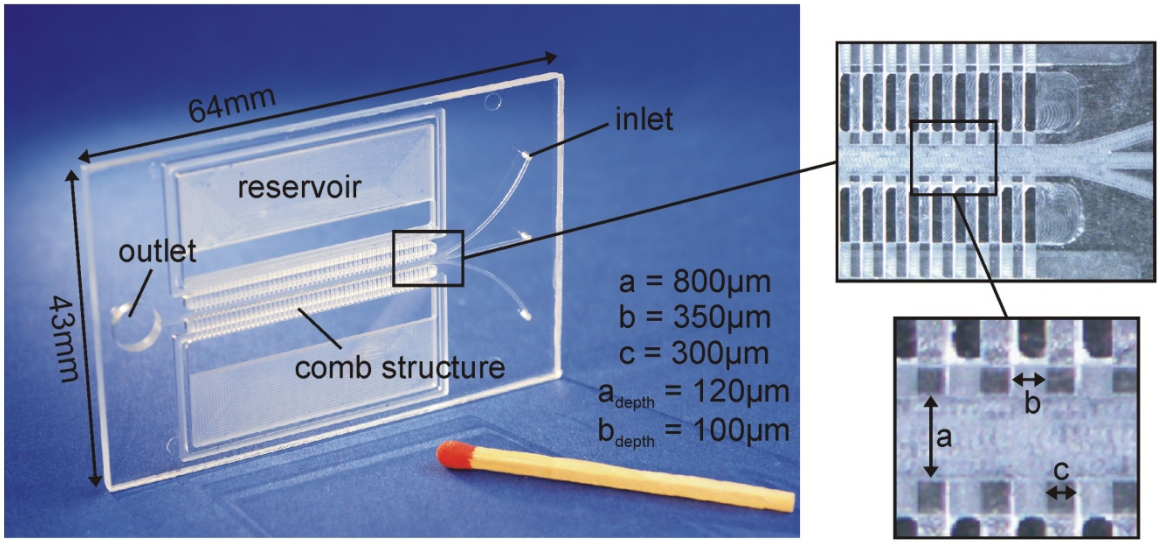


*Fig. 7-14: Microfluidic chip incorporating a comb structure that is later filled with a gel matrix. During transport experiments, the chip is equipped with additional reservoir walls and electrodes.*

Therefore, the channel walls of the fifty gel gaps are pre-coated with PEG by dynamic coating in order to locally reach a more hydrophilic channel surface compared to the main channel. Subsequently, the reduced contact angle leads to an accelerated filling of the agarose gel due to increased capillary forces. This is essential since every gap has to be filled completely before the agarose gel starts to solidify. The gel point of agarose lies between 34-37 °C.

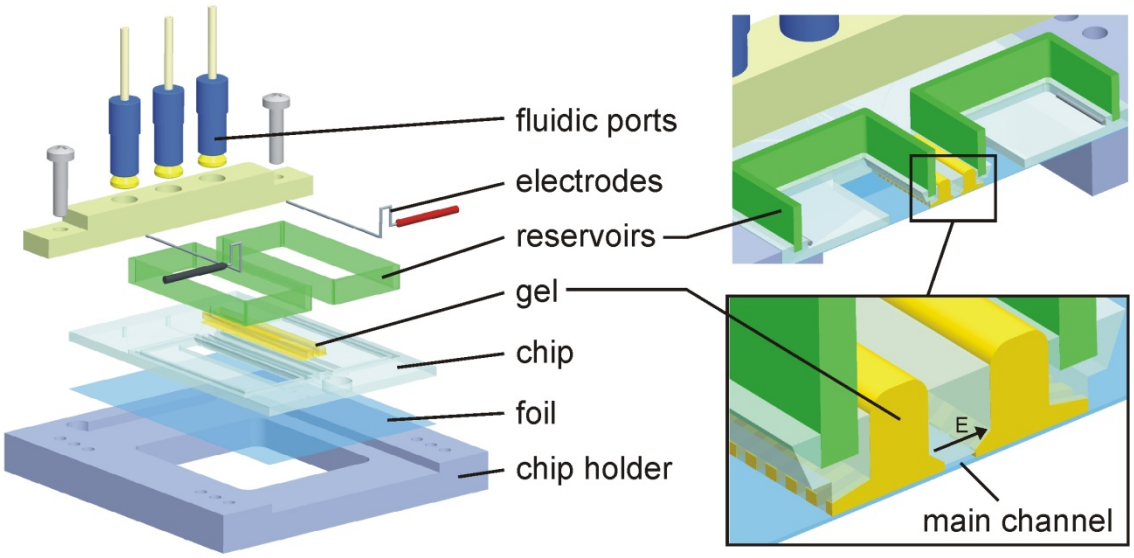


*Fig. 7-15: Components of the microfluidic setup. Instead of a membrane, gel acts as an ion bridge guiding the field perpendicular to the flow direction from one reservoir, through the main channel, into the opposite reservoir.*

This is the temperature at which an aqueous agarose solution forms a gel as it is cooled down. Furthermore, an agarose solution exhibits hysteresis in the liquid-to-gel transition, thus its gel point is much lower than its melting temperature.

In the first step of the gel filling process the chip is temporarily sealed by conventional adhesive tape. A 2.0 wt% PEG 8000 solution is injected into the gel gaps at room temperature and selectively distributes by capillary forces, cf. Fig. 7-16. It is imperative that all fifty gaps are completely wetted with the coating solution as well as no coating solution enters the main channel. This guarantees an adequate gel filling afterwards due to an abrupt change in wettability between the gaps and the main channel. The key to such an 'organized' filling lies in the channel geometry of the comb structures. The openings to the main channel and to the reservoirs act as geometrical passive stop-valves forcing the liquid to wet only those surfaces which need to be coated. Accordingly, the coating solution (or later the agarose solution), which is placed at the inlet slit by using a pipette, is drawn inside the microchannel by capillary forces and stops at the stop-valves. A short description of the functionality of the stop structures is given in a subsequent paragraph.

After approximately three minutes the PEG solution and the adhesive tape are removed. For drying, the gaps are flushed with nitrogen. After a final sealing of the channels a 1.5 % agarose solution is heated up to 100 °C and filled into the gaps of the comb structure from the backside of the chip. Again, driven by capillary forces the gel solution flows towards the main channel and stops at the openings to the channel which act as barriers for hydrophilic solutions, cf. Fig. 7-17. The comb structures on the opposite side are connected to reservoirs on the backside of the chip which, after the agarose solution has gelled, are filled with the same buffer as used for preparing the two-phase system.

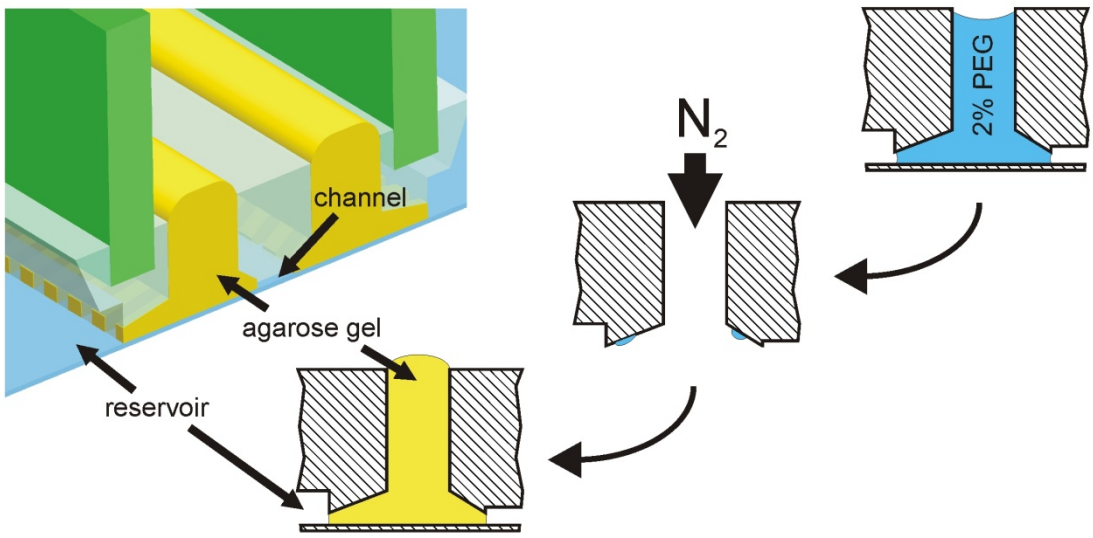


*Fig. 7-16: Gel filling process. In the first step a PEG solution is introduced into the channel network in order to improve the hydrophilicity of the surface. After drying the network is filled with a gel matrix acting as an ion bridge.*

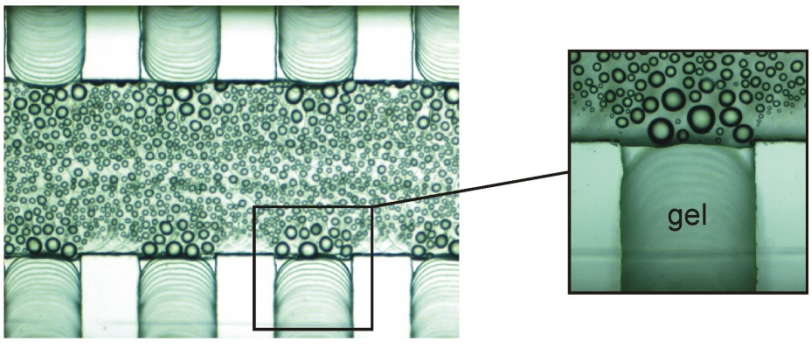


*Fig. 7-17: Main channel directly after gel filling. Due to the hot gel inside the comb structure water condensed at the main channel surface (small droplets).*

In this paragraph the principle of a fluidic and passive stop structure is outlined. It is assumed that the solution was already placed at the inlet hole and that the liquid interface in the rectangular channel is driven towards an abruptly diverging section as shown in Fig. 7-18. When the liquid meniscus is still located in the straight section of a rectangular channel, the pressure difference between the pressure inside $P_I$ and outside the liquid $P_0$ under equilibrium is given by the Young-Laplace equation

$$\Delta P = P_0 - P_I = -2\gamma \cos\theta \left(\frac{1}{w} + \frac{1}{h}\right) \qquad (7.1)$$

where $w$ and $h$ are again the width and the height of the channel, respectively [170-172]. Due to Eq. (7.1) and in case of a hydrophilic surface, $\theta < 90°$ ($\theta_{H2O} \approx 75°$ on PMMA), the pressure inside the liquid and near the meniscus will be lower than the surrounding atmospheric pressure $P_0$. The resulting pressure gradient $\Delta P_A$ drives the liquid through the straight microchannel.

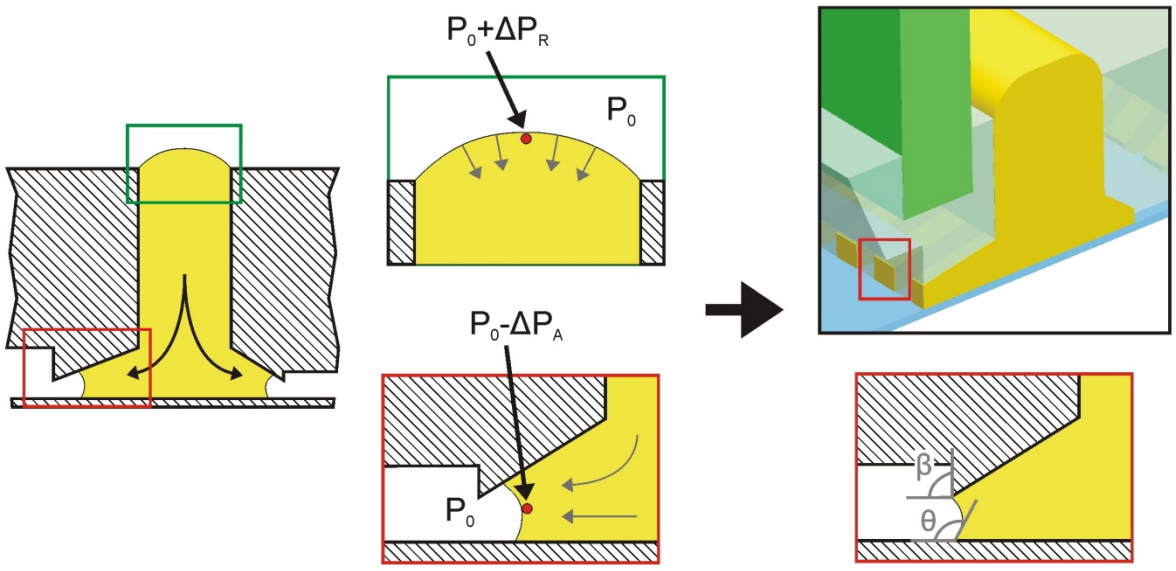


*Fig. 7-18: Filling of the comb structure. The abruptly expansion of the channel acts as a stop structure allowing a defined and easy filling.*

This capillary filling will be supported by a contrary pressure drop $\Delta P_R$ across the meniscus at the inlet, driving the fluid in the same direction. When the liquid reaches the expansion, cf. Fig. 7-18, the meniscus has a contact angle of $\theta$ with the channel wall in equilibrium. In order to drive the liquid forward, the applied pressure difference must be sufficient to force the meniscus to achieve the same wetting angle $\theta$ with the diverging wall. In contrast to the stop structure presented here, in microfluidic chip systems one often encounters the situation that only the width of a rectangular channel increases while the height stays fix, i.e. the curvature of the liquid interface stays the same in the height, while the curvature is changed for the width. Accordingly, the pressure required to drive the liquid forward can be expressed by

$$\Delta P_F = -2\gamma \left( \frac{cos\,(\theta + \beta)}{w} + \frac{cos\,\theta}{h} \right) \qquad (7.2)$$

where $\beta$ is the diverging angle [170,172]. It has to be considered that for very shallow channels the wettability of the top and bottom may dominate the behavior. That means that in case of a hydrophilic system a sudden expansion of a shallow channel may not work as a passive stop valve as the total energy may be further reduced by filling the expansion-cavity. Hence, in this study the channel expansion is equipped with an additional step in channel height obtaining a higher value of $\Delta P_F$ avoiding an unwanted capillary filling of the main channel. Additionally, due to PEG coating and the reduced contact angle not only the filling velocity for the agarose solution is increased but also the 'strength' of the stop structure, cf. Eq. (7.2).

However, independent from the kind of ion bridges, membrane or gel bridge, the integrated buffer reservoir of approximately 300 µl has to be expanded to guarantee a stable pH value during transport experiments, see chapter 9.3.4. Therefore, an additional PDMS element (Sylgard 184 silicone elastomer kit, Sasco Holz Frankfurt GmbH, Germany) was molded and simply attached to the chip by pressing it into a small slit. This leads to an increased reservoir volume of 3000 µl.

## 7.3 Sealing of Channel Network

Often the sealing of channels is a critical step in micro fabrication. For example, voids or gaps lead to capillary effects which cause unwanted loss of material. Additionally, it is also important to establish a pressure-tight bond between chip and cover which does not distort the cross section, e.g., by channel deformation or sagging of the cover lid after the sealing process. Especially for chips used in a bioanalytical context, the compatibility of the material with chemicals and biomolecules of the assay has to be ensured. For polymeric microfluidic devices a variety of suitable bonding methods have been used, including solvent bonding [173,174], thermal bonding [175,176] or bonding processes based on surface treatments by, e.g., oxygen plasma or ultraviolet-ozone [177-179].

In this study two different bonding processes, solvent and adhesive bonding, have been applied. For solvent assisted bonding the chip substrate and the cover foil should consist of the same or similar material. A suitable solvent is spin-coated on the foil (for PMMA chips: PMMA XT foil, Cadillac Plastic GmbH, Germany / for COC chips: COP 1420R foil, Ibidi GmbH, Germany). Afterwards the foil is pressed onto the polymeric chip at isothermal conditions leading to a channel sealing of high bonding strength paired with minimal mechanically induced deformation of the channel cross section.

Another method which was often used in this study for chips with decoupled electrodes is sealing by adhesive tape. The application of adhesive tape is advantageous since the sealing

process is less time consuming and the foil can be removed after usage. Hence, the channel network can be easily cleaned after experiments allowing the application of the chips for several times. In this connection it was observed that conventional adhesive tape (here Scotch® clear packaging tape E5020D, 3M, Germany) has to be used with special care. The whole surface of the tape is usually covered with adhesive agents and thus a specific amount of agents is always exposed to the liquid which is driven through the channel network. Ingredients of the adhesive agent may dissolve and influence the composition of the test liquid, as observed for the PEG-dextran two-phase system under investigation. Although the two liquids are immiscible the phase boundary between them vanished within a specific time span after they get in contact. Such a behavior was not observed using solvent assistant bonding processes. To avoid those problems and still benefit from the advantages of temporarily sealing an adhesive tape consisting of microcapsules (polyolefin adhesive tape, 3M, Germany) was applied. The pressure sensitive tape allows the adhesive to release from small microcapsules, a few µm in diameter, only when pressure is applied causing a rupture of the capsules. Accordingly, the adhesive agents are placed in areas where the chip and the foil get in contact. Only an insignificant small amount of adhesive ingredients is exposed to the liquid close to two channel corners which allows keeping the composition of the liquid constant. As comparable to solvent bonding the adhesive tape is pressed on the polymeric chip at isothermal conditions and the sealed chip can be used immediately and placed in the chip holder.

# 8 Aqueous Two-Phase Flow

*One important parameter governing the hydrodynamics of a bilaminated flow is the interfacial tension between the two liquid phases. Systems with a very large interfacial tension tend to become unstable when they are bilaminated inside a microchannel, whereas systems with a small interface tension usually have less stability problems, but consist of components which are physico-chemically more similar. For systems consisting of two immiscible phases of aqueous solutions of PEG and dextran, the interfacial tension becomes small compared to aqueous-organic two-phase systems allowing high flow stability and regular flow patterns within microchannels.*

## 8.1 Flow Patterns and Flow Stability

Attempting to study the electrophoretic or diffusive transport of sample molecules orthogonal to the phase boundary, it is important to hold the flow velocity of the liquids in the channel sufficiently small. Only this guarantees entirely detectable transport processes across the channel width while the samples flow through the main channel. Alternatively to the continuous flow configuration, for the examination of the diffusive transport across the phase boundary, a stopped flow configuration with vanishing liquid velocity was applied, as described in chapter 10. By realizing this configuration, problems initially occurred since the more viscous phase displaces the less viscous phase from the channel when the flow was switched off. These problems could be traced back to fluidic capacities in the feeding system upstream of the test device. Accordingly, the problems could be considerably reduced by using glass syringes and tubes as well as connections commonly used in HPLC as described in chapter 6.3. However, avoiding capacities is generally important since the minimization of fluidic capacities in the feeding system becomes essential for stable flow patterns, especially when flow rates are varied and lamellae are removed or additionally introduced.

As described in chapter 5, the flow behavior of two immiscible fluids in microchannels mainly depends on the interplay between the wetting behavior of each fluid on the surface, the interfacial tension between the fluids, the channel geometry and flow velocities. Although aqueous two phase systems show low interfacial tensions (typically values for the systems under investigation are in the order of $10^{-4}$ N m$^{-1}$ [180]), the resulting flow patterns in microchannels may become unstable. As an example, in Fig. 8-1 a flow pattern of a PEG- and dextran-phase is shown which initially consists of two parallel lamellae. The channel dimension is 300x200 µm (w x h) and the flow velocities are in order of a few mm s$^{-1}$. Nevertheless, the dextran-phase detaches from the wall and penetrates into the center of the channel. This behavior can be initiated by different effects. First of all, differences in the wettability leads to a contact angle dextran-phase/PEG-phase/PMMA of considerably more than 90° (contact angle instrument G-1, Krüss GmbH, Germany). This implies a curved phase boundary and also a detachment of the dextran-phase from the walls. Since the PEG-phase shows a lower contact angle on PMMA compared to the dextran-phase, this status is energetically more favorable. The further movement into the center of the channel can be described by the tendency to minimize the overall energy of the system. For illustration of such behavior and to present the two-phase flow velocity profile, in the subsequent section some basic theoretical aspects are discussed.

The laminar and steady-state flow through microchannels is also known as a Hagen-Poiseuille flow. Here, the fluid is driven through a long, straight, and rigid channel by imposing a pressure difference between the two ends of the channel [181].

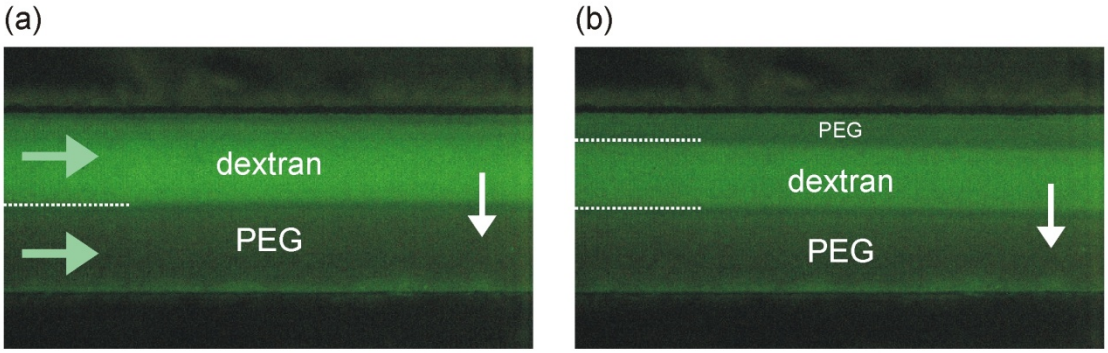


*Fig. 8-1: Flow pattern of a PEG- and dextran-phase in an almost rectangular channel. (a) The dextran- and PEG-phase were separately injected into the main channel. (b) After approximately 10 mm the dextran-phase observably starts to detach oneself from the upper wall, see right arrow.*

Originally developed for channels with circular cross-sections the analytical description of the flow behavior can also be adapted to channels having different cross-sectional shapes, e.g., rectangular cross-sections. Due to the large aspect ratio of many microfluidic channels, the geometry can be simplified and approximated by parallel plates [181]. Within such an approximation the flow is governed by the one dimensional stokes equation

$$\partial_z^2 u_x(z) = -\frac{\Delta p}{\eta L_{cl}} \tag{8.1}$$

with no slip boundary conditions at the walls. The solution of the differential equation is a simple parabola, cf. Fig. 8-2:

$$u_x(z) = \frac{\Delta p}{2\eta L_{cl}}(h - z)\, z \tag{8.2}$$

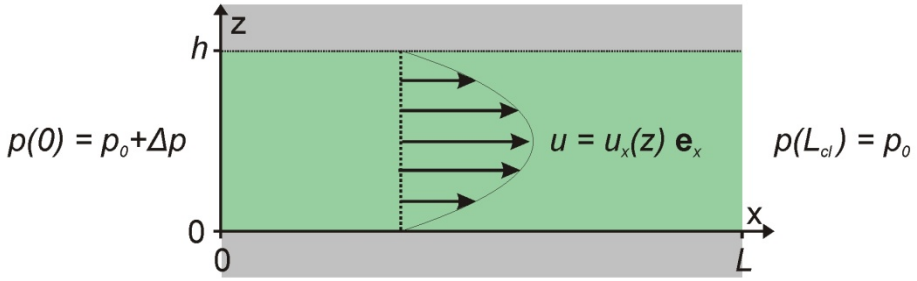


*Fig. 8-2: Due to a pressure drop $\Delta p$ over the channel length of $L_{cl}$ the fluid flows in x direction exhibiting a parabolic flow profile inside the microchannel.*

In case of a two-phase Poiseuille flow a steady-state flow of two different liquids with a flat interface at $z = h_i$ is assumed as shown in Fig. 8-3. Accordingly, in this case no Young-Laplace pressure arises across the interface. The liquids are driven by a pressure drop of $\Delta p$ and the viscosities of the bottom layer, $0 < z < h_i$, and of the top layer, $h_i \leq z < h$, are denoted by $\eta_1$ and $\eta_2$, respectively. Additionally, the system is assumed to be translation invariant along the $x$ and the $y$ axis leading to a velocity and pressure field in the form of

$$\mathbf{u} = u_x(z)\boldsymbol{e}_x, \qquad 0 < z < h \tag{8.3}$$

$$p(x) = p_0 + \left(1 - \frac{x}{L_{cl}}\right)\Delta p \tag{8.4}$$

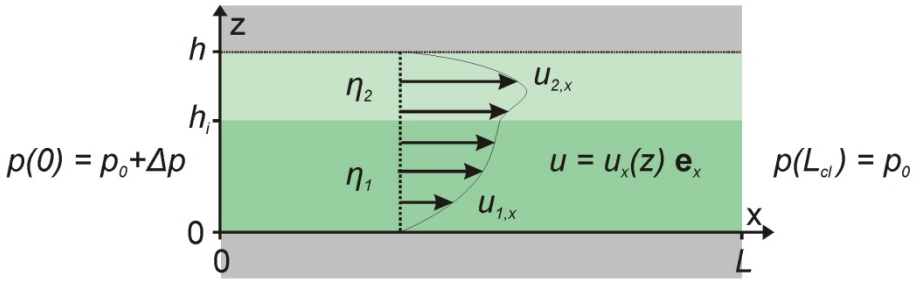


*Fig. 8-3: Flow profile of a two-phase flow with different viscosities of the phases, $\eta_1$ and $\eta_2$. The interface at $h_i$ is characterized by a flow profile transition.*

For a two-phase flow regime the velocity field $u_x(z)$ can be divided into $u_{1,x}(z)$ and $u_{2,x}(z)$:

$$u_x(z) = \begin{cases} u_{1,x}(z), & \text{for } 0 < z \le h_i \\ u_{2,x}(z), & \text{for } h_i \le z < h \end{cases} \tag{8.5}$$

In this simple model the boundary conditions for the velocity field are no slip at the walls and continuous velocity $u_x$ and shear stress $\sigma_{xz}$ at the interface $z = h_i$,

$$\begin{aligned} u_{1,x}(0) &= 0 \\ u_{2,x}(h) &= 0 \\ u_{1,x}(h_i) &= u_{2,x}(h_i) \end{aligned} \tag{8.6 a-c}$$

$$\sigma_{1,x}(h_i) = \sigma_{2,x}(h_i) \tag{8.7}$$

According to Eq. (8.2) for the single-phase Poiseuille flow velocity field and the above mentioned boundary conditions the expressions for $u_{1,x}(z)$ and $u_{2,x}(z)$ result in:

$$u_{1,x}(z) = \frac{\Delta p}{4\eta_1 L_{cl}}(a_1 - z)z \tag{8.8}$$

$$u_{2,x}(z) = \frac{\Delta p}{4\eta_2 L_{cl}}(h - z)(z - a_2) \tag{8.9}$$

where $a_1$ and $a_2$ are constants which especially consider the dependence on the last two boundary conditions describing the transition at the interface of the two phases.

At a given pressure drop and due to the further boundary condition that both liquid phases have equal flow rates, the position of the interface can be determined since it only depends on the viscosity ratio. Therefore the equation was solved with the program Mathematica 5.1 [182]. The viscosity $\eta_1$ stays constant. The resulting two-phase flow profile and the effect of decreasing viscosity ratio $\eta_1/\eta_2$ are schematically shown in Fig. 8-4a.

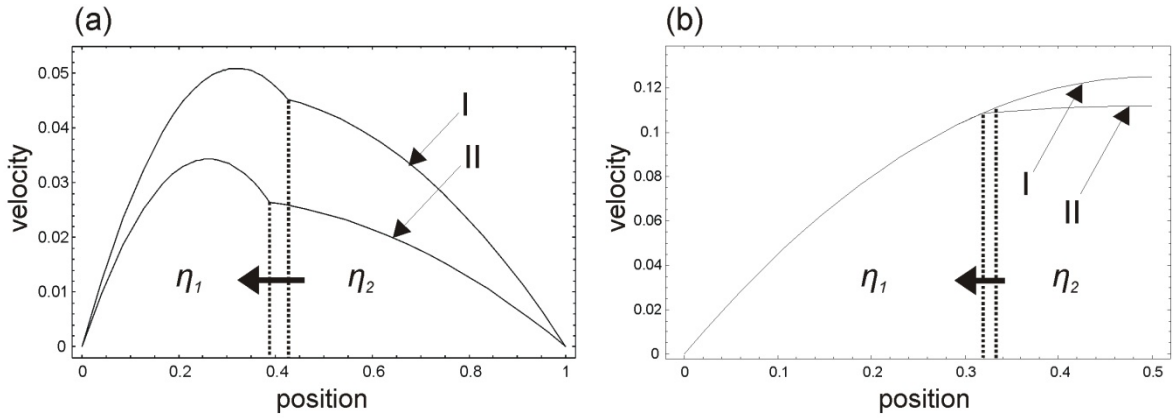


*Fig. 8-4: (a) Exemplary velocity profile of a two-lamellae arrangement across a channel width of 1. The liquid right from the interface (dotted line) has a higher viscosity than the left one. By increasing its viscosity, compared to the left liquid, also the required space increases (I → II). (b) Three-lamellae arrangement (only half channel is visible). I: equal viscosity; II: the viscosity of the centered liquid was increased by a factor of five.*

The decreasing ratio leads to a displacement of the interface position $h_i$ and to a strong reduction of the overall flow rate in case of a side by side flow configuration, cf. Fig. 8-5. Coming back to the above mentioned flow behavior of the dextran-phase lamella which, once detached from the wall, moves into the center of the channel, a flow pattern consisting of three lamellae was additionally examined for comparison. For the outer lamellae the viscosity is kept constant while for the center lamella the viscosity increases. For simplicity only one half of the channel height is calculated leading to a flow profile that is shown in Fig. 8-4b. The lamella of higher viscosity is positioned in the center of the channel.

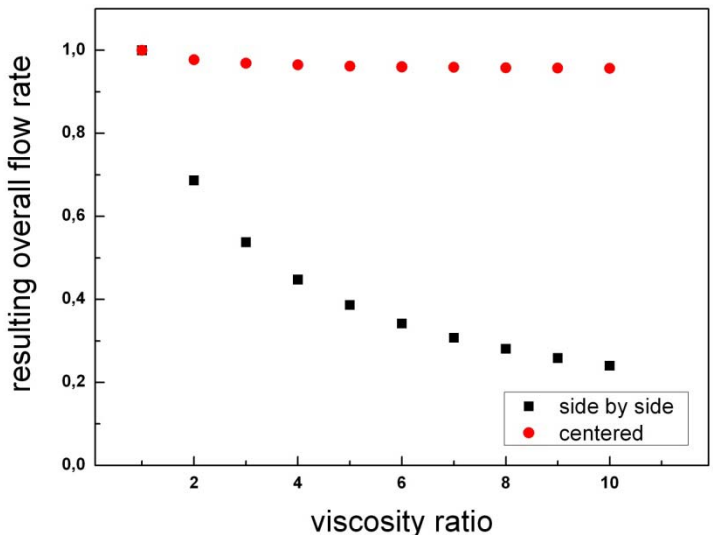


*Fig. 8-5: Comparison of the resulting overall flow rate for two different flow patterns.*

Accordingly, the shear rate within this lamella, given by

$$\dot{\gamma}_z = \frac{\partial u_x}{\partial z} \qquad (8.10)$$

is drastically reduced compared to a position near to the wall surface. Since the pressure drop stays constant and the resulting flow rates of both phases is defined to be equal, the increase of the viscosity ratio leads to a displacement of the interface position. But in contrast to the side by side flow configuration, the resulting overall flow rate decreases much slower with increasing viscosity ratio. Accordingly, a flow system energetically prefers to place the lamella of higher viscosity into the center of the channel, cf. Fig. 8-5. Additionally, this behavior is supported by another effect of energy minimization: a fluid of high viscosity surrounded by a fluid of low viscosity also prefers a centered position since the cross section of the fluid of high viscosity as well as the interfacial area between the two fluids are minimized. In the present case the dextran-phase has a much higher viscosity compared to the PEG-phase. As expected, in case of a detached dextran-phase lamella, a movement of the lamella into the center of the microchannel was observed, where the lamella was stabilized.

This simple flow model intends to give an impression of the velocity profile in two-phase flows and to explain the movement of the dextran-phase lamella into the center of the channel flow. As presented hereby, it was established that the final arrangement of the two phases does not invariably follow the injection pattern. Although the interfacial area is reduced due to the small channel height, the ratio between the interfacial area of the two liquids and the interfacial area of the liquids and the surrounding wall is still high. As described in chapter 5, a flat and wide microchannel helps to reduce the interfacial area and to stabilize the flow. Accordingly, for experiments in this study aspect ratios of 0.15 (depth divided by width) or less were chosen. But still the interfacial area between the liquid lamella and the wall surface is important. Especially in the three lamella arrangement drop formations may occur as it does for instance happen within flow focusing devices [183,184]. The center lamella only touches the top and bottom wall and the ratio between the interfacial area of the two liquids and the interfacial area of the lamella and the wall surface is increased again.

Fig. 8-6 shows a sequence of a continuous stream of dextran-phase flowing in the center of a channel and being surrounded by an immiscible PEG-phase.

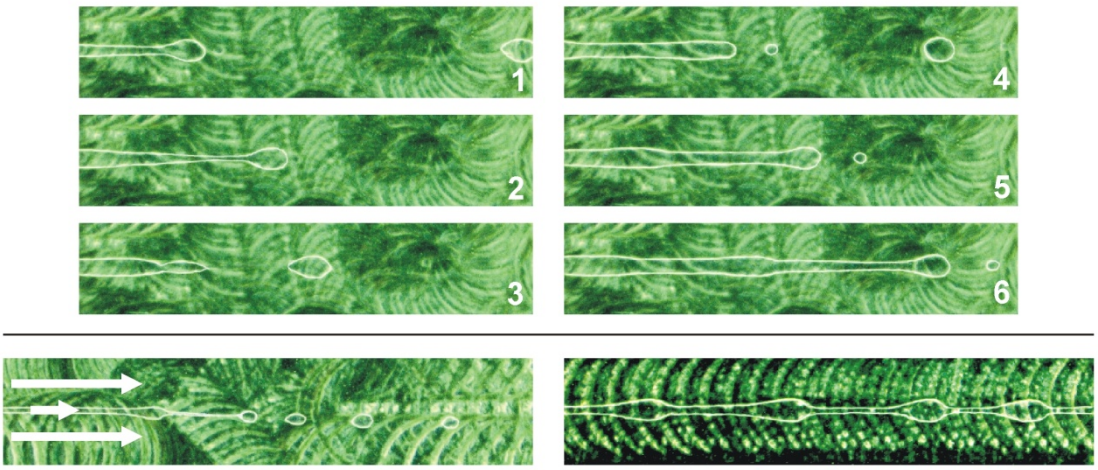


*Fig. 8-6: Top: Sequence showing dextran droplet formations within the PEG-phase. The width of the entering dextran lamella is approximately 50 µm, the channel height is 120 µm. Below: further examples of lamella instabilities.*

Due to the applied flow rates the center stream is forced into a thin lamella and breaks up into droplets. This behavior is similar to the decay of a liquid jet which is driven by the Rayleigh-Plateau instability.

In the course of these experiments, up to five stable lamellae were successfully created in a channel of 800 x 120 µm (w x h). But it has to be mentioned that even more lamellae would be possible. It was observed that the width of a central placed lamella can be approximately reduced to 100-150 µm for the ATPSs under study.

However, to introduce a stable lamella including a sample, a simple injection procedure was applied. First, the desired flow pattern was generated with lamellae without any biomolecule samples included. As soon as the flow pattern becomes stable one of the lamellae was replaced by a lamella of the same liquid which now includes the sample to be examined.

## 8.2 Viscosity Adjustment

Generally, the PEG- and dextran-phases used in the experiments have different flow viscosities inside the microchannel at constant flow rates. Therefore the flow velocity inside the PEG-phase is usually much higher than the velocity in the dextran-phase, cf. Fig. 8-4a. The viscosities in this study were measured by a rheometer (ARES, TA-Intruments GmbH, Germany) and are summarized in Table 8-1. The occurrence of different flow velocities in both phases complicates an accurate estimation of the transport behavior across the phase boundary. Biomolecules which are transported from the lamella of higher viscosity into the lamella of lower viscosity are accelerated which leads to thinning effects. Vice versa, biomolecules are decelerated when transported into the lamella of higher viscosity leading to local enrichment effects. In order to minimize the velocity mismatch between the phases a viscosity adjustment in a microchannel was performed. This helps reducing the above mentioned side effects and to examine the molecule transport across the phase boundary in more detail. Both, polymer concentration and the molecular weight of the used polymers may show strong influences on the viscosities of the PEG- and dextran-phases [185]. For the standard system (system A) and the P-PEG system (system B) the viscosity of the dextran-phase is about seven times higher compared to the PEG-phase.

| ATPS | Viscosity PEG-phase [Pa·s] | Viscosity dextran-phase [Pa·s] | Viscosity ratio |
|---|---|---|---|
| A - Standard system | 0.00416 | 0.02984 | 0.14 |
| B - P-PEG system 10% | 0.00425 | 0.03311 | 0.13 |
| C - Equal Viscosity | 0.02219 | 0.02105 | 1.05 |

*Table 8-1: Viscosities of the aqueous two-phase systems.*

Accordingly, three strategies are examined to adjust the viscosities. Initially, either the molecular weight of the PEG was increased or that of the dextran was decreased, while the amount of polymer (wt%) remained constant. But only if the molecular weights of both polymers have been changed, a viscosity adjustment could be performed. Starting at a pure PEG 8000 / dextran 10,000 two-phase system, PEG 8000 was partially replaced by PEG 35,000, cf. Table 8-2. For finding the point of equal viscosity a microchannel (800 x 100 µm) was used as viscosimeter [186,187]. The measurement is based on a given

flow rate and the resulting interface location between the co-flowing streams in a microchannel.

After preparing two-phase systems with different portions of PEG 35,000, the PEG- and dextran-phase have been injected into the microchannel separately by keeping the flow rates constantly equal but changing the values (0.05, 0.1, 0.5 and 1.0 ml $h^{-1}$). Since the two phases are immiscible but Newtonian liquids, a clear and stable phase boundary was detectable in all cases, cf. Fig. 8-7.

| System | PEG 8000 [wt%] | PEG 35,000 [wt%] | dextran 10,000 [wt%] | water [wt%] |
|---|---|---|---|---|
| I | 10.0 | 0.0 | 12.5 | 77.5 |
| II | 8.0 | 2.0 | 12.5 | 77.5 |
| III | 6.0 | 4.0 | 12.5 | 77.5 |
| IV | 4.0 | 6.0 | 12.5 | 77.5 |
| V | 2.0 | 8.0 | 12.5 | 77.5 |
| VI | 0.0 | 10.0 | 12.5 | 77.5 |

*Table 8-2: Compositions of ATPSs for viscosity adjustment. The amount of PEG 8000 is stepwise replaced by PEG 35,000 in order to increase the viscosity.*

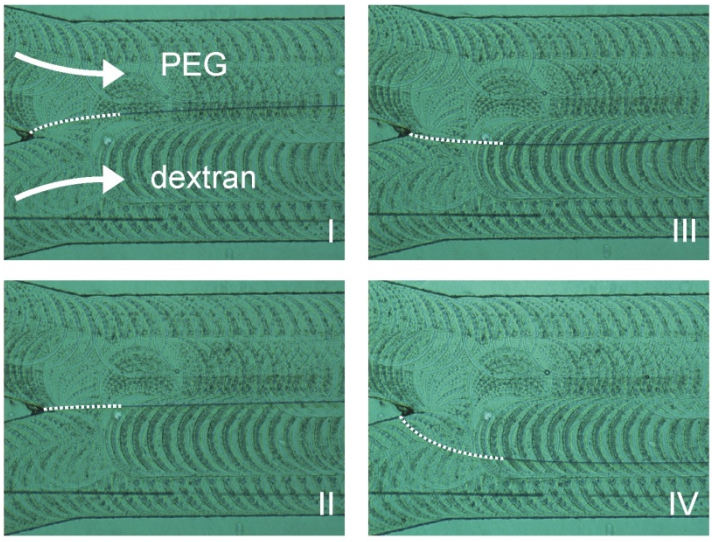


*Fig. 8-7: Resulting position of the interface (dotted line) due to different viscosity ratios (I-IV) while the PEG- and dextran-phase have identical flow rates.*

As illustrated above, at equal viscosities the phase boundary is expected to be located in the center of the channel. Therefore, the widths of both lamellae at different flow rates were compared with each other; near the entrance, halfway along the channel and close to the outlet. Afterwards the width ratios were averaged and compared to different polymer compositions, cf. Fig. 8-8. After a linear fit, the amount of PEG 35,000 for equal viscosities of

both phases could easily be determined (2.28 wt%). Finally a two-phase system of equal viscosity was created and verified by viscosity measurements using a rheometer. The measured viscosity ratio of 1.05 demonstrates a very good confirmation of the viscosity adjustment with the help of a microchannel, cf. Table 8-1. The entire composition of the two-phase system of equal viscosity is summarized in Table 3-1.

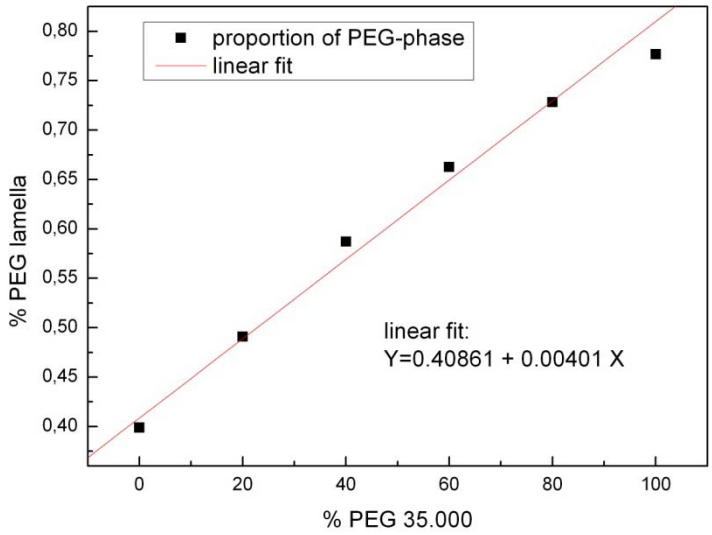


*Fig. 8-8: Linear fit of the measurement results. By increasing the amount of PEG 35,000 and simultaneous decreasing the amount of PEG 8000, the width of the PEG lamella increases steadily until approximately 78% of the channel width is occupied by the PEG-phase.*

## 8.3 Phase Separation

Since liquid naturally seeks the path of least resistance, controlled phase separation in microfluidic systems becomes essential. Often the separation at the outlet is given by channel geometries, i.e. cross section and length, and the resulting pressure drop [65]. In order to achieve individual separation adjustments one possibility is to extend the microfluidic chip by additional integrated micro valves for back pressure adjusting. Often, microfluidic valves are only used to open and close channels completely [188,189] or are made of hydro gels [190]. In this study an easier and more variable setting of the channel cross-section is intended.

The principle of the valve is illustrated in Fig. 8-9 and Fig. 8-10. The valve consists of a hemispheric valve chamber, a membrane and a pin also having a hemispheric protrusion on one side. The pin has a fine thread and is mounted inside the chip holder system. By turning the screw-pin the cross-section of the chamber can be regulated. Accordingly, the back pressure of the individual channel outlets can be adjusted and also the amount of liquid leaving the particular channel.

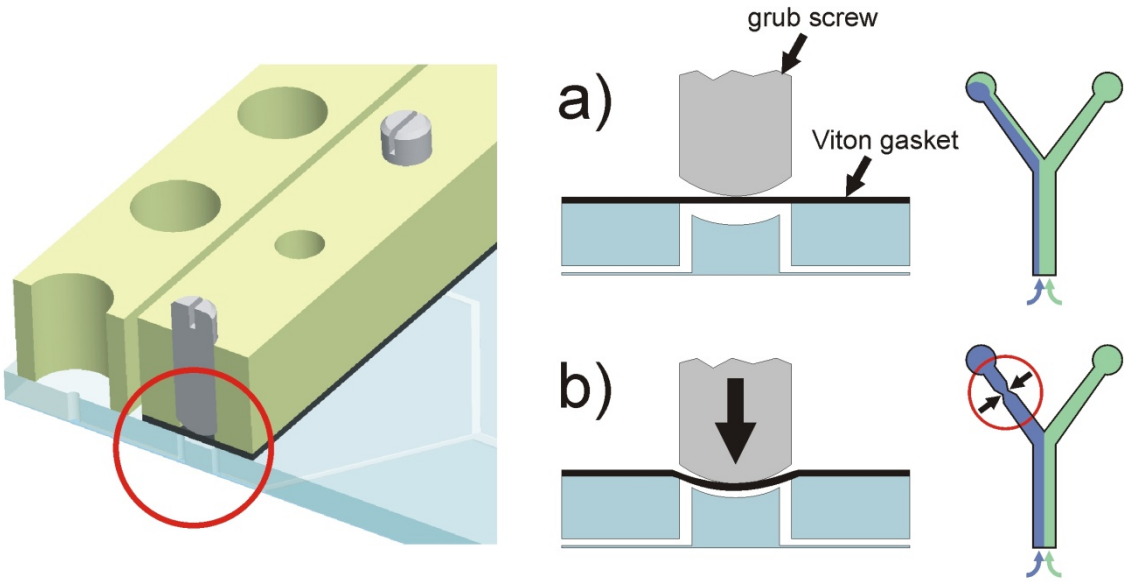


*Fig. 8-9: Principle of phase separation at the outlet. By turning the grub screw (b) the cross-section of the channel decreases and, accordingly, the flow resistance increases. By combining different screw positions, this technique allows an easy adjustment of the phase separation.*

Despite of a successful development of integrated microfluidic backpressure valves, most test chips were equipped with only one outlet due to simplification purposes. Moreover, the main focus primarily lies on the transport behavior of biomolecules across a phase boundary and therefore an accurate separation of both phases is not necessary.

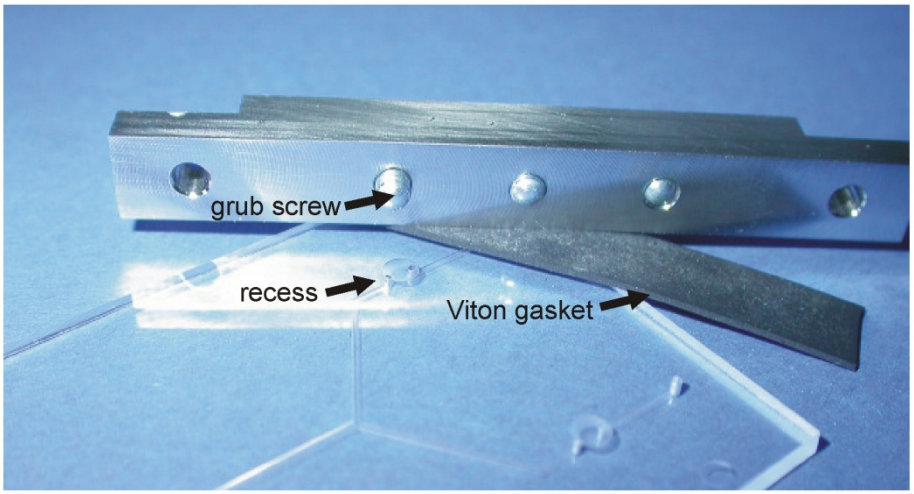


*Fig. 8-10: Test chip with integrated flow separation valves*

# 9 Transport of Biomolecules in Microchannels

*In the microfluidic systems under study there are two different ways how biomolecules or other kinds of molecules can be transported. The most famous mechanism is diffusion and has often been utilized in simple T-sensors [40]. Additional electric fields can help to move molecules in a desired manner. In case of two-phase systems both principles are applicable and have been examined here to study the interaction between the molecules and the phase boundary. In this chapter the diffusive transport as well as the active transport is introduced. In case of the active transport, it can be shown that especially decoupled electrodes allow a reliable transport of the molecules within a stable environment.*

## 9.1 Diffusive Transport

Diffusion describes the transport of material by Brownian molecular motion resulting in a net transport of molecules from regions of high concentration to regions of low concentration. In other words, diffusion counteracts the formation of non-uniform molecule concentrations leading to an increase in entropy which is thermodynamically more favorable. Accordingly, in absence of other driving forces like potential gradients, systems tend to assume a state of equal concentration. The flux can be derived from Fick's law, which states that the flux $J$, the net movement of diffusing molecules per unit area of section, is proportional to the gradient in concentration:

$$J = -D\nabla c \tag{9.1}$$

where $D$ is the diffusion coefficient or diffusivity and $c$ the molecule concentration. Referred to thermodynamics, where the driving force for diffusion can be described by the gradient of the chemical potential of the molecules, and within a 1-D domain Fick's law can be written as:

$$J = -\frac{Dc}{RT}\frac{\partial \mu}{\partial x} \tag{9.2}$$

where $R$ is the universal gas constant, $T$ is the absolute temperature and $\mu$ is the chemical potential. Generally, $D$ depends on the temperature, the viscosity of the fluid and the molecule size according to the Stokes-Einstein relation.

However, so far all presented microfluidic approaches of aqueous two-phase extraction systems are solely based on diffusive transport [29-31,33,76,77,191] and only in macroscopic systems protein or amino acids extraction has been electrophoretically enhanced [78-85], cf. Fig. 9-1.

## 9.2 Active Transport by Integrated Electrodes

As shown by Levine and Bier [80] and other groups [78,82,83] the application of additional electric fields influences the transport behavior of proteins and finally the partitioning in aqueous two phase systems. For instance, these groups have shown that proteins can be directed first into one phase and afterwards into the other one by simply reversing the direction of the electric field. During the active transport process they additionally observed some transport 'resistance' directly at the phase boundary leading to enrichment effects. Since all presented two-phase electrophoresis systems show a more or less macroscopic character, cf. Fig. 9-1, a detailed study of the molecular transport across the phase boundary is only possible with limitations.

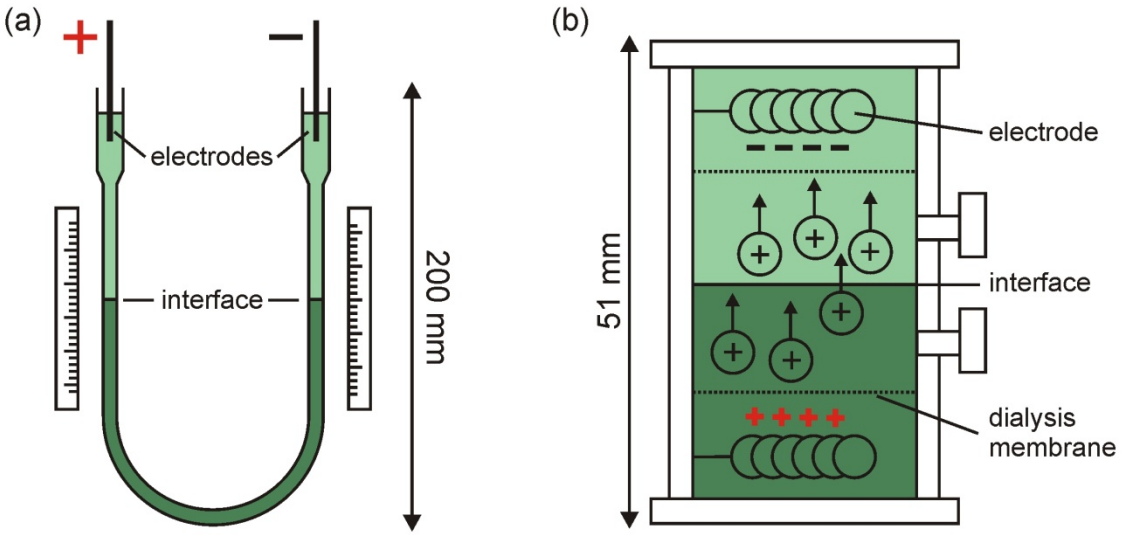


*Fig. 9-1: Macroscopic test devices of (a) Levine and Bier [80] and (b) Clark [82].*

In contrast, microfluidic systems offer the great opportunity to analyze all transport processes within both phases at once and to study the molecular transport across the phase boundary in more detail. For an active transport of biomolecules by means of an electric field, two strategies of electrode integration have been examined. In this study, first well-defined gold electrodes have been integrated into the main channel, as described in chapter 7.2.1, where the electrodes cover the vertical channel walls of the polymeric chip. As already mentioned, usually in aqueous solutions electrode potentials larger than 1.6 $V_{dc}$ may cause electrolysis and bubble generation which can lead to blockage of the narrow microchannels. This value also depends on the used electrode material. Accordingly, the applied voltage has to stay below this critical value. Even if the electrodes should be totally shielded by counter-ions at low dc voltage, there still exists an effective electric field which induces particle migration, cf. Fig. 9-2. The strength of the field strongly depends on the used buffer system as well on the flow velocity. Different groups have shown that due to the double layer the electric field is effectively reduced to less than 3% of the applied field value but high enough for inducing a movement of biomolecules within the electric field [151,153]. The use of such a setup was first explored by studying the electrophoretic transport of BSA molecules dissolved in water, which leads to an increased concentration in the vicinity of one of the electrodes, cf. Fig. 9-2. In order to investigate the transport phenomena related to electrophoresis in stratified two-phase systems, the standard two-phase system (system A, cf. Table 3-1) was prepared. For such a binary system with aqueous solutions of PEG and dextran, an electric field can be easily employed to transport the sample molecules perpendicular to the phase boundary, owing to the similar permittivities of the two phases. Fig. 9-3 shows a series of snapshots taken from a section of the channel where the voltage between the electrodes was gradually increased from 0 to 5 $V_{dc}$. Initially, the BSA molecules were injected in the dextran-phase. When the voltage was increased, the molecules were focused into an increasingly narrow band at the phase boundary. Finally electrolysis and bubble formation was observed, as to be expected in this voltage range.

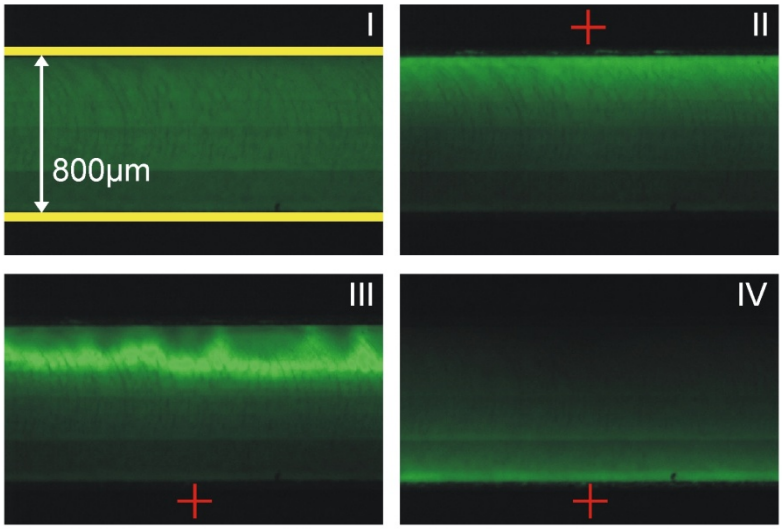


*Fig. 9-2: Time sequence of the enrichment and transport of BSA molecules in an aqueous solution (no PEG or dextran added) inside a closed microchannel with integrated electrodes (yellow). (I) No electric field is applied, (II) enrichment at upper electrode (2 $V_{dc}$), (III) BSA movement after switching the field direction and finally (III) enrichment and quenching effects at the electrode with the positive electrical potential and which is denoted with +.*

Generally and at a dc voltage of up to 2.5 $V_{dc}$, no gas bubbles occurred during a specific period of time and at constant flow rates. But also at this low voltage the formation of very small bubbles with dimensions of a few microns was observed at the electrodes. Higher voltages could only be applied for a short period of time, a few seconds, since channel blocking rapidly occurs.

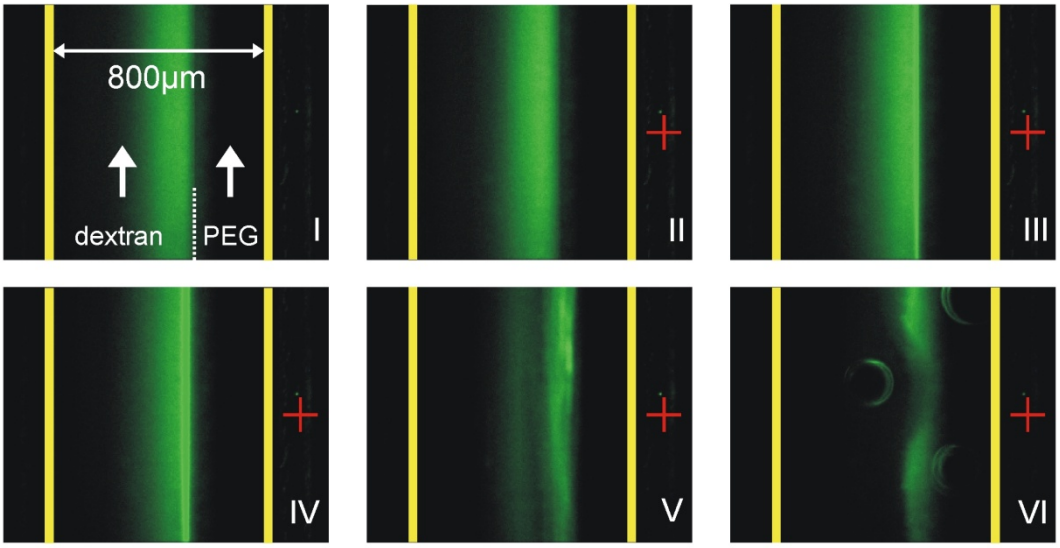


*Fig. 9-3: Snapshots showing the formation of a small band of BSA molecules initially injected in the dextran-phase. After a further increase of the applied voltage, up to 5 $V_{dc}$, the stability of the two lamellae arrangement vanished (V) and finally electrolysis and bubble formation are observed (VI).*

When comparing these results to the results of the analogous experiment with the sample molecules initially dissolved in the PEG-phase it was found out that the BSA molecules are able to penetrate the phase boundary and transfer into the dextran-phase very easily. Thus, it seems that the interface between the two phases has a diodic function for the electrophoretic transport of proteins.

Further experiments of BSA transport within single phase systems revealed more complex behaviors. In a single phase system consisting of the PEG-phase the solution apparently helps to concentrate BSA molecules not at the electrodes but in the center of the channel after reversing the electric field direction several times with a period of two minutes, cf. Fig. 9-4. After a further increase of the applied dc voltage up to 3.5 $V_{dc}$, the development of a small concentration band of about 20 µm thickness was observed, cf. Fig. 9-4 III and IV. The underlying mechanisms are not clearly understood yet, but might resemble a polymer arrangement forming a transport barrier for proteins or an isoelectric focusing step.

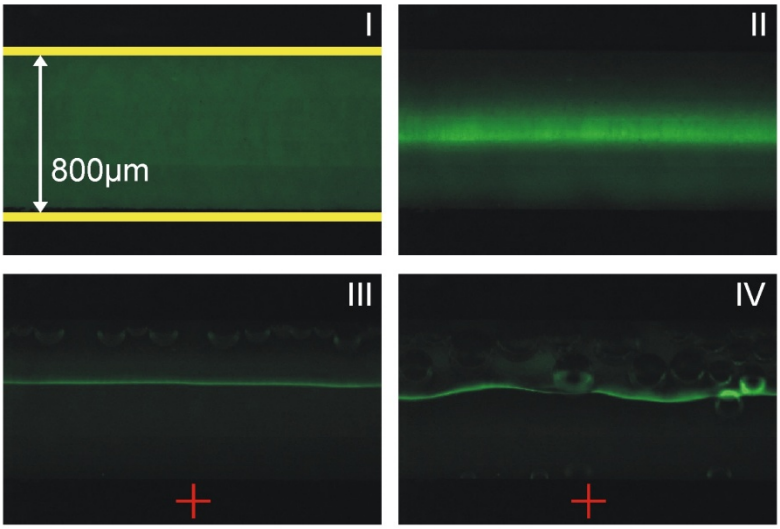


*Fig. 9-4: After reversing the electrical field several times (I-II) an enrichment of BSA molecules was achieved. After increasing the driving voltage the enrichment transferred into a small band of about 20 µm thickness (III). Finally, bubble formation due to electrolysis occurred (IV).*

However, the main problem of integrated electrodes in dc mode was induced intensity instabilities of the fluorescence protein marker. Although the fluorescence emission of the Alexa Fluor® 488 fluorophore is independent of pH as long as the value lies between 4 and 10 [92], strong fluctuations were observed for a two-phase arrangement. Fig. 9-5 shows the integral of the fluorescence intensity over the channel width at different times after a voltage of 1.5 $V_{dc}$ was applied. The amount of protein remains unchanged. The direction of the electric field was switched twice leading to further fluctuations. Due to the small liquid volume inside the channel compared to the electrode surfaces it is assumed that already small generations of oxygen and hydrogen at the electrodes leads to a strong alteration of local pH values, also lower than 4 or higher than 10. Accordingly, such behavior eliminates the possibility to determine the amount of proteins at different points within the channel and to characterize the transport behavior across the phase boundary in detail.

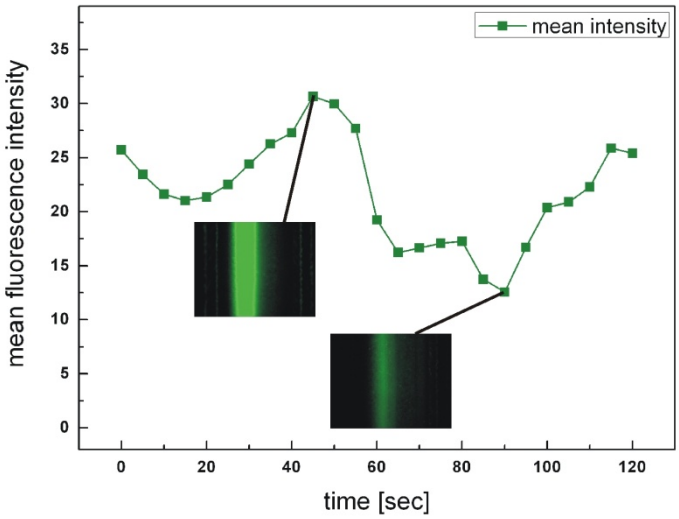


*Fig. 9-5: Mean fluorescence intensity of BSA dissolved in a two-phase arrangement of PEG and dextran. During the application of an electrical field the mean intensity is strongly oscillating although the mean BSA concentration of the sample stays constant.*

### 9.2.1 Influence of Voltage Shape

The effective electric field strength can be increased by applying an alternating or cyclical electrical field which does not allow the complete built up of an electric double layer [153,192]. Additionally, bubble formation should be significantly suppressed. But since an applied uniform ac voltage would not automatically initiate a net transport of molecules in one direction, the waveform has to be modified. And since proteins are not polarizable the underlying transport mechanism is different from dielectrophoresis [97].

The amount of gas generated at the electrodes is proportional to the amount of net charge transferred to the $H^+$ ions in solution resulting in a steady current [193,194]. Accordingly, gas generation can be avoided if the driving waveform causes no net current. The current-voltage characteristics can be approximated to be linear only when either the applied potential is small (< 100 mV) or the applied frequency is high (> 100 Hz). But for higher potentials or lower frequencies a non-linear current-voltage behavior occurs due to activation control as expressed in the Butler-Volmer equation [61,194]. In the framework of a bubble-free electrokinetic pump [194], it has been shown that a non-uniform current waveform with a zero average current lead to a non-uniform but non-zero average voltage response. This effect has been used to drive liquids through microchannels by electroosmosis. However, since the major part of the transport experiments in this thesis are performed with decoupled electrodes, the origin of the net transport by ac voltage will not be discussed here in detail. For further information the reader is referred to [193-195].

Due to non-uniform waveforms, which have been also applied to a two lamella arrangement of the aqueous two phase system, bubble generation is suppressed and voltages higher than 5 $V_{ac}$ can be applied. But although an electrophoretic net transport of proteins towards one electrode was induced, the application of an alternating electric field of low frequency comes along with mixing effects [167-169] leading to an unacceptable disturbance and disruption of the phase boundary. Ac voltages at low frequency usually induce stronger disturbances, but also the application of dc voltages leads to comparable mixing behaviors. Accordingly, these mixing effects will also occur using decoupled electrodes [163,196].

## 9.3 Active Transport by Decoupled Electrodes

The disadvantage of a microfluidic system with embedded metallic electrodes deposited on the channel walls is the development of bubbles above a threshold voltage due to electrolysis. Thus the field strength that can be applied to induce electrophoretic motion is rather limited. For this reason the electrodes and the main channel were fluidically decoupled by designing a channel with gaps inside the walls that are filled with hydrogel or slits where dialysis membranes are placed in. The chip, cf. Fig. 7-9, comprises a microchannel with a number of inlets, two buffer reservoirs on both sides of the channel and a bridging structure allowing a fluidic decoupling of the buffer reservoirs from the channel. The preparation of the gel matrix as well as of the dialysis membrane has been already described in 7.

The ions in the buffer reservoirs can diffuse into the gel matrix or membrane, thus ensuring that the electric field is guided from one electrode in the buffer reservoir through the bridging structure, further across the microchannel, through the bridging structure on the opposite side to the second electrode. That way an electric field perpendicular to the interfaces between two immiscible aqueous phases can be applied without introducing gas bubbles to the channel. The buffer reservoirs are open to the environment. Accordingly, bubbles created by electrolysis can easily escape from the system.

### 9.3.1 Dialysis Membranes

To decouple the flow inside the main channel from the electrodes, dialysis membranes have been used as ion bridges. They are permeable for buffer ions but not for small biomolecules, like proteins. The fabrication steps have been described in chapter 7.2.2.1. The membranes act as a part of the channel wall and are humidified prior to transport experiments. Besides Nadir® membranes also other kinds of dialysis membranes have been examined; Visking dialysis membrane (regenerated cellulose, MWCO 12-14 kDa, 44130.01, SERVA Electrophoresis GmbH, Germany) and Servapor dialysis membrane (regenerated cellulose, MWCO 12-14 kDa, 44148.01, SERVA Electrophoresis GmbH, Germany). The main problem of the two latter mentioned types of membrane was their considerable autofluorescence, cf. Fig. 9-6, which strongly interferes the analysis of the protein transport behavior.

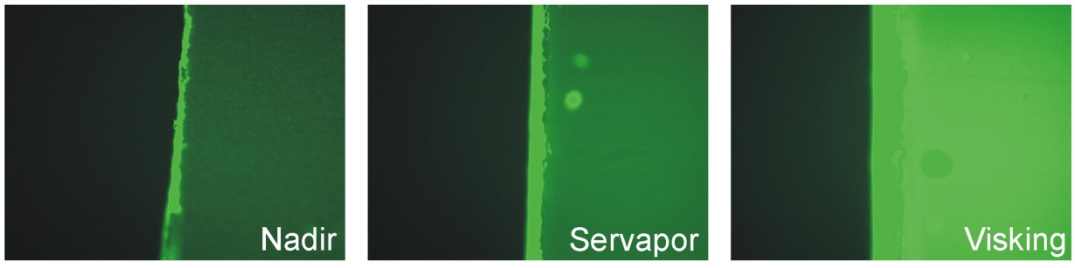


*Fig. 9-6: Autofluorescence of different dialysis membranes. The applied integration time is comparable to that in protein transport experiments.*

But apart from the disturbing autofluorescence, the application of dialysis membranes for such purposes comes along with another disadvantage compared to hydrogels. Dialysis membranes consist of a spongy matrix of crosslinked polymers with pore diameters of approximately 25 Å (Servapor 44148). That means that the membrane consists of countless small nanochannels which end into the main channel. In combination with an electric field a strong EOF is induced. In turn, this leads to an intensive disturbance of the multi-laminated two-phase flow, cf. Fig. 9-7. This disadvantage is amplified by the fact that the potential drop

occurs predominantly over the dialysis membrane. Accordingly, the resulting electric field inside the membrane is much higher compared to the field inside the main channel.

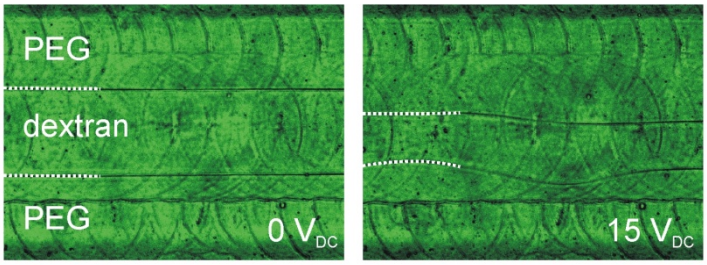


*Fig. 9-7: Interface fluctuations within a three lamellae arrangement once an electrical field has been applied. The flow is from left to right. Channel walls are not visible.*

In order to reach an adequate electrophoretic velocity of the proteins, compared to a gel bridge, a higher voltage is necessary, see chapter 9.3.2. But this again results in a higher EOF inside the nanochannels disturbing the two-phase flow before the proteins have covered a desired distance. As an example, the current/voltage characteristic of a dialysis membrane is illustrated in Fig. 9-8.

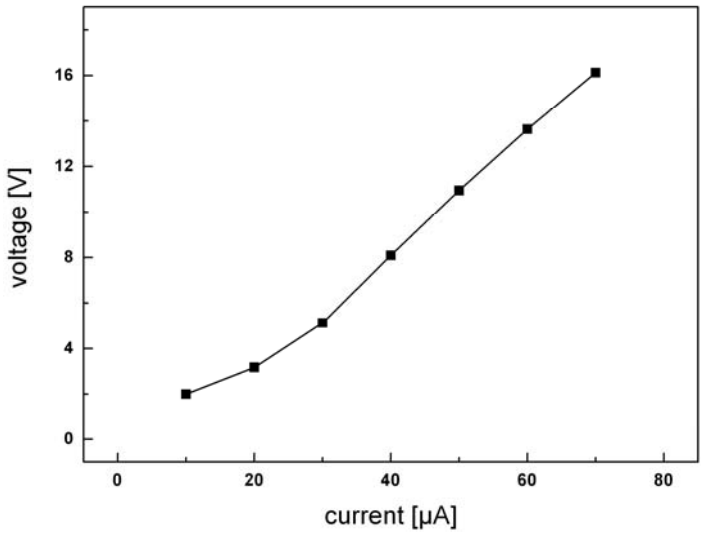


*Fig. 9-8: Current/voltage characteristic of a chip with integrated dialysis membranes.*

But in spite of the above mentioned disadvantages, dialysis membranes allow protein enrichments inside a microchannel directly at the membrane itself. Experiments without flow show that after a certain time most of the proteins are concentrated at one of the side walls, since they are not able to penetrate the membrane, cf. Fig. 9-9.

Although dialysis membranes facilitate to keep proteins inside the main channel, the disturbance of the laminated flow does not allow a solid examination of the transport behavior of proteins and other molecules across phase boundaries.

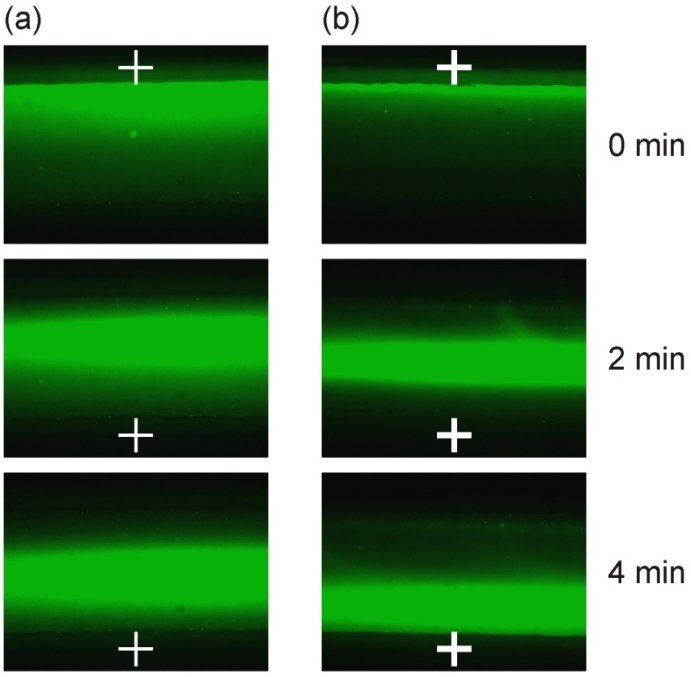


*Fig. 9-9: After proteins have been concentrated at the upper membrane at a current of (a) 40 µA and (b) 60 µA, the orientation of the electrical field was reversed. The BSA molecules were transported towards the lower membrane with different velocities due to the difference in the electric field strength.*

### 9.3.2 Hydrogels

In contrast to dialysis membranes, proteins are not efficiently retained by agarose gels. But using gel as a decoupler helps reducing the voltage drop over the ion bridges considerably. The electric resistance of a dialysis membrane (e.g. Servapor 44148) is, for instance, three times as large as the resistance of the gel system. For example, when 4 $V_{dc}$ is applied, the resulting overall current of the gel system is approximately 80 µA, cf. Fig. 9-10. The resulting electric field inside the main channel depends on the conductivity of the buffer system. Generally, for an integrated examination of the transport behavior of proteins inside a 5 mM buffer system a minimum current of 200 µA is necessary leading to sufficient electrical field strengths. In contrast and in order to reach the same field strength inside the main channel of a membrane system more than 40 $V_{dc}$ is needed (extrapolated, cf. Fig. 9-10). In summary, gels used as decoupler are a good way to banish the problem of electrolysis from miniaturized channels.

The electrical field strength inside the main channel can be estimated by the applied current and resistivity of the liquid volume. As an example, the electrical field in the main channel of the gel chip is estimated as described in the following section.

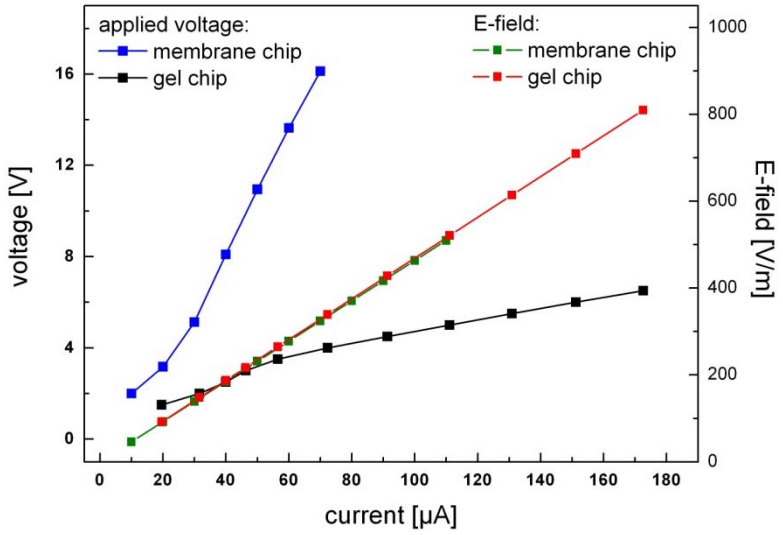


*Fig. 9-10: Current/voltage characteristic of both chip designs, with an integrated dialysis membranes as well as a gel matrix. According to the current and since the liquid volume inside the main channel is similar also the resulting electrical field within the main channel is almost equal. But in case of the gel chip much less voltage is necessary to reach the same field strength.*

The main channel was equally filled with two lamellae, one PEG- and one dextran-lamella of 5 mM buffer strength. The measured resistivities $\rho_{el}$ of the PEG- and dextran-phase (Labor-Konduktometer 703, Knick Elektronische Messgeräte, Germany) are 1712.5 Ω cm and 1913.0 Ω cm, respectively. For the resulting resistivity an average value of 1812.8 Ω cm is assumed. With

$$R_{el} = \frac{w}{L_{cl} \cdot h} \rho_{el} \qquad (9.3)$$

and

$$E = \frac{R_{el} \cdot I}{w} \qquad (9.4)$$

the electrical field strength can be calculated, where $w$ and $h$ are the channel width and height, $L_{cl}$ the length of the channel located between the electrodes. $I$ is the applied current and $E$ the resulting electrical field perpendicular to the channel orientation. Accordingly, for, e.g., $I$ = 70 µA the corresponding electric field is approximately 330 V m$^{-1}$. Furthermore, also in case of $I$ = 70 µA and if the voltage drop inside the buffer reservoirs is neglected, the resulting electrical field inside one gel matrix or one dialysis membrane is approximately 620.7 V m$^{-1}$ or 7915 V m$^{-1}$, respectively.

### 9.3.3 Interface Instabilities

Flow in microchannels is often stable and laminar. But under certain conditions, due to the coupling between conductivity gradient and applied electric fields, an unstable flow field owing to electrokinetic instabilities may occur [166]. This phenomenon was first described by

Melcher and Taylor in the 1960's [197]. In microsystems very large electric fields can be achieved by applying relatively small voltages. For instance, a voltage of 10 V applied across a length of 800 µm leads to an electric field strength of 12.5 kV $m^{-1}$. Accordingly, electrokinetic instabilities may become dominant. Those instabilities can be utilized for rapid mixing [167-169]. In the present system, however, such instabilities are undesirable leading to a disruption of the phase boundary of a two-phase system. The coupling between electric fields and ionic conductivity gradients results in an electric body force (per unit volume), $\rho_q E$, of the form

$$\rho_q E = (\varepsilon E \cdot \nabla \sigma_{ion}) E \qquad (9.5)$$

where $\rho_q$, $\varepsilon$, $\sigma_{ion}$ are the charge density and the local values of permittivity and ionic conductivity, respectively [168,181]. This kind of electric body force is generated wherever applied electric fields interact with conductivity gradients. Accordingly, the instability occurs at the interface of adjacent streams of the aqueous phases, since at this area the conductivity gradient is steepest. The conductivity gradient itself occurs due to the non-uniform distribution of the ions in both phases.

For a system driven by decoupled electrodes the influence of the electric field on the flow pattern of the multi-laminated flow is exemplified in Fig. 9-11. It was shown in a number of experiments that the bi-laminated PEG-dextran system can typically withstand voltages of about 7 to 15 $V_{dc}$, depending on the concentration and molecular weights of the used polymers and the salt concentration of the buffer solution. This, however, poses no limitations to most of the experiments performed, because at these voltages already a considerable electrophoretic motion of protein molecules is observed.

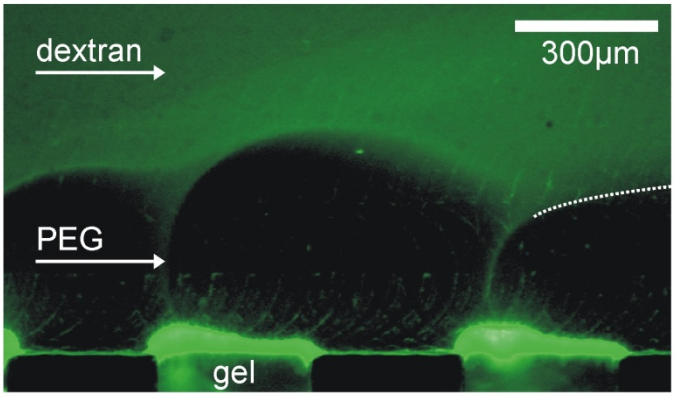


*Fig. 9-11: Perturbations of the phase boundary in high electric fields. Only the lower PEG-phase and two of the gel channels are visible. The BSA molecules are dissolved in the dextran-phase and some of the proteins have already accumulated at the gel surface.*

### 9.3.4 Buffer Reservoir

To guarantee stable conditions with respect to pH value and electric field, the buffer reservoirs play an important role during active transport processes. Accordingly, the buffering capacity of the reservoirs has to be considered. Using the Henderson-Hasselbach equation for a buffer, which describes the relationship between the strength of corresponding acids-base pairs and their capacity to preserve a specific pH value, desirable tolerances for changes in pH in

combination with the applied charge can be estimated. During the transport experiments in this study the applied current lies usually between 50 and 150 µA. Accordingly, for a 5 mM buffer system and a constant current of approximately 100 µA over a period of 60 minutes the buffer reservoir should occupy at least 1200 µl. In this case the change in pH will not be more than 0.2 [198].

Typical transport experiments start at 0 $V_{dc}$ and the applied voltage is increased stepwise. Furthermore, a single experiment can possibly last up to two hours. During this time a constant pH value has to be ensured. In case of 300 µl reservoirs and a stepwise increase of 1 V every ten minutes, a change of the pH value inside the buffer reservoirs is already detectable after 30 minutes, cf. Fig. 9-12. After 60 minutes the ΔpH reaches a value of 1.0 and after 90 minutes a ΔpH of 3, demonstrating that the buffer capacity is expended.

In order to avoid notable pH shifts, the volume of each buffer reservoir was increased to 3000 µl. For such a reservoir no pH shift was detected over a time period of two hours under typical experimental conditions. Thus the increased reservoirs ensure constant buffer conditions for biomolecule transport processes.

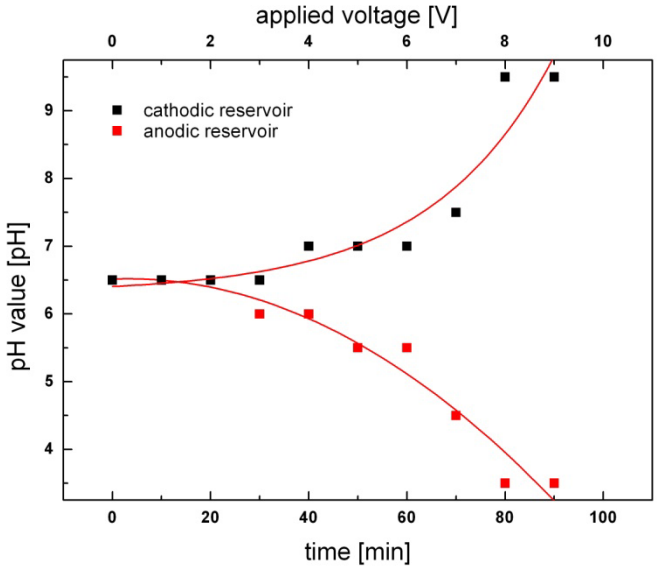


*Fig. 9-12: During transport experiments the pH value of the buffer, 5mM, placed in 300 µl reservoirs starts to increase or decrease after 30 minutes.*

# 10 Diffusive Protein Transport

*With the aim to investigate if local effects at the phase boundary cause a retardation of proteins, here a detailed study of the diffusive transport of proteins across fluid phase boundaries within ATPSs is presented. Possible modifications of interfacial mass transfer could be due to protein adsorption at the phase boundary or local electric fields from electric double layers. The experiments have been performed with a microfluidic system in which protein diffusion within a bilaminated configuration of two phases is analyzed. A one dimensional model, incorporating phase-specific diffusion constants and the difference in chemical potential between the phases, has been formulated. A comparison of experimental and simulation data shows a good overall agreement and suggests that a potential local influence of the phase boundary on protein transport is insignificant for the systems under investigation.*

## 10.1 Introduction

In a simple picture a biomolecule such as a protein is considered as a nanoparticle of an effective radius $r$. It is not difficult to show that the interface always represents a potential-energy minimum for such a particle, where the depth of the minimum depends on the particle radius, the contact angle with the interface and the interface tension [199]. If this energy scale is small compared to the thermal energy $k_BT$, it is expected that the fluid interface does not significantly influence the diffusive transport of particles from one side to the other. However, simple estimates show that for a nanoparticle of the size of a typical protein molecule considered here, the energy scale for adsorption at the interface is of the same order of magnitude as the thermal energy. For this purpose typical interfacial tensions of aqueous two-phase systems of the order of $10^{-4}$ N m$^{-1}$ [180] have been assumed. Thus, it is natural to speculate that reversible adsorption could occur, as observed by some authors [200,201].

Likewise, it is expected that in this case the fluid interface acts as a transport barrier, retarding the biomolecule transport from one phase to another. This is due to the fact that particles can get trapped in a potential-energy minimum for a considerable time before their Brownian motion continues in either one of the two phases [202]. Another effect that could lead to a suppression or augmentation of mass transfer in ATPSs is the formation of an electric double layer at the phase boundary. In typical ATPSs, consisting of polyethylene glycol (PEG) and dextran, salts with polyvalent anions, like phosphate, partition unevenly between the top and the bottom phase leading to an electrostatic potential difference of a few mV across the interface with electrical double layers formed on both sides [78,80,104,107,108]. Electric double layers give rise to a localized electric field causing an additional force on a charged molecule in the vicinity of the phase boundary. Order-of-magnitude estimates show that the corresponding energy scale can be significant in comparison to the thermal energy. Depending on the direction of the electric field with respect to the direction of diffusive transport, either retardation or augmentation of mass transfer could result. But due to the nature of thermally activated processes it becomes clear that a retardation is the most likely process to be detected experimentally [78].

Despite the practical relevance of protein partitioning in ATPSs, the microscopic details of diffusive transport of proteins across the boundary between the two aqueous media seem to have never been studied before. Therefore, here the concentration profiles in the vicinity of the phase boundary are examined experimentally and compared to model predictions. Specifically, bilaminated ATPSs based on PEG and dextran are formed inside a microchannel to examine the transport of different proteins across the phase boundary as a function of their different affinities to the polymer phases. In order to achieve a larger range of partition

coefficients (protein concentration in the PEG-phase divided by protein concentration in the dextran-phase in equilibrium) of different proteins, PEG has been partly replaced by P-PEG that is modified by additional hydrophobic side groups, as described in chapter 3.5.1; the compositions of the used ATPS with P-PEG (type B) can be found in Table 3-1. The hydrophobic side groups strongly influence the protein partitioning between the two phases leading to increased partition coefficients in most cases. For example, without P-PEG the major part of bovine serum albumin (BSA) is found in the dextran-phase, while when a specific amount of PEG is replaced by P-PEG, the partition coefficient strongly increases [113-115]. Due to the hydrophobic ligand P-PEG now offers additional hydrophobic binding sites. This leads to a higher affinity to proteins exposing hydrophobic groups at their surface, and therefore the partition coefficient of hydrophobic proteins usually increases. Higher partition coefficients lead to higher mass fluxes if the proteins are initially dissolved in their non preferred phase.

The experiments are complemented by a simple mathematical model accounting for the diffusive protein transport driven by a chemical potential gradient. This model just accounts for the free-energy change of proteins in the bulk phases but does not include any interfacial contributions such as an adsorption energy or an electric field caused by electric double layers. In that sense the mathematical model serves as a hypothesis that is tested by comparing the experimental data with the model predictions. It is shown that the two data sets agree quite well, thus suggesting that the driving force for diffusive transport is the usual chemical potential gradient within and between the two phases themselves, while any specific contribution of the phase boundary seems to be negligible.

For all diffusion experiments 10 µl of the labelled proteins solution were initially mixed with 250 µl of one of the two aqueous phases leading to a final concentration of 5.6 µg $ml^{-1}$ (0.85 µM) and 4.7 µg $ml^{-1}$ (1.04 µM) for BSA and ovalbumin, respectively. Accordingly, due to this low protein concentration the risk of self-quenching can be neglected. Furthermore, usually PEG chains tend to repel intruding molecules for reason of osmotic pressure and are used as a salting-out agent [203]. But again, due to the low protein concentration of far less than 0.1 g $l^{-1}$ paired with a moderate PEG amount, it can be assumed that in this study the salting-out of proteins induced by PEG can be also neglected [204].

## 10.2 Adapted Microfluidic Setup

The experimental setup for diffusion experiments is comparable to the setup already described in chapter 6. Since for the examination of the diffusive behavior of proteins no electric field is necessary, the power supply and integrated electrodes are left out, cf. Fig. 10-1.

Accordingly, the diffusion test chip only consists of two inlets (1,2), one outlet (4) and an additional vent hole (3) as well as a main channel. The width, depth and length of the main channel are 500 µm, 50 µm and 38 mm, respectively. All other parts of the experimental setup are equal to the setup described above. This also applies to the analysis of the fluorescence intensity distribution.

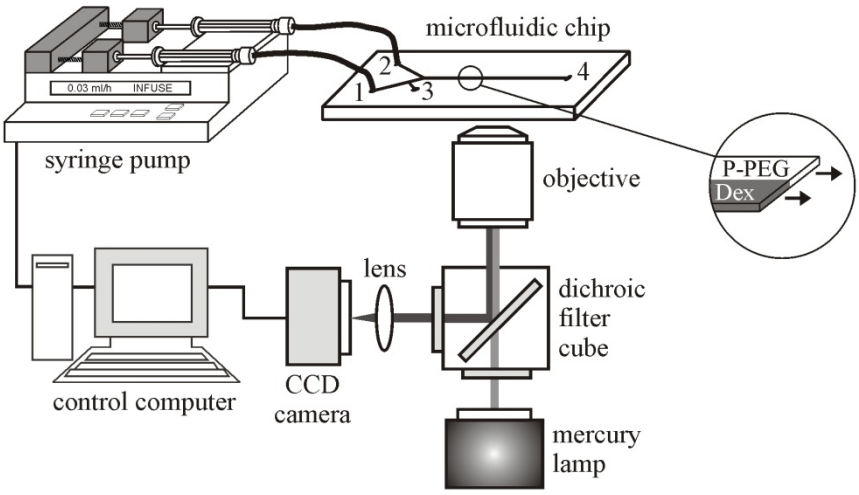


*Fig. 10-1: Schematic of the microfluidic chip integrated in the experimental setup including an inverse fluorescence microscopy system. The dextran- and the P-PEG-phase are injected through inlet 1 and 2, respectively.*

## 10.3 Single Phase Diffusion

Owing to the fact that the ATPS consists of two phases with different viscosities and different diffusion coefficients of the dissolved species, the diffusion coefficients of the used proteins were determined first, separately in each phase. To this end, one syringe is filled with either the P-PEG- or the dextran-phase, while a second syringe is filled with the same liquid with fluorescence-marked proteins dissolved in. At the beginning of the experiment the vent hole is closed by adhesive tape and the injected liquids flow towards the outlet. Since the same type of liquid is fed into both inlets, equal flow rates (0.1 ml $h^{-1}$; this value corresponds to an average velocity of 2.22 mm $s^{-1}$ of each lamella) yield a step-like initial protein distribution, where one half of the channel (in width direction) is filled with proteins while in the other half no proteins are found. The flow rates during filling were chosen such that the diffusive mass transport of the proteins to the other liquid just slightly broadened the initially step-wise concentration profile across the liquid-liquid interface.

After the two lamellae are formed inside the channel the outlet port is sealed, simultaneously the syringe pumps are switched off and the vent hole is opened allowing any residual flow to escape. The residual flow is caused by fluidic capacities (material compliance) in the feeding system and has to be bypassed in order to avoid any convective transport effects within the main channel. At this moment the first fluorescence image of the protein distribution is taken 10 mm behind the channel intersection, i.e. approximately five seconds after the two lamellae got into contact. Further images follow within certain time intervals. In addition to that, each time images with transmitted light are taken shortly afterwards. These images allow to identify the channel walls unambiguously. After approximately two minutes the vent hole is closed again in order to suppress any possible evaporation. Since the outlet is still closed and the fluid to be investigated is located in a microfluidic ‘dead-end’ the evaporation and the closing afterwards has no observable effect on the two lamellae arrangement inside the main channel. All experiments with single-phase as well as those with two-phase systems were carried out at room temperature.

## 10.4 Diffusion across Phase Boundary

The experimental procedure is almost identical to the diffusion experiments performed on single-phase systems as described above. Here, instead of one type of liquid both phases, P-PEG- and dextran-phase, are simultaneously injected into the main channel. Owing to their different viscosities the flow rates have to be adjusted in order to create two lamellae of approximately equal widths. For this purpose the chosen flow rates are 0.18 ml $h^{-1}$ and 0.03 ml $h^{-1}$ for the P-PEG- and the dextran-phase, respectively (these values correspond to average velocities of 4.00 mm $s^{-1}$ and 0.66 mm $s^{-1}$ in each phase). Viscosity measurements using a rheometer (ARES, TA-Instruments GmbH, Germany) yield viscosity values of 4.2 mPa·s for the P-PEG- and 32.8 mPa·s for the dextran-phase, respectively. These values are in qualitative agreement with the applied flow rates [205]. The subsequently discussed experiments refer to the case where the proteins under study are dissolved in the non-preferred phase (dextran-phase). This configuration leads to a higher mass flux across the phase boundary compared to the reverse case. As a cross-check, the reverse case, i.e. the proteins are initially dissolved in preferred phase, was analyzed as well and it has been assured that the same partition coefficient is obtained.

Again, after the outlet port has been closed, the two-lamellae arrangement inside the microchannel is 'frozen' and any remaining pressure gradient is relaxed by opening the vent hole. Pictures are taken within shorter time intervals as compared to the single-phase measurements. Images with transmitted light are taken shortly after each fluorescence image for localizing the channel wall as well as the position of the phase boundary.

## 10.5 Theoretical Background[1]

In the simplest picture, the time dependence of the concentration profiles observed in the microchannel filled with two liquid phases can be modeled by two diffusion equations governing the mass transport within each phase, where both equations are coupled via the mass transfer occurring across the interface. For the sake of simplicity, any solute-wall interactions at the bottom and at the top of the microchannel are neglected and a flat fluid interface forming a right angle with the wall boundaries is assumed, which allows the application of a one-dimensional (1-D) model approach. In order to derive the governing equation for diffusive mass transfer in a 1-D domain comprising two fluid phases, a spatially varying chemical potential, being the free energy of a dissolved species, is introduced. For a dilute, ideal solution the chemical potential is given by [206]

$$\mu(x) = \mu^0(x) + RT \ln c(x,t) \qquad (10.1)$$

where $c(x,t)$ denotes the concentration as function of the position in direction of the width of the channel (cf. Fig. 10-4) and time, $R$ is the universal gas constant and $T$ the absolute temperature. $\mu^0(x)$ is the standard potential of the dissolved molecules. Here, a sharp interface between both phases located at $x = 0$ is assumed, so that the standard potential is given by a step function

[1] The theoretical model as well as the simulation of the intensity profiles, cf. chapter 10.6, have been primarily developed and carried out by Prof. Dr. Friedhelm Schönfeld (FH Wiesbaden, Germany).

$$\mu^0(x) = \begin{cases} \mu_-^0 & \text{for } x < 0 \\ \mu_+^0 & \text{for } x > 0 \end{cases} \tag{10.2}$$

where the subscripts + and – refer to the different phases. Specifically, the model does not contain any special term describing a possible interfacial adsorption of molecules to the phase boundary at $x = 0$ or a local electric field. Equilibrium between both phases implies equal chemical potentials, so that the difference in standard potentials $\Delta\mu^0 = \mu_-^0 - \mu_+^0$ is connected to the partition coefficient $k$ by

$$k = \frac{c_-^{equ}}{c_+^{equ}} = e^{-\Delta\mu^0/RT} \tag{10.3}$$

or

$$\Delta\mu^0 = -RT \cdot \ln k \tag{10.4}$$

where $c_\pm^{equ}$ in Eq. (10.3) denote the equilibrium concentrations in the phases located at $x < (>) 0$.

Any gradient in the chemical potential drives a corresponding molecular flux given by

$$J(x,t) = -c(x,t) \cdot \mu_m(x) \cdot \partial_x \mu(x) \tag{10.5}$$

and inserting Eqs. (10.1) and (10.4) results in

$$J(x,t) = -D(x)\{\partial_x c(x,t) - c(x,t) \cdot \ln k \cdot \delta(x)\} \tag{10.6}$$

Here $\mu_m(x)$ and $D(x) = \mu_m(x) \cdot RT$ denote the mobility and diffusion coefficient of the molecules in the solvent, respectively, and $\delta(x)$ is the Dirac delta distribution. The spatial dependences of the quantities are explicitly accounted for to emphasize that the chemical potentials as well as the diffusion coefficients differ in the different phases. As for the standard potentials, cf. Eq. (10.2), a step profile for the diffusion coefficient is assumed:

$$D(x) = \begin{cases} D_- & \text{for } x < 0 \\ D_+ & \text{for } x > 0 \end{cases} \tag{10.7}$$

Finally the time evolution of the concentration field is governed by the continuity equation

$$\partial_t c(x,t) = \partial_x J(x,t) \tag{10.8}$$

Eqs. (10.6), (10.7) and (10.8) together with the appropriate initial and boundary conditions determine the complete time evolution of the concentration field. For the particular case of two infinite media filling two half spaces and a stepwise initial concentration the time dependence of the concentration field in both phases is given by error functions [207]. For the general case with an arbitrary initial condition extracted from experimental data and a finite system ($-L < x < L$) with zero flux boundary conditions at the channel walls the equations can be solved numerically. For this purpose the finite-element software package COMSOL [208], being controlled via a MATLAB [209] script, has been employed. As mentioned above, the

model neglects additional transport effects at the interface that are due to hypothetical very localized extrema of the chemical potential or electric fields due to electric double layers. Therefore, it has to be regarded as a hypothesis that either needs to be falsified or corroborated by the experimental data.

In order to allow for an unbiased comparison between the mathematical model and the experimental data, the three model parameters, viz. $D_-$, $D_+$ and $k$ have to be determined first. The diffusion coefficients are determined by comparing experimental data for single-phase diffusion with the time evolution of the concentration field predicted by the standard 1-D diffusion equation, i.e. Eqs. (10.6) and (10.8), with a single, constant diffusion coefficient and $k$ set to one. Again, to allow for an arbitrary initial concentration profile taken from the experiment, Eq. (10.8) is solved numerically. The single-phase diffusion coefficients are determined by fitting the numerical data to the experimentally determined concentration profiles of the first three recorded time steps using a MATLAB optimization routine [209,210]. The partition coefficient k is derived from the experimental concentration profiles at the end of an experimental run with the two-phase system where the system is very close to equilibrium. There the concentration profiles show clear plateaus from which the partition coefficient can be determined (cf. Eq. (10.3)).

## 10.6 Results

In the following subsections the results of the diffusion experiments are presented. In the first step the diffusion coefficients of the proteins in each phase are determined in detail. Additionally, such determination becomes important since the application of the Stokes-Einstein relation to ATPSs has to be handled with care. In the next step the protein diffusion across the interface is examined and compared to a mathematical model.

### 10.6.1 Diffusion in Single Phase Systems

The first experiments inside the microchannel aimed at the determination of the diffusion coefficient of the chosen proteins, here BSA and ovalbumin, in each of the two phases. After stopping the flow inside the microchannel, pictures were taken within certain time intervals. Afterwards, intensity profiles across the channel width have been generated from each picture. Due to the fact that the mercury lamp showed a certain intensity fluctuation over time and the total amount of proteins inside the channel and within each cross section stays constant in the absence of any axial species transport, the integral of all intensity profiles was renormalized to a fixed value of one. Additionally, since the linearity between protein concentration and fluorescence intensity was confirmed, all further calculations are carried out with normalized concentration values [211]. A comparison between the normalized experimental data and the simulations results for BSA in the P-PEG-phase is exemplarily shown in Fig. 10-2. The determined protein diffusion coefficients are summarized in Table 10-1.

| Protein | P-PEG | dextran |
|---|---|---|
| BSA | $2.4 \cdot 10^{-11}$ | $1.4 \cdot 10^{-11}$ |
| Ovalbumin | $2.1 \cdot 10^{-11}$ | $1.3 \cdot 10^{-11}$ |

*Table 10-1: Protein diffusion coefficients in the different phases given in $m^2\ s^{-1}$, determined by minimizing the deviation between the experimental data and the model results.*

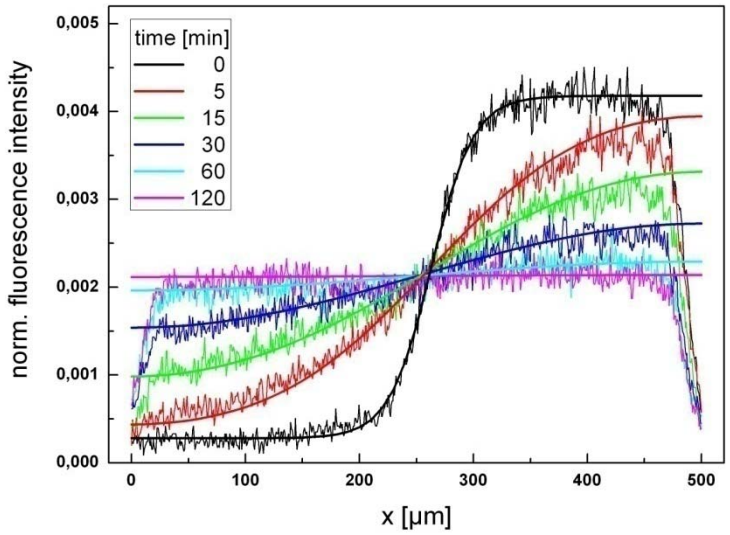


*Fig. 10-2: Experimental and simulated normalized (see text) intensity profiles for BSA diffusion in the P-PEG-phase. After approximately two hours equilibrium is reached.*

With respect to the recorded intensity profile a further comment is made regarding the decreasing intensities close to the channel walls. Due to the manufacturing process the channel walls on each side form an inclined plane leading to a trapezoidal channel cross section. These planes have a projection in $x$ direction of 50 µm and more, cf. Fig. 10-3. Therefore a decreasing of the intensity close to the side walls, as observed in the experiments, has to be expected, cf. Fig. 10-2.

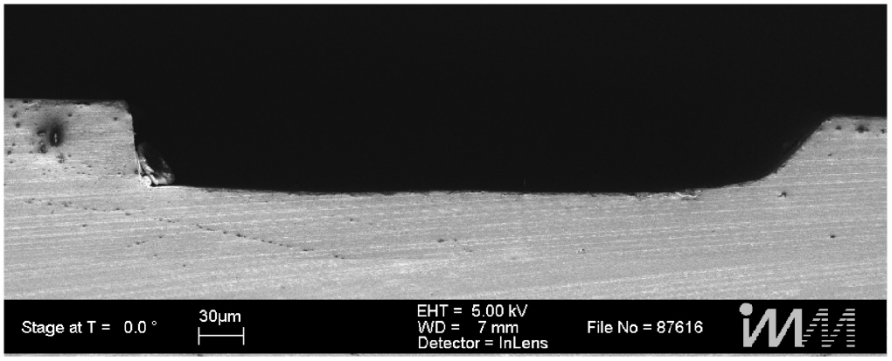


*Fig. 10-3: SEM picture: cross section of the main channel of one test chip. The shape of the cross section can vary from test chip to test chip.*

As a consistency check, the Stokes-Einstein relation can be applied to relate the derived diffusion coefficients to reported and corresponding diffusion coefficients in water. Based on literature values for the latter (BSA: $D = 6.3\ 10^{-11}\ m^2\ s^{-1}$ [212,213]; ovalbumin: $D = 7.7\ 10^{-11}\ m^2\ s^{-1}$ [213,214]) and on the measured viscosity of the P-PEG-phase, one finds $D = 1.5\ 10^{-11}\ m^2\ s^{-1}$ for BSA and $D = 1.8\ 10^{-11}\ m^2\ s^{-1}$ for ovalbumin, both in P-PEG. Thus, the diffusivities derived for the P-PEG-phase (Table 10-1) agree reasonably well with the literature data, in particular in case of ovalbumin. With respect to the deviations it has to be noted that caution is advised when applying the Stokes-Einstein relation to the ATPS under study. While the relation is well established for homogeneous solvents, it stands on shaky foundations when applying it to inhomogeneous systems containing, for instance,

macromolecular cosolvents. Therefore, in the case of water/dextran mixtures Lavalette et al. distinguish between macroscopic and microscopic viscosities where the latter is found to be of particular importance for the diffusion of proteins, since they are mainly exposed to the solvent showing low viscosity [215,216]. When comparing the observed diffusion coefficient of BSA in the dextran-phase to the results of Lavalette et al., who studied the translational diffusion of BSA in a similar macromolecular environment, very good agreement is found (within 10%) [215]. Estimating the diffusion coefficients in the dextran-phase based on the measured viscosity and the Stokes-Einstein relation reveals a considerable discrepancy with the values given in Table 10-1. This, however, signals the breakdown of this relation in complex environments rather than inconsistencies in the investigated data.

Since the diameter of BSA is larger than that of ovalbumin [214,217,218] one would intuitively expect a lower diffusion coefficient of BSA compared to the one of ovalbumin. But for the high concentrations of polymeric macromolecules used in the experiments it is observed that the relation between the diffusivities of the two proteins is reversed. The reason for that is probably that the interactions between the proteins and the dissolved polymers are different from the protein-solvent interactions which manifests itself in changing transport properties when a protein is more likely to closely encounter polymer chains at higher concentrations. Furthermore, the three-dimensional structure of the proteins may have an influence on their diffusion behavior, since BSA displays a rather convex elongated shape, whereas ovalbumin consists of two sub-domains [219].

### 10.6.2 Protein Diffusion Across the Interface

After the ATPS showed a stable and sharp phase boundary located in the middle of the channel, the flow was frozen as described above. Again, pictures have been taken within certain time intervals recording the mass flux of the fluorescent proteins, cf. Fig. 10-4. Since the location of the phase boundary sometimes changed within a certain range (up to 20 µm) during the experiment, all subsequent evaluations were performed relative to its actual position, i.e. the phase boundary was assigned to a position $x = 0$, cf. Fig. 10-4. The shift of the interface is possibly due to the fact that it does not appear completely straight after the lamellae have been formed inside the channel, so subsequently the residual curvature smoothes out.

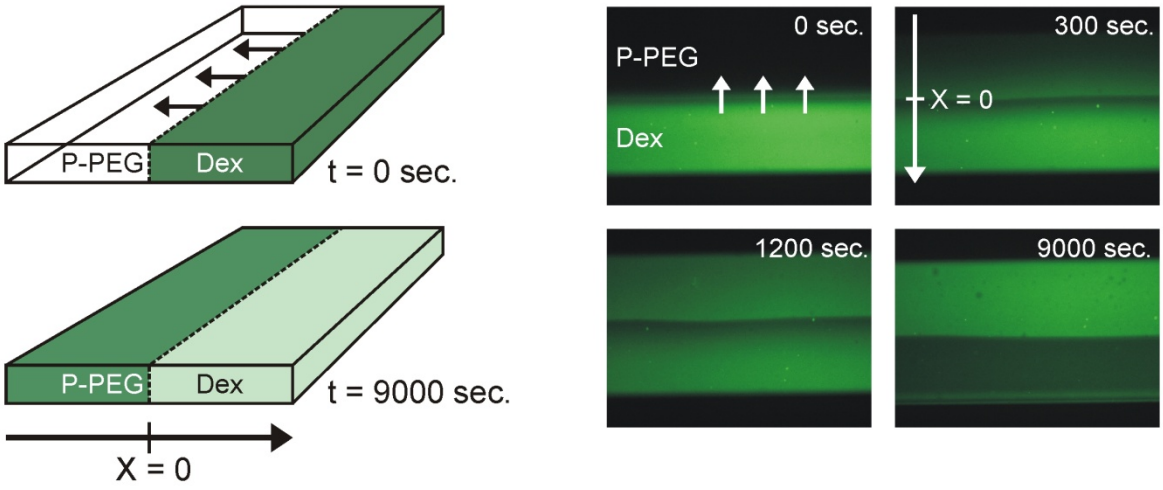


*Fig. 10-4: Diffusion of BSA across the phase boundary. Left: schematic of protein diffusion. The boundary itself was always identified with x = 0. Right: fluorescence intensity related to the protein distribution at various points in time after the flow has been stopped.*

Again, owing to the above mentioned reasons, the integral of all profiles has been normalized. Moreover, because artifacts, such as intensity peaks, were observed close to the channel walls (minimum and maximum $x$ coordinate) in some cases, a subset of the experimental data had to be discarded. To this end margins of 50 µm were defined close to the channel walls which were not included in the subsequent analysis steps. The origin of which can be traced back to the filling process at the beginning of the experiment. It has been observed that at the beginning of the filling process the two-lamellae flow structure is not fully developed in some cases. Accordingly, sometimes one phase, either the P-PEG- or the dextran-phase, touches the opposite wall and is deposited as a thin film occupying small regions near the channel edges. In this case, the film can get visible at the end of the experiment, cf. Fig. 10-4 - 9000 sec. However, the corresponding intensity peak constitutes less than 1% of the total integrated fluorescence intensity and should therefore only have a minor influence on the overall mass balance. Furthermore, in order to allow for a clear comparison between experimental data and model results, scattering of the former has been removed by smoothing using a Fast-Fourier-Transform filter [220]. Data oscillations with wavelength below about 14 microns have been neglected.

Another possible problem that may corrupt the analysis of experimental data is protein adsorption to the channel walls. However, because of the high PEG concentration in the microchannel the adsorption of BSA to the PMMA surface is strongly suppressed. Thus and as mentioned above PEG is also often used for dynamic wall coatings to prevent protein adsorption during polymerase chain reaction [26,221]. In order to quantify the amount of protein adsorbed to the channel walls, the channel was flushed with pure water after each experiment and a fluorescence image with the same camera settings was taken. These images showed no significant fluorescence emission at all. For comparison, a PMMA channel was flushed with BSA dissolved in water not containing any PEG. When removing the BSA solution after 30 minutes, the channel surface showed a strong adsorption of BSA molecules visualized by fluorescence emission, cf. Fig. 7-2.

Comparisons between the experimental data and the model results for BSA and ovalbumin are shown in Fig. 10-5. At first sight the experimental results shown in Fig. 10-5 look similar to the concentration profiles reported by Baumann and Mühlfriedel, who studied the mass transfer of rhodamine B across the phase boundary of water and butanol [211]. Yet, in contrast to the present study the authors find a rather smeared out concentration profile close to the interface, where the concentration ‘jump’ extends over a range of above 1 mm. Moreover, equilibrium partitioning is not found to be attained in the course of their experiments. Therefore, the authors conclude that mass transfer is not solely governed by the classical theories. Here, however, a good overall agreement between experimental data and simulation based on the conventional theory is found. As mentioned above, the partition coefficients are deduced from the plateaus of the concentration profiles of the last experimental time step, while the diffusion coefficients are derived from the single-phase measurements. Thus, the numerical approach does not contain any free parameters that could be adjusted to fit the experimental data for the two-phase system.

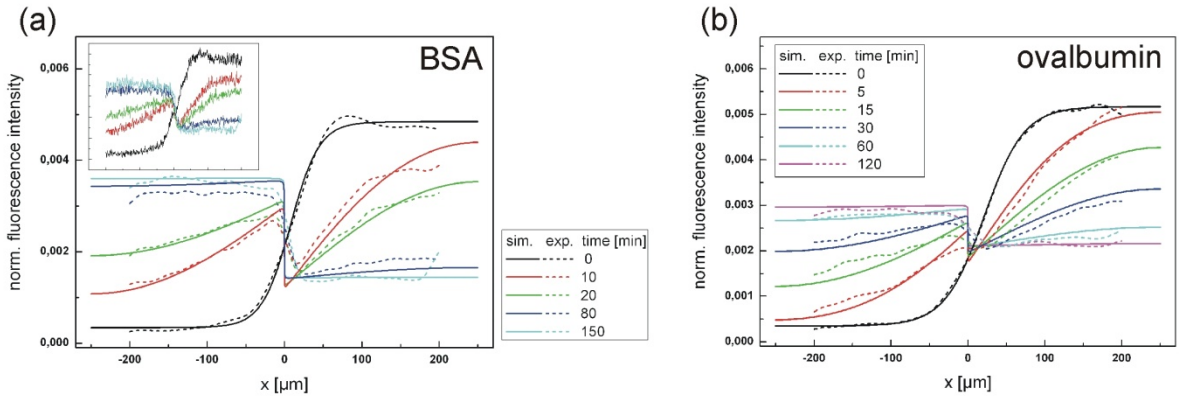


*Fig. 10-5: Intensity profiles of BSA (a) and ovalbumin (b) diffusing across the phase boundary from the dextran-phase into the preferred P-PEG-phase. Dashed lines denote the smoothed experimental data, solid lines the model results for $k_{BSA}$ = 2.53 and $k_{oval}$ = 1.42, respectively, and the diffusion coefficients given in Table 10-1. As an example, the inset in (a) shows raw data of the recorded intensities.*

One of the most striking differences between the model results and the experimental data is the fact that the concentration jump across the interface predicted by the model is smeared out in the experiments. Note that this effect is not significantly affected by the performed smoothing. The reason for the smeared out jump can be assigned to an expected curvature of the phase boundary inside the microchannel in combination with the integral view of the experiment. A difference in the wettability of the wall material with both phases leads to a contact angle different from 90° and thus implies a curved phase boundary, cf. Fig. 5-2. Within independent measurements the contact angle α: dex-phase/P-PEG-phase/PMMA was determined as 132° on average (contact angle instrument G-1, Krüss GmbH, Germany). Due to the low protein concentration and the fact that no significant adsorption of BSA or ovalbumin onto the surface was observed in either phases, the contact angle measurements were carried out without proteins. Hysteresis effects have been determined to be in a range of about ± 20° (estimated from advancing and receding contact angle measurements of single droplets (liquid/solid/air) of each aqueous phase; contact angle instrument DSA 100, Krüss GmbH, Germany). Since the contact angle is considerably larger than 90° every fluorescence image taken from the phase-boundary area actually comprises a mixture of both P-PEG- and dextran-phase within a range of about 4.9 – 15.0 µm, depending on the actual contact angle and possible pinning effects, as shown in Fig. 10-6.

Yet, apart from the differences close to the phase boundary which are probably due to curvature effects neglected within the chosen 1-D approach, both the experimental and the theoretical curves show a very similar behavior. Most importantly, an influence of the phase boundary on the transport of proteins, due to a possible potential-energy minimum or electric field, is not visible.

While the chosen approach does not allow resolving the concentration fields in the close vicinity of the interface in detail, an additional transport resistance would manifest itself as a slowing down or speeding up of the overall mass transfer. Specifically, it would lead to reduced or increased concentration levels in the P-PEG-phase compared to the model predictions.

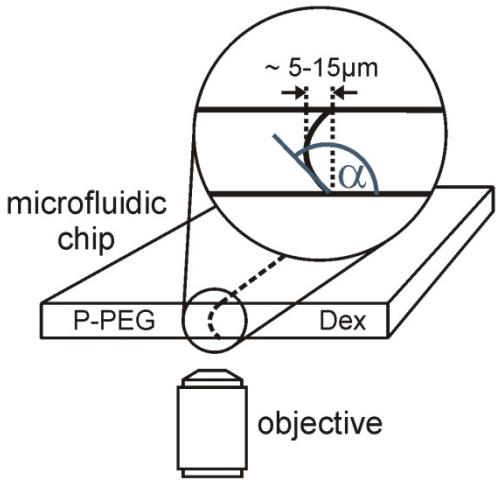


*Fig. 10-6: Deformation of the phase boundary inside the microchannel.*

Such effects are not seen in Fig. 10-5, leading to the conclusion that within the accuracy of the experiments performed, the model of Eqs. (10.6) to (10.8) is adequate to describe the mass transfer of the studied systems of proteins within ATPSs.

The partition coefficients deduced from the experiments, viz. $k = 2.53$ for BSA and $k = 1.42$ for ovalbumin, have been corroborated by independent equilibrium measurements. The respective differences in chemical potential are about 1 for BSA and about 1/3 for ovalbumin, in units of the thermal energy $k_bT$. Moreover, it has to be stressed that the good agreement between the experimental and simulated data sets is only obtained for the diffusion coefficients given in Table 10-1. The simulated concentration profiles are observed to depend sensitively on the underlying diffusivities. A change of their values in excess of 20% leads to a noticeable reduced agreement between both data sets.

## 10.7 Conclusion

In this chapter a detailed and important study of the diffusive transport of proteins across a phase boundary within an ATPS has been presented. Experiments with a microfluidic system have been performed in which a bilaminated configuration of two liquid phases containing P-PEG and dextran is formed. Initially, proteins with attached fluorescence markers are dissolved in one of the phases and subsequently diffuse into the other. The corresponding concentration profiles as a function of time were recorded using a fluorescence microscope. The profiles were compared with model results based on the numerical solution of the diffusion equation in both phases. The model only incorporates the phase-specific diffusion constants and the difference in chemical potential between the phases.

ATPSs are widely used for separation and purification of proteins, but it seems that the details of protein mass transfer between the two phases have not been studied so far. In a hypothetical scenario, the phase boundary itself acts as a potential-energy minimum for molecules or particles in its vicinity. Alternatively, electric fields close to the interface could have an influence on molecular transport. Such scenarios would usually lead to a slowing down of the diffusion processes from one phase to the other. A comparison of experimental and simulation data suggests that such local effects related to the phase boundary can be neglected for the systems under investigation. Rather than that, the diffusive mass transfer between the phases is governed by the diffusion dynamics within the bulk phases and the difference in chemical potential between the phases. These processes have been included in the simulation model

that allows to reproduce the experimentally derived concentration profiles with reasonable accuracy. The fact that no local effects of the phase boundary on protein transport could be identified could have several reasons. On the side of wetting forces leading to protein adsorption, the contact angle of the two-phase system could deviate noticeably from 90°, thereby reducing the adsorption energy to values significantly below the thermal energy scale [199]. It should be noted that such an argument is only relevant in a scenario where the very concept of wetting is meaningful at all. If, however, the extension of a phase boundary between two liquids is of the same order or larger than the diameter of the molecule considered, wetting ceases to be a meaningful term. With a molecular diameter of BSA of about 10 nm and phases containing large polymer chains, this could be the case. To the best of knowledge, no experimental evidence on both, the contact angle of proteins in ATPSs and the spatial extension of the liquid-liquid interface, exists. Therefore, the current state of affairs does not allow drawing any specific conclusions on the role of wetting forces on protein adsorption at the interface. On the side of electrostatic forces due to electric double layers, a similar size effect involving the lengths scales of the protein and the double layer could play a role. The concept of a charged molecule experiencing a force within a Debye layer is only meaningful if the molecule is smaller than the thickness of the layer. Again, due to the comparatively large size of the proteins considered, such a picture may easily break down but will be further discussed in chapter 11.4 in more detail.

The absence of sophisticated local effects due to the phase boundary promotes the practical applicability of the computational model developed here. A model, based on the above findings, for the dynamics of protein mass transfer could be important to better understand and optimize many separation and purification processes in ATPSs. For an efficient process not only the equilibrium configuration itself is important, but also how fast this equilibrium is reached.

Although the diffusive transport of proteins across the phase boundary of ATPSs are not significantly influenced by the boundary itself, active enrichment and separation of biomolecules at and by utilizing the phase boundary are still possible and will be presented in the following chapters.

# 11 Active Transport and Enrichment of Proteins

*Basically, this study aims at the exploration of a new class of methods for electrophoretic separation and enrichment of biomolecules in a system of stratified layers. In the previous chapter the diffusion behavior of proteins was examined. It is found that the diffusive transport of proteins across the phase boundary of ATPSs is not significantly influenced by the boundary itself but primarily depends on the chemical potential of the protein in each phase. Here, in this chapter the active transport of proteins by an electric field is described showing that under certain circumstances such an additional force helps to induce a new principle of continuous enrichment of biomolecules.*

## 11.1 Introduction

In contrast to organic-inorganic two-phase systems, for a binary system made of aqueous solutions of PEG and dextran, an electric field can be easily employed to transport the sample molecules perpendicular to the phase boundary since both phases have a similar electrical conductivity. An additional advantage is that the biocompatibility is essentially ensured since both phases largely consist of water.

As already described above, the application of dialysis membranes as well as of gold electrodes deposited on the main channel walls show several disadvantages. Hence, all following transport experiments using electric fields are carried out with the microfluidic setup incorporating gel electrodes as a decoupler.

The aim of the active transport experiments is to investigate how the electrophoretic motion of a protein is influenced by the phase boundary and the difference in (electro) chemical potentials $\Delta\mu$. The series of experiments starts with the standard ATPS (type A) showing a moderate partitioning coefficient and accordingly a moderate $\Delta\mu$. After a detailed description of the transport behavior of proteins in this standard two-phase system giving an introduction into such kind of transport experiments, modified ATPSs are introduced showing an increased $\Delta\mu$ and leading to obvious enrichment effects of proteins directly at the phase boundary.

## 11.2 Standard Aqueous Two-Phase System

In the first experiments fluorescence labelled BSA molecules are dissolved in the dextran-phase of the standard system (type A), as shown in Fig. 11-1. If the system is based on a potassium phosphate buffer at low pH values, the BSA molecules prefer the dextran-phase, while the transport into the PEG-phase is retarded. By contrast, if the BSA molecules are first dissolved in the PEG-phase the gradient in the chemical potential leads to an increased mass flux into the preferred dextran-phase without any observed hindrance at the phase boundary. These phenomena indicate a pronounced asymmetry of the protein mass flux between the two phases which has already been discussed in chapter 10 in more detail.

In the first experiments BSA was initially dissolved in the preferred dextran-phase. The two different phases are injected into the microchannel, cf. Fig. 11-1. An equilibrium time is needed because first the channel is completely filled with the PEG-phase and afterwards the dextran-phase lamella is injected. Owing to the small flow rates during the experiments, typically 0.05 ml $h^{-1}$ in case of the PEG-phase and 0.01 ml $h^{-1}$ in case of the dextran-phase, it takes some time until the final three-lamella arrangement is fully developed over the complete channel length. After approximately ten minutes of equilibration time allowing the system to become stable and form equal lamella widths, the images were recorded with the CCD camera setup, cf. Fig. 6-1.

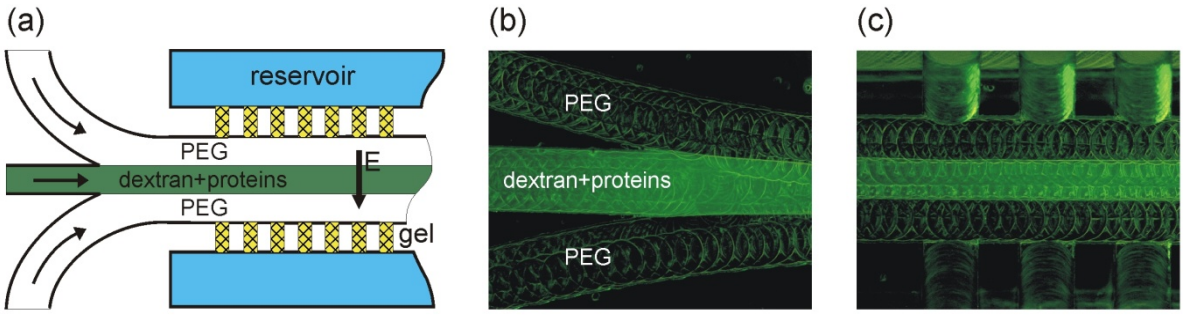


*Fig. 11-1: (a) Setup of the microfluidic chip in case of ion bridges made of gel. Proteins are dissolved in their preferred phase, here dextran-phase, and injected into the main channel (b). The fluorescence intensity of the proteins is superimposed on a transmitted-light image showing the phase boundaries. As soon as the protein solution reaches the gel channels their movement can be influenced by an adjustable external electric field (c).*

The first image was recorded while the electric field was switched off. Afterwards, an electric field is applied and increased stepwise. The next images are recorded five minutes after each increase of the electric field strength, allowing the system to respond to the electric field change. All images are taken 30 mm downstream of the confluence of the three feed streams, close to the exit of the channel.

Up to approximately 2.5 $V_{dc}$ the majority of BSA molecules is confined within the dextran-phase but move towards one of the phase boundaries to the neighboring PEG-phase, depending on the direction of the applied electric field. This leads to a non-uniform fluorescence intensity distribution across the dextran lamella and a (low) enrichment at the respective phase boundary, cf. Fig. 11-2.

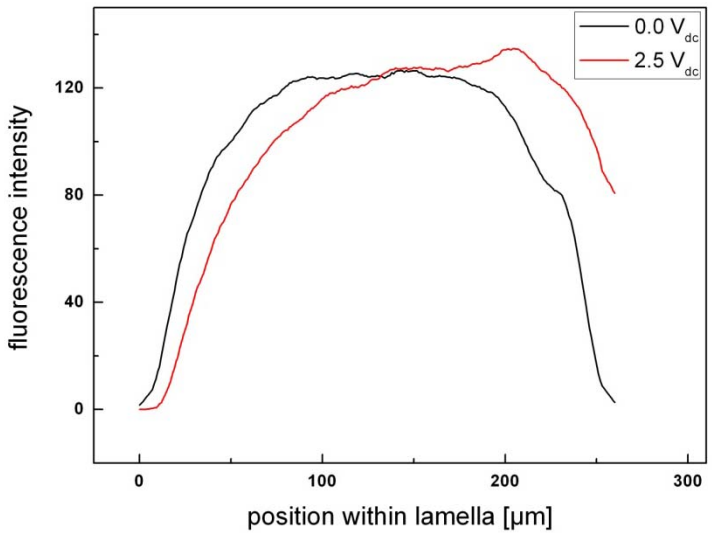


*Fig. 11-2: Fluorescence intensity (smoothed) across the dextran-phase lamella. In order to smooth out noise, an average over 15 neighboring data points was taken. The phase boundaries to the PEG-phase are located at x-values 0 and 220 µm, respectively. At 0.0 $V_{dc}$ the fluorescence shows a uniform distribution with a fall-off towards the phase boundaries. At 2.5 $V_{dc}$ the BSA molecules move towards one phase boundary which leads to a shift of the intensity curve depending on the electric field direction. Buffer: potassium phosphate, 5 mM, pH 7.0.*

The bell-shaped curve obtained at 0 $V_{dc}$ with a fall-off towards the fluid interfaces can be explained by assuming a diffusive mass transfer into the neighboring phase. Thus, the initially rectangular concentration profile is smeared out by diffusion, which is, however, so slow that it does not lead to a significant depletion of the dextran-phase within the times considered here. In addition, it has to be pointed out that only after reaching a voltage value of approximately 1.6 $V_{dc}$ a significant electric field is present. Below this value the electrodes placed in the reservoirs are almost completely shield by a double layer. Accordingly, only after exceeding this value, an active transport induced by electrophoresis is expected.

In order to investigate not only the active transport of proteins within its preferred phase but also across the phase boundary the field strength was further increased by applying a voltage of more than 2.5 $V_{dc}$ with the result that the proteins increasingly overcome the phase boundary, cf. Fig. 11-3.

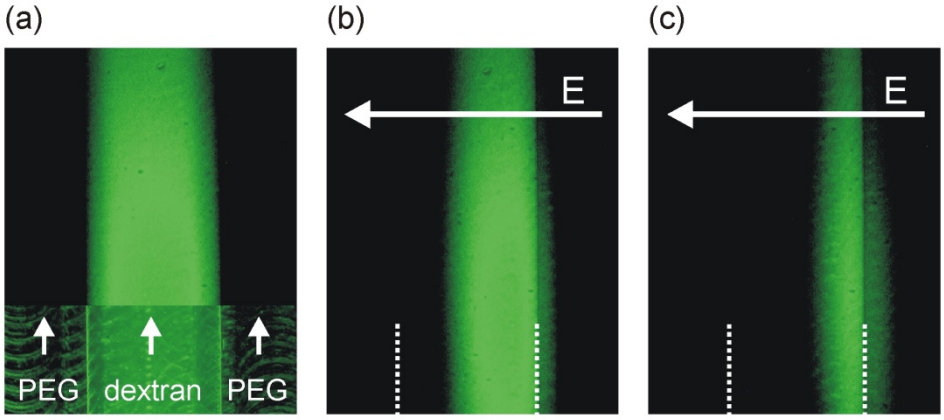


*Fig. 11-3: (a) Uniform distribution of BSA within the dextran-phase without electric field; upper part: fluorescence intensity, lower part: fluorescence intensity superimposed on transmitted-light image showing the phase boundaries. (b)-(c) Proteins concentrate at the right phase boundary under applied voltages of 3.5 and 4.5 $V_{dc}$. For 3.5 $V_{dc}$ a small number of BSA molecules have already overcome the boundary. At 4.5 $V_{dc}$ most of the molecules have left the preferred dextran-phase. The inhomogeneous intensity of the fluorescence light source leads to a reduction of fluorescence intensity at the top of the picture. Buffer: potassium phosphate, 5 mM, pH 7.0.*

Fig. 11-4 shows the average fluorescence intensity (averaged over the width of the dextran lamella) at the observation point close to the exit of the channel as a function of applied voltage. The data points recorded in the experiments are displayed together with fitting functions of the form

$$y = A_2 + \frac{A_1 - A_2}{1 + 10^{(x - \log x_0)}} \qquad (11.1)$$

(lines) where x represents the applied voltage. At small voltages a plateau is formed showing that less proteins penetrate the phase boundary. When the voltage is increased, the average fluorescence intensity in the dextran-phase shows a steep decrease and finally levels off at a value close to zero, indicating that virtually all of the molecules have been transferred to the PEG-phase. It should be emphasized that the slope in Fig. 11-4 indicating a decreasing fluorescence intensity does not necessarily reflect the equilibrium of the system, but depends on the kinetics and speed of the transition of proteins between the two phases.

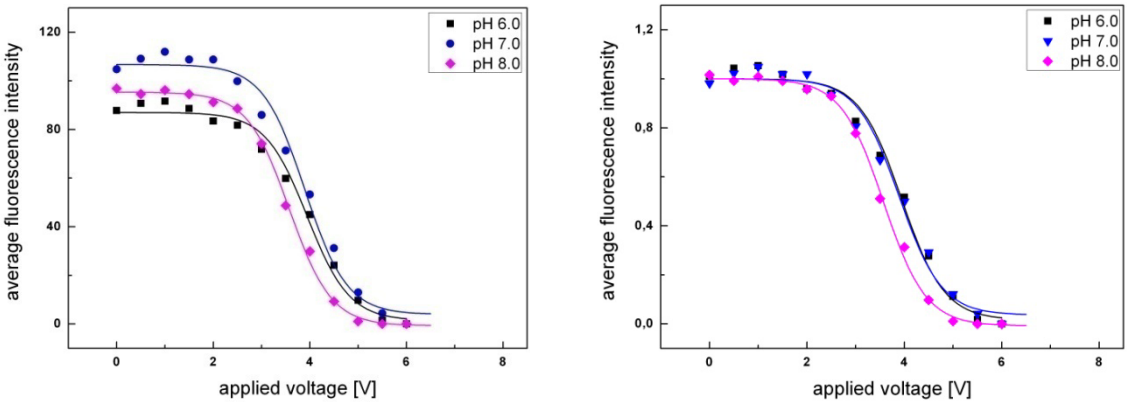


*Fig. 11-4: Left: Average fluorescence intensity within dextran-phase. The intensities of all pixels of a line within the lamella were added and divided by the number of pixels to eliminate influences from variations within the lamella width. Right: Normalized intensity curves with all data divided by their values at U = 0 $V_{dc}$. After a voltage of about 2.5 $V_{dc}$ is reached, the BSA molecule start to penetrate the phase boundary.*

Owing to the finite residence time in the microchannel, only the fraction of proteins remaining in the dextran-phase after a specific time span is recorded. In fact, measurements conducted at reduced flow rates indicate that the decrease of fluorescence intensity shown in Fig. 11-4 occurs at a slightly smaller voltage. This suggests that the recorded data do not reflect an equilibrium situation, but a dynamic process which shows a nonlinear behavior as a function of the applied voltage. These experiments have been performed at three different pH values, pH 6, pH 7 and pH 8. The isoelectric point of BSA lies at a value of approximately pH 4.7. Therefore, the pH variations leave the sign of the protein charge unchanged. Rather than studying the influence on the protein charge, the pH variations were done to examine a possible influence on the transport barrier between the phases, since it is known that the double-layer potential at the phase boundary is a function of pH [107,108]. When normalizing the intensity curves as done in the right part of Fig. 11-4, apparent differences between different pH values disappear. The conclusion has to be drawn that the electrophoretic transport of BSA across the phase boundary is largely independent of pH, at least in the range between pH 6 and pH 8. Deriving a pH-dependence from the curves in Fig. 11-4 seems to be without support, since for the microfluidic chip used here (predecessor to the chip presented in chapter 7) the gel preparation process in each experiment may lead to slight differences in size of the gel barriers and by that to different electric field strengths within the main channel at the same applied voltage. Due to this fact, the voltage drop across the channel may vary slightly although the applied overall voltage is the same.

To compare the active transport behavior of the proteins in the reverse direction BSA was also initially dissolved in the non-preferred PEG-phase. As mentioned before, the proteins easily diffuse into the dextran-phase after the two phases get in contact. An additional electric field leads to an enhanced and directed transport into the preferred dextran-phase. This additional electrophoretic migration across the phase boundary starts immediately when the E-field is switched on and leads to a rapid decrease of fluorescence intensity within the PEG lamella, also at low voltages, cf. Fig. 11-5.

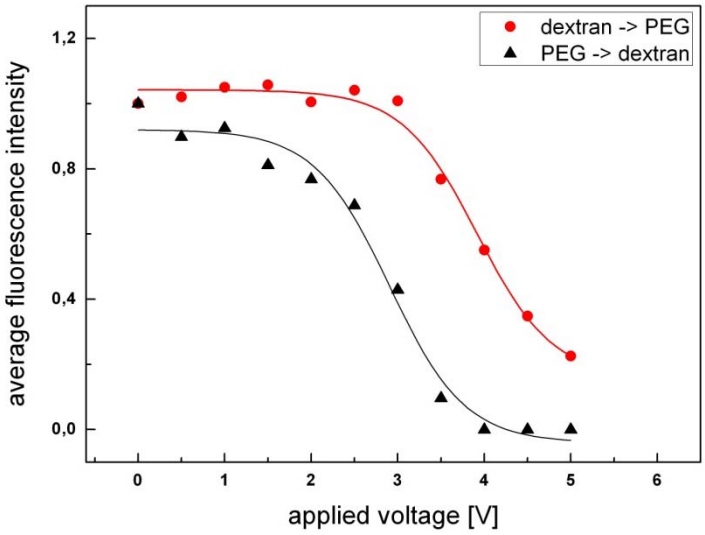


*Fig. 11-5: Comparison of fluorescence intensity of BSA within the lamella into which BSA is injected. PEG→dextran: BSA is injected in the non-preferred PEG-phase. By applying an electric field the proteins rapidly leave the phase and penetrate the phase boundary without any hindrance. Dextran→PEG: BSA is injected in the preferred dextran-phase, the phase boundary impedes protein transport. Only when a voltage of about 3.0 $V_{dc}$ is reached, the BSA molecules increasingly penetrate the phase boundary. Buffer: potassium phosphate, 5 mM, pH 7*

It is straightforward to check the potential of the setup described above for protein separation, which, in its most general form, is based on exploiting different protein properties, such as protein size, its hydrophobicity, or its isoelectric point. In order to examine if there is any dependency on the type of protein, the experiments on electrophoretic transport in PEG/dextran systems were performed with different proteins. In addition to bovine serum albumin (BSA, 66 kDa), protein samples of beta-galactosidase (116 kDa) and carbonic anhydrase (29 kDa) were examined.

Similar to the observed behavior of BSA, the other protein types also display a higher affinity to the dextran-phase. This means that if the proteins are injected into this phase they hardly leave it by diffusion. After applying an electric field all tested protein species show a movement and redistribution within the dextran-phase, but still no increased movement across the phase boundary itself as long as the field strength stays below a certain threshold value. For a specific voltage range the average fluorescence intensity (averaged over a dextran lamella) stays at a constant level until the proteins start to leave the preferred phase and penetrate into the PEG-phase. This finally leads to a decrease in fluorescence intensity. Of course, because of their charges all types of proteins will start to leave the dextran-phase sooner or later. Remarkably, however, in the case of the PEG/dextran system, all protein species start to overcome the phase boundary within nearly the same voltage range of about 2.5-3.0 $V_{dc}$. Only in the downward slope there seems to be some difference between the different protein types, cf. Fig. 11-6.

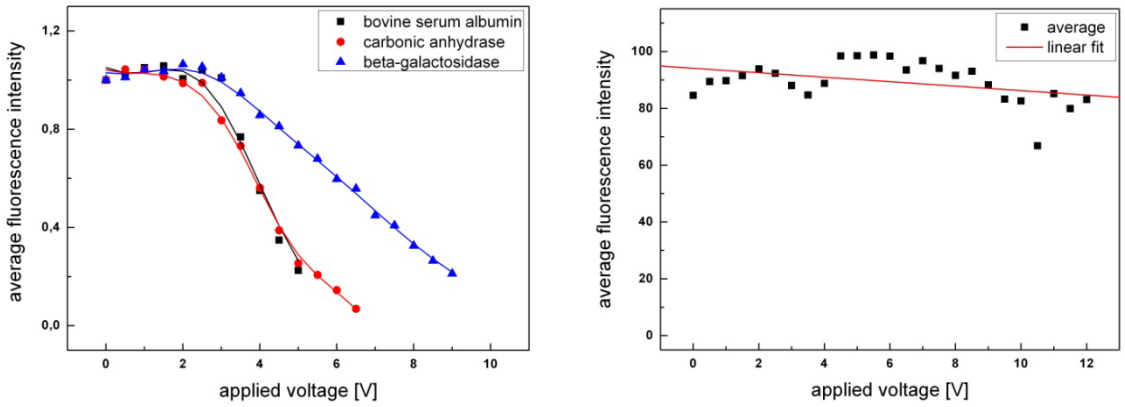


*Fig. 11-6: Left: Comparison of the fluorescence intensity of different proteins, which are injected in the preferred dextran phase. A notable transport of proteins into the PEG-phase is observed for applied voltages of about 3 $V_{dc}$ and above. Right: Fluorescence intensity of BSA molecules dissolved in a buffer system at the isoelectric point of BSA. Due to the small net charge most of the molecules will stay within the initial phase, also at high applied voltage values.*

Thus, it could be speculated that the observed behavior has to be attributed to a quite universal mechanism dominating the transfer of molecules between the phases. Since all of the studied proteins have a higher physico-chemical affinity to the dextran-phase compared to the PEG-phase, this difference in chemical potentials itself retards transport by diffusion or electromigration. This explains the protein behavior that was discovered by Levine et al. [80] during an active transport from the preferred into the non-preferred phase leading to an enrichment of proteins at the phase boundary. However, measured protein partition coefficients in ATPSs [222] suggest that the proteins under study possess different chemical potential barriers. Therefore, it can be further speculated that the transport resistance due to the different affinities to the phases is not the dominant effect. The most natural explanation for the "universal" shape of the fluorescence intensity curves could be, for example, the formation of an electric double layer at the phase boundary. As already mentioned and discussed by several authors [104,107-110], the ions of the buffer solution will usually have different affinities to the two different aqueous phases. Consequently, they partition between the phases, resulting in charge separation and the formation of an electric double layer at the phase boundary. In this double layer an electric field can be formed in such a way that it opposes the transport of proteins from the dextran to the PEG-phase. Since the electric-double layer potential difference is the same for all protein species, the corresponding transport resistance would be the same, thus possibly offering an explanation for the observed "universality" of the curves in Fig. 11-6. Additionally, this would be consistent to the observations of Theos et al. [78]. They have found evidence of protein accumulation at the phase boundary in systems with phosphate buffer, known to provide a significant electric double-layer potential (1.5 to 2.2 mV, depending on the pH value) [107,108]. An interfacial accumulation was not observed for, e.g., Tris/Bes buffer with a low double-layer potential of 0.3 mV [78].

But the results of the diffusion experiments do not support such an assumption of retardation by a double layer or other possible interfacial effects, see chapter 10. Furthermore, it has to be mentioned that although the partition coefficients $k$ of all three proteins used here in this kind of ATPS are different, the differences $\Delta k$ itself are in the range of ±0.5. Accordingly, the influence of the partition coefficient itself during an active transport across the phase

boundary has been examined in more detail. For this purpose, the two-phase system was modified. The results of the corresponding study are presented in the following section.

Additionally, due to the macroscopic setup of Levine et al. and Theos et al. a quantitative study of this phenomenon was difficult. The use of a microfluidic setup and fluorescence labelled proteins enables a more detailed examination of the influence of the phase boundary in ATPSs on the transport behavior of proteins.

## 11.3 Modified Aqueous Two-Phase System

For a standard ATPS the partition coefficient of, for example, BSA is about $k = 0.5$, i.e. approximately 66% of the initially dissolved amount of BSA is located in the dextran-phase while 33% can be found in the upper PEG-phase. That means, in contrast to cells, see chapter 12, proteins are usually more or less present in both phases. Furthermore, for a standard PEG-dextran system and all examined proteins there was only a minor enrichment of proteins observed during the active transport from the preferred into the non-preferred phase. The resulting fluorescence intensity curves can be interpreted in such way that the protein transport across the phase boundary is dampened and does not allow for an adequate enrichment of biomolecules at the phase boundary. In order to clarify the role of the fluid interface with respect to protein transport, an additional series of experiments were performed with a PEG-dextran system forming again parallel layers in a microchannel. For this purpose and in order to reach higher or lower partition coefficients the aqueous phases were either modified by additional hydrophobic groups, as it has been done in the diffusion experiments, or by varying the molecular weight of the used polymers, as it has been used for viscosity adjustment.

### 11.3.1 Effect of PEG-Palmitate

The effect on the partition coefficient of P-PEG on BSA and ovalbumin is described in chapter 3.5.1, where higher values of $k$ lead to higher mass fluxes. In order to study the influence of palmitate in more detail, partition coefficients of different protein types have been initially determined off-chip by adsorption measurements using a photometer (Biophotometer, 6131000.012, Eppendorf AG, Germany) in combination with micro cuvettes (Plastibrand UV cuvette, 8,5mm, 70-850 µl, 7592, Brand GmbH & Co. KG, Germany). Due to the low protein concentration during the transport processes, also for the off-chip adsorption measurement protein concentrations of 50 µg ml$^{-1}$ have been applied in order to be comparable to experiments on-chip. Different ways are possible to measure the protein concentrations, for example, the direct photometric measurement at a wavelength of 280 nm or using protein assay kits like Bradford (595 nm) or BCA (562 nm). Within a preparatory test series it was found out that for proteins dissolved in PEG-dextran ATPSs the µBCA test, see next paragraph, was the most reliable one. Additionally, the determined values of the partition coefficient by a µBCA test are in good agreement (within 10%) with $k$ values determined from fluorescence pictures of the two-phase systems during diffusion experiments.

For the µBCA test the proteins were initially dissolved in the PEG-phase (or P-PEG phase) with the concentration adjusted to 100 µg ml$^{-1}$. Subsequently, the PEG-phase was mixed with the dextran-phase (one to one) leading to a final concentration of 50 µg ml$^{-1}$. The resulting solution was vortexed and allowed to settle overnight. After 12 hours 50 µl of either the top or the bottom phase was mixed with 1 ml of the BCA working reagent (BCA protein assay kit, 23225, Pierce Biotechnology, Inc., USA) and treated for 30 minutes at 37°C. Afterwards, 200 µl of the solution were transferred into micro cuvettes and analyzed by the photometer (measuring method: ‘BCA micro’ for low concentration range). For control purposes, it was

determined that the difference between the partition coefficients of proteins which are initially dissolved in the dextran-phase and afterwards mixed with the PEG-phase compared to those partition coefficients which are realized the other way round, first dissolving the proteins in the PEG-phase, is negligible (< 4%) and within the error of measurement. The values of the partition coefficient measurements are summarized in Table 11-1. In case of the more hydrophobic proteins, e.g. bovine serum albumin or hemoglobin, the presence of palmitate leads to a significant increase of the partition coefficient and to a high preference to the P-PEG-phase.

| Protein | *k* Standard system | *k* P-PEG system 10% |
|---|---|---|
| Bovine serum albumin | 0.69 | 2.53 |
| Ovalbumin (chicken egg) | 1.11 | 1.42 |
| Conalbumin (chicken egg) | 0.58 | 0.55 |
| Hemoglobin (bovine) | 0.39 | 8.85 |
| β-Lactoglobulin (bovine) | 0.78 | 2.65 |
| α-Chymotrypsinogen A (bovine) | 1.08 | 1.12 |

*Table 11-1: Partition coefficients of proteins dissolved in the standard (type A) and P-PEG (type B) ATPS.*

For a better illustration of the effect of P-PEG, Fig. 11-7 shows three reaction tubes with BSA dissolved in a standard two-phase system, a system where PEG 8000 was only replaced by PEG 6000 as well as in a P-PEG system (P-PEG 6000).

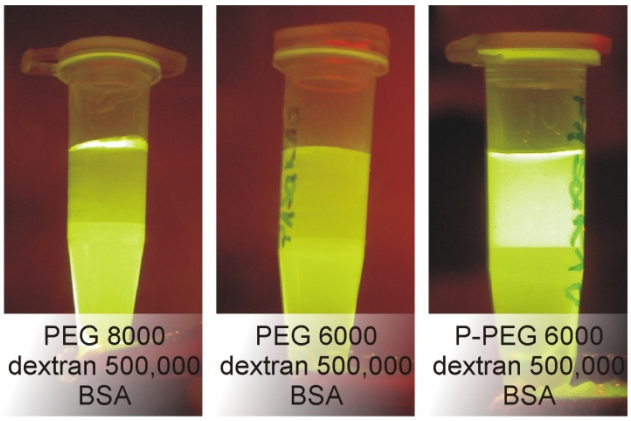


*Fig. 11-7: Left: The affinity of BSA to the lower dextran-phase is slightly higher compared to the PEG-phase. Center: Due to the reduced molecular weight of PEG the affinity to the PEG-phase increases. Right: Since BSA offers hydrophobic side chains the affinity to the P-PEG-phase is strongly increased. Lower: Chemical structure of P-PEG.*

In case of the latter one most of the BSA molecules can be found in the upper P-PEG phase whereas changing the molecular weight of PEG from 8000 to 6000 has only a minor effect in increasing the affinity to the upper PEG-phase. However, again a three lamellae arrangement was examined where the phase of higher affinity, P-PEG, was placed in the center. The molecules, BSA (exemplary), were initially dissolved in their preferred P-PEG-phase and injected into the main channel. Fig. 11-8 shows the difference between the transport behaviors of BSA in a standard system compared to a P-PEG system. Again, all images were taken close to the exit of the channel, 30 mm downstream of the confluence point of the three feed streams. In case of the standard system and without an electric field, observable diffusion across the phase boundary takes place. Applying a voltage of 4 $V_{dc}$ most of the BSA molecules have left their initial phase without showing a significant enrichment at the phase boundary. Accordingly, the phase boundary itself seems to have only a minor transport resistance effect.

By contrast, in case of a higher partition coefficient of BSA not only the transport by diffusion is reduced but also the transport across the phase boundary. Additionally, the fluorescence images show an intensity peak directly at the boundary revealing an enrichment of molecules by a factor of approximately 1.4, cf. Fig. 11-9. A higher value of enrichment by increasing the portion of P-PEG (more than 0.44%, cf. Table 3-1) was not achieved since also the partition coefficient of BSA only barely changed with the increase of P-PEG concentration. That applies also for other kinds of proteins.

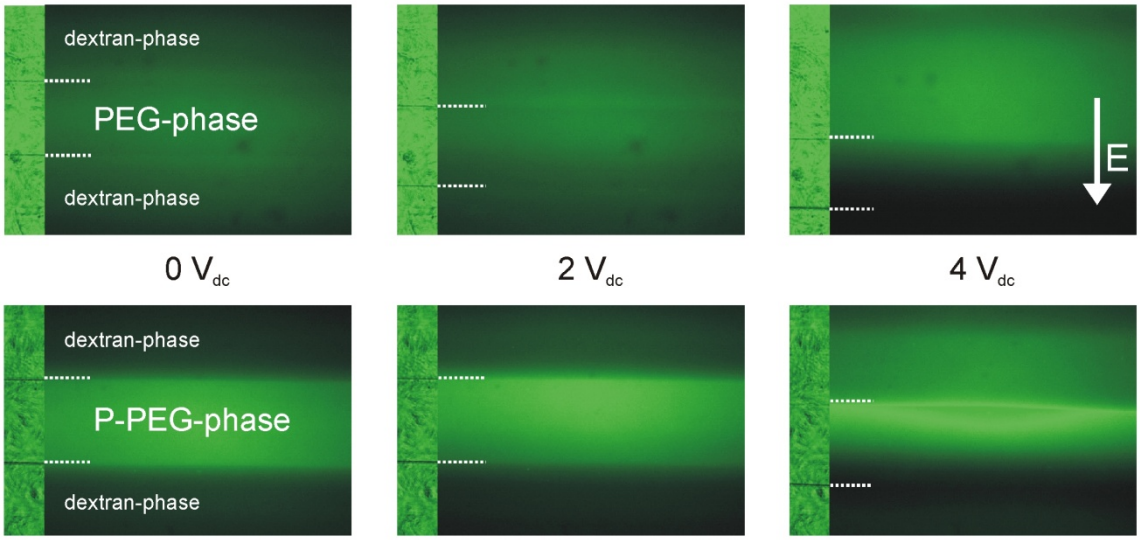


*Fig. 11-8: Effect of P-PEG and the increased affinity to the P-PEG-phase in regard to the transport behavior across the phase boundary.*

Finally, minor increases of partition coefficients compared to the standard system lead to more visible retardation effects at the phase boundary suggesting that neither double layer effects nor an energy minimum directly at the phase boundary determine the active transport of proteins across the phase boundary. This is consistent with the results of the diffusion experiments and their comparison to simulation data. In order to corroborate this finding, the preference to one of the two phases was further increased by changing the molecular weight which is described in the following subchapter.

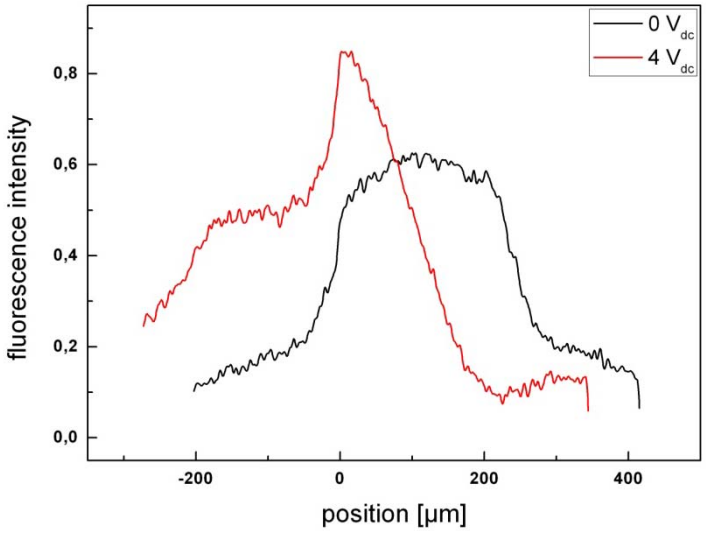


*Fig. 11-9: Enrichment of proteins at the left phase boundary (position = 0) at 4 $V_{dc}$. For comparison the distribution at 0 $V_{dc}$ is also displayed. The intensity curves are smoothed.*

Besides protein enrichment the increased affinity to the P-PEG-phase can also be utilized for protein separation. Therefore, the same arrangement of fluidic lamellae as well as the reduced diffusion out of the preferred phase is combined with the characteristics of proteins at their isoelectric point. As described in chapter 2.1, the net charge of a protein becomes zero at its isoelectric point. Accordingly, the transport induced by an electric field is negligible when using buffer systems at the isoelectric point of the target protein. Such proteins stay in their initial phase while proteins with a different pI can be removed from their initial phase. Fig. 11-10 shows the different transport behaviors of BSA, ovalbumin and hemoglobin at pH 7.

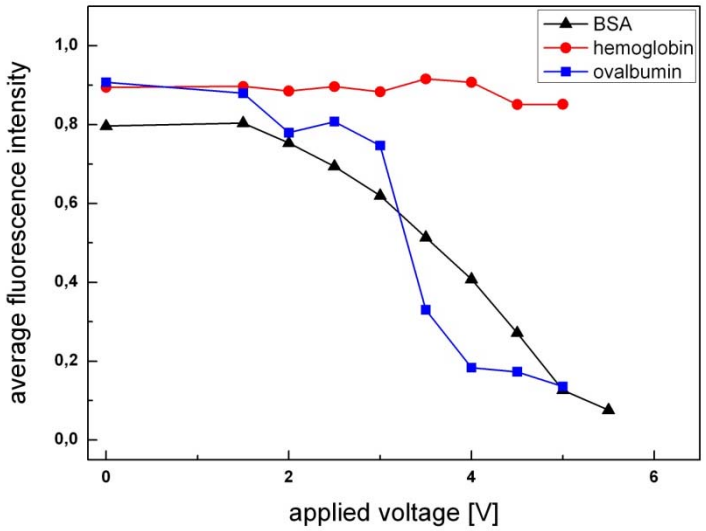


*Fig. 11-10: Transport behavior of different proteins in case of a P-PEG-dextran two-phase system at pH 7.0. Since the isoelectric point of hemoglobin is near to pH 7.0 its net charge is strongly reduced. Accordingly, also its transport behavior induced by an electric field is minimized.*

Also at high electric field strengths hemoglobin molecules (pI 7.1) remain in the P-PEG-phase while BSA and ovalbumin left the P-PEG-phase almost completely. In this configuration, such a system allows a selective and continuous purification of specific proteins and is similar to miniaturized isoelectric focusing (IF) devices [12,44,47,49]. But in case of such IF devices the preparation of the pH gradient within the microchannel is always a challenge. The advantage of using a two-phase system is that no pH gradient is necessary since the target proteins are held back in their lateral position because of their partition coefficient and it can potentially operate continuously.

### 11.3.2 Effect of Molecular Weights

The change of the molecular weight of the used polymers during this study had two reasons. On the one hand, it is possible to reach a viscosity adjustment, i.e. both phases have the same viscosities. By that the velocity gradient close to the phase boundary is reduced and the proteins dissolved in different phases are transported to the outlet with no velocity distortion at the phase boundary. On the other hand the molecular weights of the polymers usually have a strong effect on the partitioning of biomolecules. If, for a given phase composition, one polymer is replaced by the same type of polymer having a smaller molecular weight, partitioned molecules such as proteins will favor more the phase containing the polymer with lower molecular weight [27]. Relating to the standard ATPS, dextran 500,000 is replaced by dextran 10,000 and PEG 8000 is partly replaced by PEG 35,000. The resulting partition coefficients of different proteins and for the system of equal viscosity are summarized in Table 11-2. Virtually all proteins show a high affinity to the dextran-phase. For example, the amount of conalbumin inside the dextran-phase is fifty times higher compared to the amount in the PEG-phase. Also if in case of the ATPS type C the PEG is partly replaced by P-PEG the very high affinity to the dextran-phase remains unchanged. That means that the hydrophobic binding sites have no observable effect on the partition coefficient when dextran of low molecular weight is present.

| Protein | $k$ Standard system | $k$ P-PEG system | $k$ Equal viscosity |
|---|---|---|---|
| Bovine serum albumin | 0.69 | 2.53 | 0.10 |
| Ovalbumin (chicken egg) | 1.11 | 1.42 | 0.06 |
| Conalbumin (chicken egg) | 0.58 | 0.55 | 0.02 |
| Hemoglobin (bovine) | 0.39 | 8.85 | - |
| β-Lactoglobulin (bovine) | 0.78 | 2.65 | 0.08 |
| α-Chymotrypsinogen A (bovine) | 1.08 | 1.12 | 0.66 |

*Table 11-2: Partition coefficients of proteins dissolved in different ATPSs, additionally the data of the system with equal viscosities are given.*

For a better illustration of the effect of P-PEG and changing the molecular weights of the used polymers on the partitioning behavior of the proteins, Fig. 11-11 shows reaction tubes with BSA dissolved in a P-PEG system and in a system with equal viscosities. Furthermore, in case of an active transport across the phase boundary by an electric field the strong modification of the partition coefficients leads to stronger enrichment effects at the phase boundary, as

illustrated in Fig. 11-12. Additionally, the higher affinity of the proteins to the dextran-phase requires a higher electric field to drive the proteins towards the phase boundary and especially across it. Instead of 5-6 $V_{dc}$ for a standard system, where usually all proteins have crossed the boundary, here it needs more than 8 $V_{dc}$ until a significant transport across the boundary is observed. At the optimum of 6.5 $V_{dc}$ a nearly 3-fold continuous enrichment was reached while most of the protein molecules are retained within their initial phase.

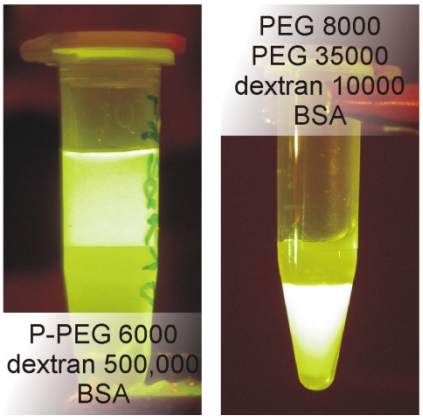


*Fig. 11-11: Left well: The affinity of BSA to the P-PEG is higher compared to the lower dextran-phase. Right: Due to the high reduction of the dextran molecular weight the affinity to the dextran is now drastically increased.*

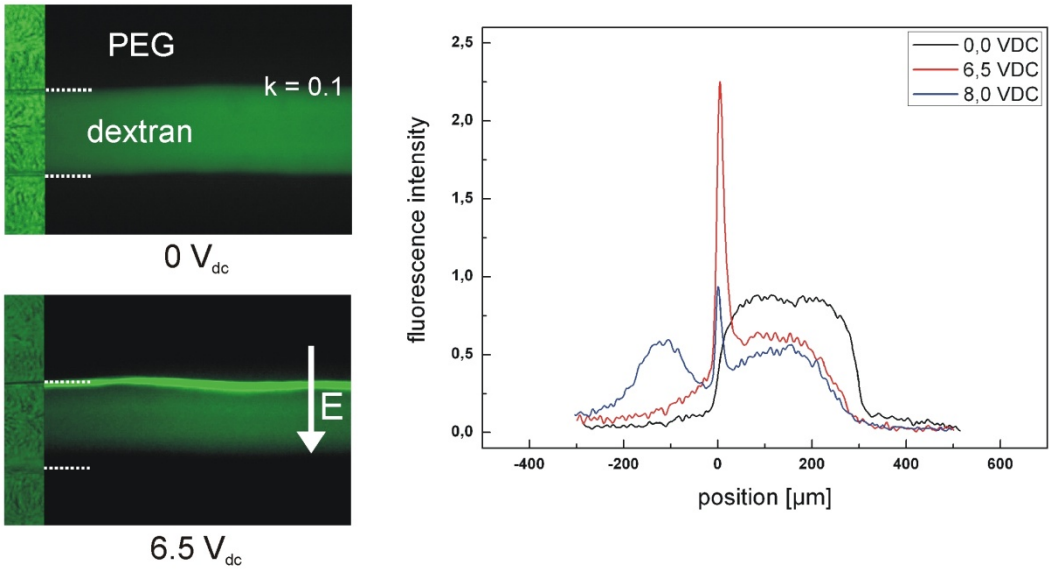


*Fig. 11-12: Enrichment of BSA molecules at the phase boundary of an ATPS of equal viscosity (type C). Right: Fluorescence intensity across the channel width. The upper phase boundary is positioned at 0 µm. At 6.5 $V_{dc}$ the majority of the proteins is pushed towards the phase boundary but kept within the initial phase. At 8.0 $V_{dc}$ the penetration of the boundary is obvious.*

## 11.4 Comparison to Existing Theories and Discussion

In this chapter the experimental results presented above will be compared to results of scientific investigations found in the literature. The forces which may influence the transport behavior of the proteins across a phase boundary are presented and discussed in detail.

The effect of protein enrichment at the interface of an ATPS during electrophoretic transport was first described by Levine and Bier [80] and later by Clark et al. [78,82,83]. Levine and Bier studied the hemoglobin migration through an ATPS and across the interface in a U-tube. They observed that the phenomenon of enrichment was directional and that the migration from the preferred to non-preferred phase yielded an enrichment, whereas migration from non-preferred to preferred phase appeared unaffected by the phase boundary. Accordingly, they concluded that a partition coefficient dependence to electrophoretic migration was caused by the difference of the chemical potential of the protein in each of the phase. Furthermore, they proposed that the electrophoretic transport across the interface can be influenced by modifying the affinity of a protein to a phase. In contrast, Clark et al. [78,82,83] observed that the enrichment of proteins at the phase boundary is controlled by an interface potential (induced by an electric double layer in the vicinity of the phase boundary) and its orientation rather than the partition coefficient.

In this study, the first time a microfluidic system was used to analyze the behavior of biomolecules within an electrical field while passing a phase boundary. Compared to the results of Levine and Bier [80] or Clark et al. [78,82,83] who both used macroscopic two-phase systems, only microfluidic systems allow a detailed examination of the phase boundary. Especially due to the small dimensions and the advantages of the fluorescence technology a quantitative measurement of the protein concentration directly at the phase boundary and its development is possible.

In several points the results of this study are consistent with the results of both groups, Levine and Bier [80] as well as Clark et al. [78,82,83]. Proteins can be transported across the interface of an ATPS in both directions: from preferred to non-preferred phase and vice versa. In all cases the proteins migrate across the interface but, although an interface potential was generally present, enrichment at the interface has only been detected during a forced transport of proteins from the preferred into the non-preferred phase. Protein enrichment during the transport from the non-preferred into the preferred phase was not observed. Additionally, by a strong increase of the affinity to one of the phases the effect of enrichment can be amplified as long as the protein is transported towards the non-preferred phase.

Diffusion is described by the simplest form of Fick's law

$$J_{diff} = -D\nabla c \qquad (11.2)$$

where $D$ is the diffusion coefficient and $c$ the molecule concentration. To combine the flux of diffusion with the electrical effect of an applied electric field the argument is used that the protein velocity $u$ is proportional to the sum of all forces acting on the protein [206]:

$$\begin{pmatrix}\text{protein}\\ \text{velocity}\end{pmatrix} = \begin{pmatrix}\text{protein}\\ \text{mobility}\end{pmatrix}\left(\begin{matrix}\text{chemical}\\ \text{forces}\end{matrix} + \begin{matrix}\text{electrical}\\ \text{forces}\end{matrix}\right)$$

$$u = -\mu_m\,(\nabla\mu + ze_0N_A\,\nabla\phi) \qquad (11.3)$$

where $\mu_m$ is the protein mobility, $z$ the protein charge depending on the pH value of the surrounding solution and $\phi$ the electrostatic potential. For a dilute, ideal solution the chemical potential is given by Eq. (10.1). To rewrite Eq. (11.3)

$$\nabla\mu = \frac{RT}{c}\nabla c \tag{11.4}$$

is combined with Eq. (11.3) resulting in:

$$-u = \frac{\mu_m RT}{c}\left(\nabla c + \frac{c\, ze_0 N_A}{RT}\nabla\phi\right) \tag{11.5}$$

With

$$-\mathrm{J} = -c\, u \tag{11.6}$$

and

$$\mathrm{D} = \mu_m RT \tag{11.7}$$

Eq. (11.3) can be converted to:

$$J = -D\left(\nabla c + \frac{c\, ze_0 N_A}{RT}\nabla\phi\right) \tag{11.8}$$

$$= -D\nabla c - D\frac{c\, ze_0}{k_B T}\nabla\phi \tag{11.9}$$

where the left hand term in the flux equation characterizes diffusion while the right hand term describes electrophoretic motion.

Based on their experimental work [80] Levine et al. later presented a mathematical model of the transport behavior of proteins across the phase boundary driven by an additional electric field [223]. The framework of their calculation is based on Eq. (11.9), the diffusive and electrophoretic transport in a single phase system. In order to apply this equation to two-phase systems two additional boundary conditions have to be added. They are necessary to describe the transport behavior across the interface and are based on [207]. There are two different possibilities which can be taken into account.

One assumption and one possibility as a boundary condition is the instantaneous equilibrium across the phase boundary that was already used for modeling of the diffusive transport. As described in chapter 10.5, the interface is set at $x = 0$. Accordingly, the partition coefficient $k$ at this point (cf. Eq. (10.3)) is described by:

$$k = \frac{c_-^{equ}}{c_+^{equ}} \quad \text{for } x = 0 \tag{11.10}$$

An alternative to this first boundary condition is the assumption of a significant resistance to transport across the interface described by a flux combined with a mass transfer expression:

$$J = \alpha\,(k\,c_+ - c_-) \quad \text{for } x = 0 \tag{11.11}$$

where $\alpha$ [m/s] represents a mass transfer coefficient.

The second boundary condition, which is combined with one of the boundary conditions mentioned above, states that all mass flowing out of one phase must flow into the opposite phase. Accordingly, the fluxes across the phase boundary have to fulfill

$$J_- = J_+ \quad \text{for } x = 0 \tag{11.12}$$

Exemplarily and presented by Levine et al. [223], Fig. 11-13a shows the modeling results of the transport behavior and enrichment of hemoglobin at the interface ($x$ = 0 µm) using Eq. (11.10) as a boundary condition. For the mathematical model initial protein concentrations left $c_{i,-\infty}$ and right $c_{i,\infty}$ from the interface of 0.20 mol m$^{-3}$ and 0.082 mol m$^{-3}$, respectively, were chosen. During the transport experiment in this study, the dextran-phase was sandwiched by two PEG-phase lamellae. The BSA molecules were initially dissolved in the preferred dextran-phase and, for comparison purposes, the experimental results are shown in cf. Fig. 11-13b. With respect to the definition of the partition coefficient $k$ in Eqs. (3.5) and (10.3) and since the PEG and dextran phase have been interchanged compared to the diffusion experiments, $k$ has to be inverted for the interpretation of the figures. The modeling results of Levine et al. [223] using Eq. (11.10) as a boundary condition are qualitatively in good agreement with the experimental results of this study. Also the width of the intensity peak is found to be similar in both curve progressions.

In case of the equilibrium model, enrichment of proteins at the interface only occurs at a transport direction from the preferred to the non-preferred phase. At a partition coefficient $k$ close to 1 no significant enrichment was observed although a potential step at the interface was always present. In contrast, the increase of affinity to one phase leads to higher protein enrichment at the phase boundary.

In case of the resistance model, cf. Eq. (11.11), that includes a mass transfer coefficient, similar simulation results can be obtained [223]. But from the diffusion experiments of this study it is observed that additional effects, which significantly could reduce the diffusive transport of a protein while crossing the interface, are not detectable. That means that the assumption of an instantaneous equilibrium across the phase boundary induced by $k$ is most likely. Accordingly, also a possible transport resistance due to interface potentials seems to be negligible.

In contrast, in the work of Theos and Clark [78] enrichment of proteins at the interface has been found in two-phase systems with an interface potential of 2.2 and 1.5 mV, independent from the direction of transport. That means enrichments have been detected during the transport from the preferred into the non-preferred phase as well as vice versa.

However, it is questionable if such an interface potential can really significantly influence the transport across the phase boundary. This point is discussed in the next paragraph in more detail. Initially, the development of interface potentials in ATPSs is explained. Subsequently, the existence of an interface potential for the ATPSs under study is proven followed by an explanation of the interplay between a protein and an interface potential.

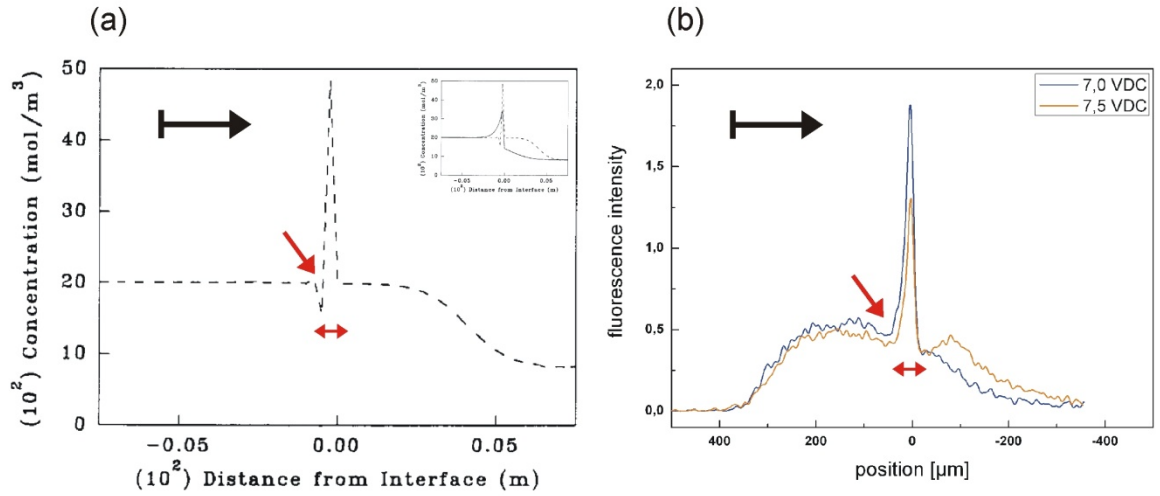


*Fig. 11-13: (a) Simulated concentration profile of hemoglobin (k = 2.44) after 1 min of electrophoresis (from left to right) according to the equilibrium model of Levine et al. [223] (for better visibility further modeling results have been removed). The original figure of the publication is displayed in the upper right corner. (b) Fluorescence intensity profile (smoothed) showing enrichment of BSA molecules moving from left to right driven by an electric field. In both cases, (a) and (b), the width of the peak, located at the interface, is about 50 µm.*

Shown by different groups, the use of a potassium phosphate buffer leads to an interface potential in the vicinity of the interface [104,105,107,108]. The partition coefficient of a charged species *i*, like an ion, can be described by

$$\ln k_i = \ln k_i^0 - \frac{z_i F}{RT}\Delta\phi \qquad (11.13)$$

where $\Delta\phi$ is the electrostatic potential difference between the top and bottom phase, $z_i$ the number of elementary charges of species *i* and F the Faraday constant. $k_i$ is the resulting partition coefficient whereas $k_i^0$ includes all interactions except that between the charge of the ion and $\Delta\phi$ [104]. In case of a salt ($A^+B^-$) and considering the boundary condition that both phases have to be electroneutral $k_{A^+} = k_{B^-}$, $\Delta\phi$ can be calculated by

$$\Delta\phi = \frac{RT}{(z_{B^-} - z_{A^+})F} \ln \frac{k_{B^-}^0}{k_{A^+}^0} \qquad (11.14)$$

Pfennig et al. showed that $\Delta\phi$ can not be directly calculated or measured but is the order of a few mV [104]. In this study, the presence of inhomogeneous ion distribution for a potassium phosphate buffer was proven by resistivity measurements, see Table 11-3.

| Molarity | $\rho_{el\_PEG}$ [Ω cm] PEG-phase | $\rho_{el\_dex}$ [Ω cm] dextran-phase | $\rho_{el\_PEG}$ /$\rho_{el\_dex}$ |
|---|---|---|---|
| 5 mM | 1712.45 | 1913.00 | 0.90 |
| 10 mM | 1002.76 | 980.19 | 1.02 |
| 50 mM | 181.65 | 177.70 | 1.02 |
| 100 mM | 98.74 | 94.94 | 1.04 |

*Table 11-3: Electrical resistivity of the standard ATPS; buffer system: potassium phosphate, pH 7.*

Since the electrical resistance is nearly the same in both phases, it seems that also the ion concentration is equalized. But due to the difference in viscosity ($\eta_{PEG}$ = 0.004 P·s, $\eta_{dextran}$ = 0.030 P·s, standard ATPS) also the ion concentration must be different. In a first and simplified estimation the ratio between the ion concentrations can be determined:

$$\frac{c_{dextran}}{c_{PEG}} = \frac{\eta_{dextran}}{\eta_{PEG}} \frac{\rho_{el\_PEG}}{\rho_{el\_dex}} \qquad (11.15)$$

leading to a ratio $c_{dextran}/c_{PEG}$ of 7.65 for a 10 mM potassium phosphate buffer system. Table 11-3 shows that for a 5 mM buffer system the maximum of the interface potential $\Delta\phi$ is not fully developed. This behavior is consistent with the experimental results of Pfennig et al. [104] where the maximum of $\Delta\phi$ and a plateau is not reached below 10 mM. But already for a 5 mM system 90% of the plateau value is achieved, explaining the small difference in the resistance ratio compared to higher molarities. However, the measurements show a linear increase of resistance depending on the molarity of the buffer system. The inhomogeneous distribution of buffer ions in ATPSs of this study was also proven by PEG-phase bubbles within a continuous phase of dextran, since they were moving as soon as an electric field was applied, cf. Fig. 11-14.

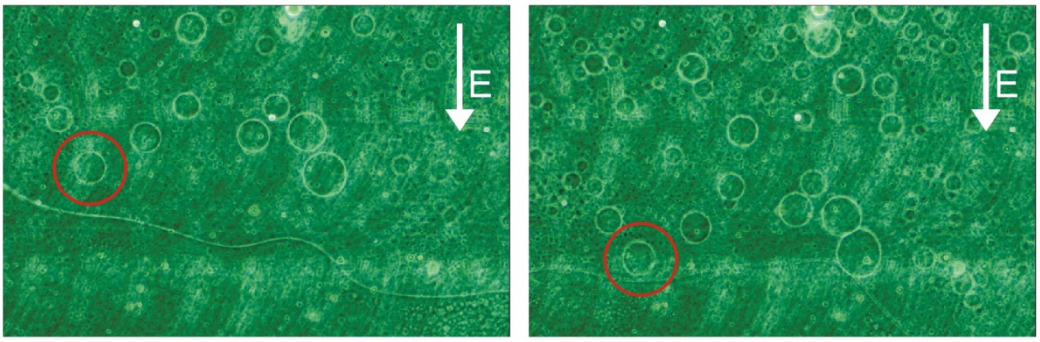


*Fig. 11-14: Movement of dextran-phase bubbles within the PEG-phase driven by an electric field. At a voltage of approximately 5 $V_{dc}$ velocities of up to 20 µm $s^{-1}$ are achievable.*

After proving the existence of an interface potential for ATPSs under study, possible forces and energies arising from the electric double layer are now discussed in more detail. For further considerations an interface potential $\Delta\phi$ of 3.0 mV is assumed; a value which is

comparable to the value derived by Theos and Clark [78]. Additionally, a phosphate buffer of 10 mM at pH 7 is assumed. The resulting Debye length

$$\lambda_D = \left( \frac{\varepsilon_w \, k_B \, T}{2 \, N_A \, I_{ion} \, e_0^2} \right)^{1/2} \qquad (11.16)$$

where the potential is reduced by a factor of 1/e, is about 2 nm. $\varepsilon_w$ is the dielectric constant of water. The ionic strength was calculated by the software Peakmaster 5.2 [224]. The resulting potential curve is shown in Fig. 11-15.

The maximum range of influence of such double layer is about 10 nm. But already at approximately 5 nm the potential is reduced to 10% of its initial value. Therefore, only in the area of a few nm the movement of the protein can be influenced. To clarify the strength of such influences possible energy values of the protein are compared.

The thermal energy $k_BT$ at a temperature of 300°K is $4.14 \cdot 10^{-21}$ J. Further on, assuming a protein as a point charge, its potential energy can be calculated by $W_p = q_{Protein} \, \phi$. For a BSA molecule its charge, $q_{BSA} = z_{BSA} e_0$, can be assumed as $-3.2 \cdot 10^{-18}$ C at pH 7, $z$ = -20 [217,225], leading to potential energy of $-9.6 \cdot 10^{-21}$ J.

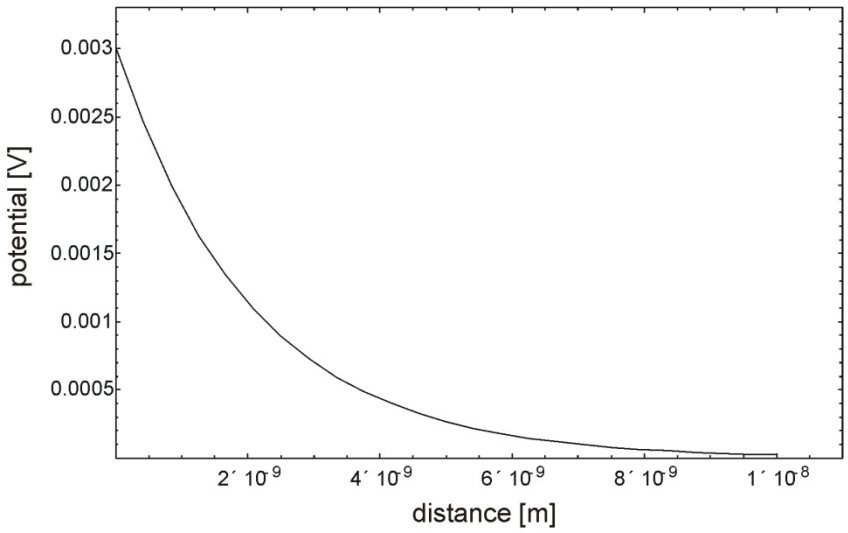


*Fig. 11-15: Potential curve for a $\Delta\phi$ of 3.0 mV.*

Thus, the thermal and electrostatic energies are of the same order of magnitude and the resulting ratio between thermal and electrostatic energy is about 2.3. Therefore, it can be expected that, although the interface potential may influence the protein movement across the interface, only insignificant local enrichments of proteins are expectable. Additionally, on the one hand, the interface between the two phases of an aqueous two phase system is not as sharp as between a wall surface and a liquid. Accordingly, also the interface double layer and the resulting electric field at the interface are expected to be less defined. On the other hand, proteins are not in the shape of an ideal point charge. In fact, there exist positively and negatively charged regions unevenly distributed all over the protein surface [118]. Accordingly, proteins can be attracted or repelled depending on their three dimensional orientation. And by their ability to rotate around their own axis a movement across the interface by finding the path of least resistance is more likely.

After this consideration of the influence of an interface potential the above assumption of a determining and instantaneous equilibrium across the phase boundary induced by $k$ remains most likely. It was shown that although an interface potential is present a resistance to transport remains negligible.

# 12 Separation of Proteins and Cells

*Since the transport of proteins across the interface in a PEG-dextran system follows comparatively simple dynamics, the study of transport processes of larger and more complex objects was self-evident. In this chapter the continuous separation of proteins from cells from lymphoblastoid cell lines (LCL-cells) is described. While proteins overcome the phase boundary and, supported by an electric field, leave the phase they have been initially dissolved in almost completely, lymphoblastoid cells are retained. They are unable to cross the phase boundary if the field strength stays below a threshold value.*

## 12.1 Cells in Aqueous Two-Phase Systems

Contrary to proteins cells are relatively large particles. One of the difficulties in partitioning mammalian cells in macroscopic systems lies in the gathering of particles onto the interface of two phases by sedimentation or flotation, since cell densities are comparable to ATPSs made of PEG and dextran [27,226,227].

Furthermore, the partition behavior of cells in ATPSs is slightly different to the behavior of proteins. Often almost 100% of the cells prefer either the PEG or the dextran-phase [27], cf. Fig. 12-1. For example, the affinity of cells to the phases can be influenced by adding sodium chloride (NaCl). At low concentrations of NaCl cells often prefer the PEG-phase but with an increasing amount of NaCl the affinity turns into a high preference to the dextran-phase [27,28].

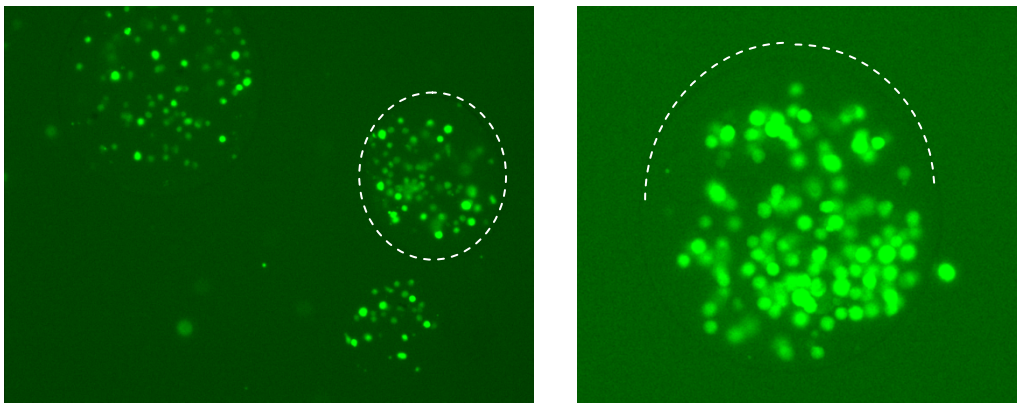

*Fig. 12-1: Partitioning of LCL cells (fluorescent dots) in an ATPS consisting of PEG and dextran. Here, all cells are found inside PEG bubbles demonstrating that cells often strongly prefer one of the two phases. In the left picture one bubble is marked by a dotted line.*

But also the molecular weights of the used polymers can have a strong influence on the partitioning behavior [28]. For the separation experiments of proteins and cells described here, the standard PEG-dextran system (A) was applied, where almost 100% of the LCL cells prefer the PEG-phase.

## 12.2 Active Separation

For an active separation immiscible aqueous phases (type A) are injected separately into the main channel that is part of the microfluidic system described above. The lower PEG-phase, cf. Fig. 12-2, partly contains a mixture of BSA molecules and lymphoblastoid cells. In order to avoid possible gravity effects the cell migration is perpendicular to the direction of gravity.

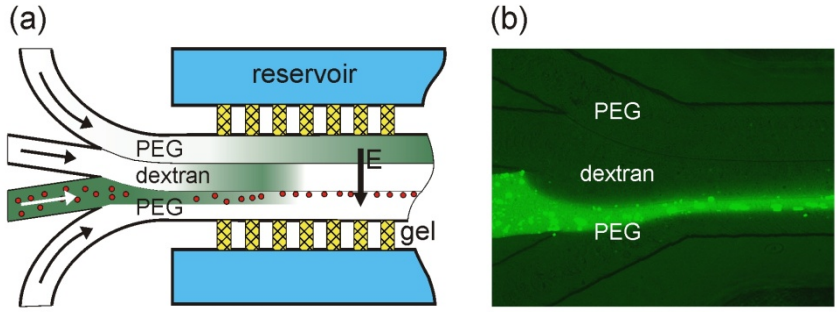


*Fig. 12-2: (a) Schematic showing the transport of proteins and cells in a tri-laminated two-phase system. Below a critical electric field strength the cells are trapped at the phase boundary. (b) Entrance of the main channel. Cells (fluorescent dots) and proteins (background fluorescence) are located in the lower PEG-phase.*

The total flow rates used in the experiments were 0.05 and 0.03 ml $h^{-1}$ for the upper and lower PEG-phases and 0.008 ml $h^{-1}$ for the dextran-phase, respectively. A detailed description of the microfluidic chip was already given in chapter 7. The labeling procedure of the proteins and cells can be found in chapter 2.

## 12.3 Results

At the entrance of the main channel both proteins and cells are dissolved in the same PEG-phase, cf. Fig. 12-2 and Fig. 12-3. Without an electric field and once the different phases get in contact, diffusion of proteins into the dextran-phase is observed. Halfway along the channel the cells are randomly distributed within the preferred PEG-phase while the proteins diffuse not only into the neighboring dextran-phase but also into the gel matrix below.

After applying an electric field the proteins start to move into the central dextran-phase and finally, near the outlet of the channel, into the upper PEG-phase and gel matrix. On the contrary, the cells are retained by the phase boundary and stay in the preferred PEG-phase. A further increase of electric field strength forces them to cross the phase boundary continuing their electrophoretic migration towards the positive electrode. Below this critical field strength, 100% of the cells are found in their preferred PEG-phase allowing a continuous separation of LCL-cells from proteins. A typical result of such an experiment at 4 $V_{dc}$ is shown in Fig. 12-3. Already near the entrance, cf. Fig. 12-3 (a), parts of the proteins have been already transported into the dextran-phase. Near the outlet, Fig. 12-3 (c), a complete depletion of the phase from proteins has been reached while the cells have been trapped in their preferred phase and collected at the phase boundary.

In order to visualize the transport behavior of the proteins the fluorescence intensities across the channel at different positions are combined in one graph, see Fig. 12-4. If no electric field is applied the proteins mainly stay in their initial phase and slightly diffuse into the ambient liquid. In case of an applied electric field and halfway along the channel the major part of the proteins has passed the first phase boundary. Near the outlet, cells and proteins are separated almost completely.

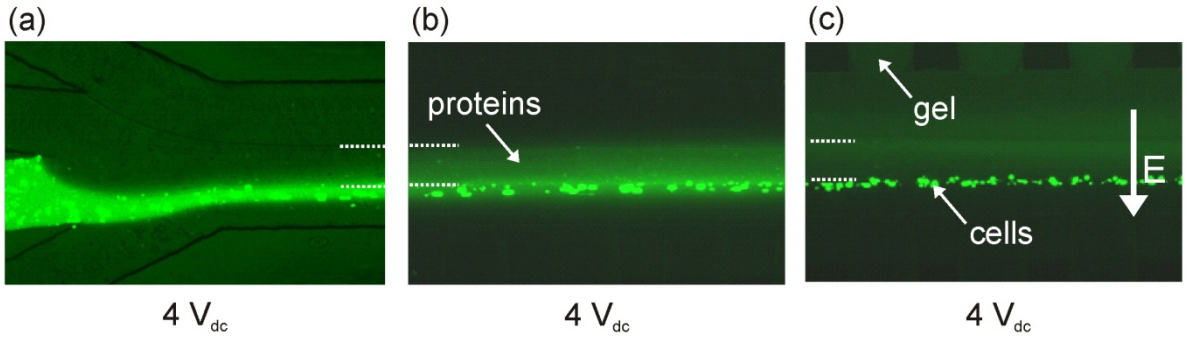


*Fig. 12-3: Separation of lymphoblastoid cells from proteins in a PEG-dextran system. The cells are visible as bright spots, while the background fluorescence is due to proteins. At 4 $V_{dc}$ and halfway along the channel (b) the proteins have been partially transported into the dextran-phase, by contrast cells are retained at the phase boundary. (c) At the end of the channel cells have been trapped in their preferred phase and collected at the phase boundary while the proteins have already crossed the intermediate dextran-phase and reached the upper PEG-phase of the trilaminated flow.*

But the separation depends not only on the applied electric field but also on the flow velocity and the width of the lamella the sample molecules are initially dissolved in. Both, a lower flow velocity and a smaller lamella width would lead to an accelerated separation within the main channel. Furthermore, cell positions in regard to the phase boundary have been analyzed, see Fig. 12-5. Near the outlet the maximum measured distance between the center of a cell and the phase boundary is reduced to approximately 30 µm. But most of the cells are located directly at the boundary and are attached to it, see Fig. 12-3. In Fig. 12-5 (right) the distribution of cells in five snapshots, within a lamella of about 100 µm and near the outlet, is analyzed. If no electric field is applied cells are randomly distributed across their initial lamella. In contrast, as soon as a field of 4.5 $V_{dc}$ is applied, approximately 70% of the cells can be found within a range of 10 µm from the phase boundary.

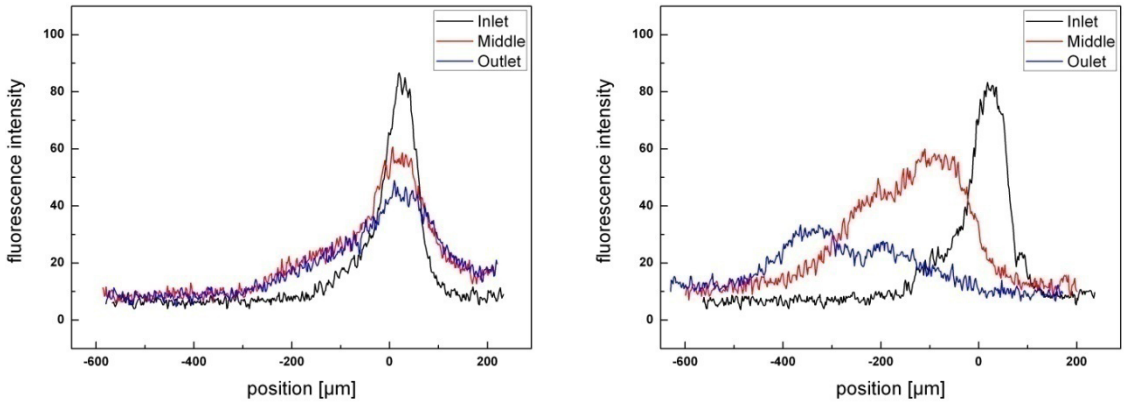


*Fig. 12-4: Left: Fluorescence intensity profiles of BSA molecules across the channel near the inlet of the channel, halfway along the channel and near the outlet when no electric field is applied. The first phase boundary is located at 0 µm. Right: Fluorescence intensity profiles at 4 $V_{dc}$, where at the outlet the proteins have left their initial phase almost completely.*

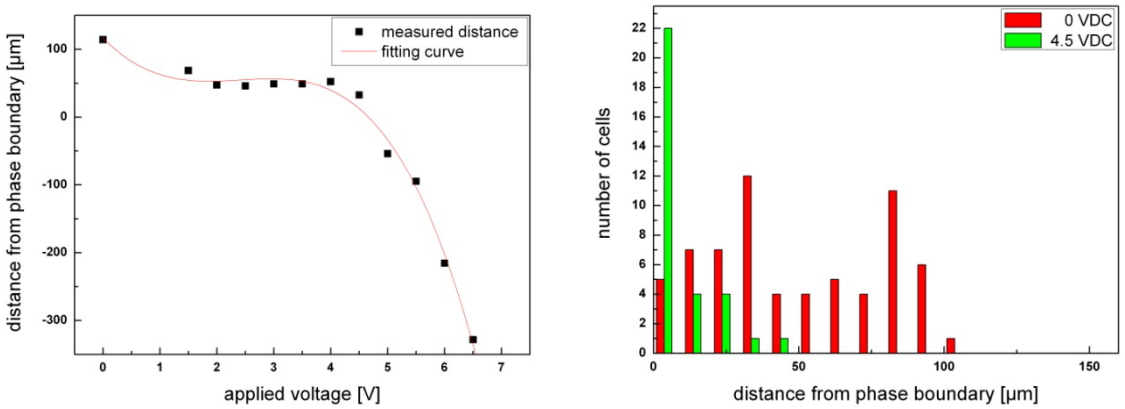


*Fig. 12-5: Left: Maximum distance of a cell from the phase boundary (y=0) at values of the applied voltage. At 4.5 $V_{dc}$ the cells start to penetrate the boundary and resume their electrophoretic motion. Below 4.5 $V_{dc}$ nearly all cells are lined up at the phase boundary like pearls on a string. Right: Number of cells at different distances from the boundary, with and without an electric field.*

## 12.4 Conclusion

The investigated PEG-dextran aqueous two-phase system allows a very gentle separation of cells and proteins. Additionally, this microfluidic setup combines the separation process with an enrichment of the desired cells directly at the phase boundary. Since also cell lysis due to high electric field strengths is avoided, it is found to be superior to typical electric field flow fractionation systems. This makes such a microfluidic device a promising candidate for further types of separation, purification and enrichment processes of biomolecules.

# 13 Further Two-Phase Systems

*One of the most important parameters governing the hydrodynamics is the interfacial tension. Systems with a very large interfacial tension tend to become unstable when bilaminated into a small channel, whereas systems with a small interfacial tension usually have less stability problems, but consist of components which are physico-chemically more similar. Besides already presented ATPSs and for the sake of completeness, in this chapter systems consisting of propylene carbonate and water as well as of sunflower oil and water are described. They are briefly described completing the large range in interfacial tension and electrical permittivities examined in this study.*

## 13.1 Propylene Carbonate-Water Two-Phase System

As an alternative to two-phase systems which are only based on water, the enrichment of proteins (BSA) at a propylene carbonate (PC) - water interface was examined. For this purpose, the fact that BSA is not readily dissolvable in organic solvents, such as PC, was utilized.

In order to obtain a significant electric field within the aqueous phase the organic phase has to be conductive. Otherwise, most of the electric potential drop would occur in the organic phase. For this purpose tetrabutylammonium hydrogensulfate (155837, 97%, Sigma-Aldrich, Germany) was added up to a concentration of 1M, which results in a conductivity of 3.8 mS in case of the PC phase.

Here, the microfluidic system, cf. Fig. 7-15, comprises two parallel lamellae and an electric field is applied perpendicular to the flow direction. At a vanishing electric field the BSA molecules show a uniform distribution within the aqueous lamella. Upon applying a voltage of 15 $V_{dc}$ an enrichment of BSA molecules is observed close to the phase boundary. The width of the band of concentrated proteins is about 60 µm, cf. Fig. 13-1.

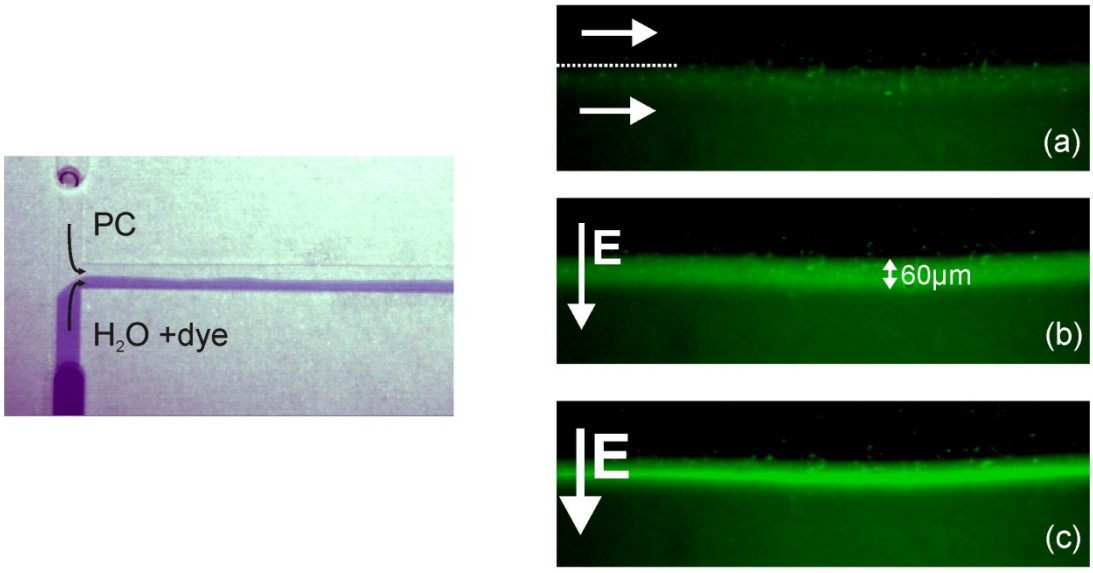


*Fig. 13-1: Left: Bilaminated PC (top) - water (bottom) system (only for demonstration). Right: PC - aqueous buffer system introduced into the gel chip. When an electric field is applied, dissolved proteins accumulate at the phase boundary. An increase of the field strength leads to an increase of protein concentration. (a) 0 $V_{dc}$, (b) 15 $V_{dc}$, (c) 20 $V_{dc}$.*

A voltage increase up to 20 $V_{dc}$ leads to a narrowing of the band down to approx. 20 µm and to an increase of the fluorescence intensity above 35 percent. A further increase of the electric field strength does not lead to a higher concentration of BSA molecules at the phase boundary but to a deformation of the boundary itself.

As the camera only captures 2D distributions this deformation manifests itself as a visible band widening. Within the examined voltage no penetration of BSA into the PC phase was observed and only small amounts of denatured and deposited BSA got visible on the channel surface after several minutes of flow.

The water-PC system has been examined as an alternative to the PEG-dextran system also applicable for a continuous enrichment of biomolecules at the interface by electrophoresis. It would also be possible to apply such a two-phase system to other charged particles, either dissolvable in aqueous or organic phases.

## 13.2 Oil-Water Two-Phase System

The sunflower oil - water system has the largest interfacial tension of all presented two-phase systems and provides strongly chemically different environments in the aqueous and organic phase. However, owing to the much higher electric permittivity of water as compared to oil, an electric field across the phase boundary is largely shielded in the water phase and electrophoretic transport becomes difficult. Also, a successful creation of a bilaminated system of liquids becomes more difficult at high interfacial tensions. Considering aspect ratios of microchannels, it was necessary to stabilize the phase boundary utilizing a special channel geometry. With such geometry it was possible to obtain a stable bilaminated oil - water configuration of high interfacial tension, as exemplified in Fig. 13-2. In contrast, for common channels with a rectangular cross section the formation of water droplets was observed.

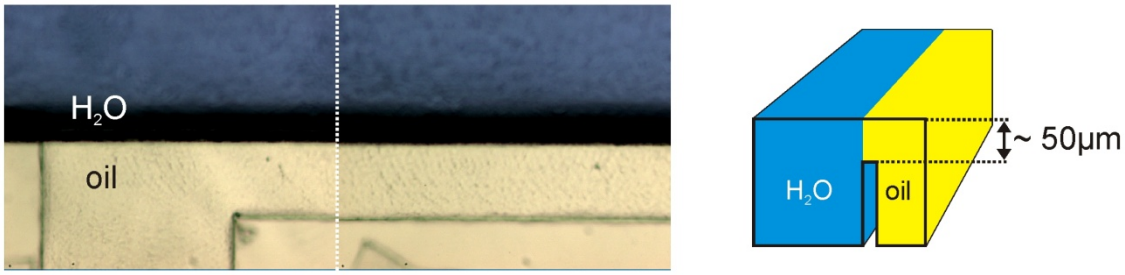


*Fig. 13-2: Bilaminated arrangement of oil and water (left) and corresponding channel cross section. The oil is located inside a bended portion of the channel as a stationary phase while the water phase with dissolved aniline blue fills a straight and deeper portion of the channel. It can be alternatively used as a stationary phase or moving phase.*

One subject of the studies of an oil-water two-phase system was the observed behavior of BSA proteins at a stable phase boundary of oil and water inside a microchannel. Due to the presence of surfactants the proteins tend to accumulate at the interface [228], cf. Fig. 13-3. This effect may be utilized for electrophoretic separation with an electric field applied parallel to the liquid lamellae (instead of perpendicular).

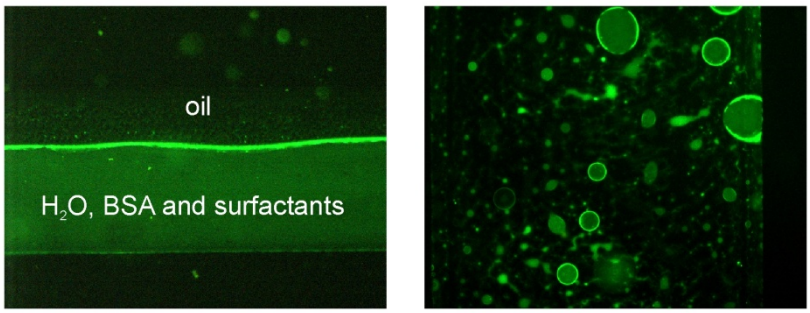


*Fig. 13-3: Accumulation of BSA molecules at the phase boundary without electric field. In the left picture the two phases are located inside a microchannel. In the right picture a mixture of the two phases are shown that is not constricted by channel walls.*

In context of this examination of the oil-water two-phase system it has to be mentioned that the main attention of this study was directed to ATPSs. Nevertheless, the results of this chapter illustrates the possibility to stabilize an oil-water system only by adapted channel shapes, which can be taken as a fundamental for a wide range of further interesting fields of research.

# 14 Conclusion and Outlook

*In summary, this work shows that the combination of electrophoresis, biomolecules and two-phase systems offers a huge variety of interesting and challenging scientific issues. In this chapter, the conclusion of this study is given followed by an outlook.*

## 14.1 Conclusion

In conclusion, the different microsystems developed in this study allow to analyze electrophoretic transport properties in virtually any kind of two- or multi-phase systems. Compared to existing macroscopic systems only such microfluidic systems permit a detailed examination of incidents in the vicinity of a phase boundary.

For the connection to the macro-world the associated and modular microfluidic setup provides easy and reliable fluidic connection ports. Besides an additional variation of the number of fluidic connections, the ports as well as the microfluidic valves can be easily adapted to the chip and don't have to be integrated into it. Such setup properties support fast design changes of microfluidic chips and of the experimental setup.

For the electrophoretic transport perpendicular to the flow direction and to the phase boundary, respectively, the external electric field was integrated into the chip via dialysis membranes or gel bridges. Since these ion conducting materials are part of the channel walls the flow of the aqueous two-phase system remains undisturbed and without any volume loss due to leakage.

The results of active as well as passive transport experiments of proteins across boundaries of aqueous two phase systems give a detailed description and understanding of their mass transfer behavior. It could be shown that mainly the affinities to different phases, expressed by the partition coefficient, define the interaction of proteins with the phases and that possible interactions with the phase boundary itself are negligible for the systems studied here. This observation is supported by an order of magnitude estimation of the involved, and known, energies. It shows, that a significant local enrichment of proteins by, e.g., electric double layers can be ruled out.

By increasing the affinity of a protein to one of the aqueous phases such a system allows at least a continuous three-fold enrichment at the phase boundary. Moreover, it is demonstrated that the setup also allows for a continuous separation of proteins by utilizing the different electrophoretic behaviors of proteins at specific pH values of the buffer system. Accordingly, even if two different proteins have a high affinity to the phase they are initially dissolved in, only the protein with a high electrophoretic mobility is removed by an applied electric field. In contrast, the other protein, showing a negligible mobility, stays in its initial phase.

In case of the protein-cell separation the phase boundary shows a higher effect of retardation for cells compared to proteins. This fact allows a gentle and continuous separation and purification of a protein-cell solution combined with an advantageous enrichment of cells directly at the phase boundary.

Accordingly and in general, such a microfluidic setup with its entire individual and numerous setting options offers a high potential for different kinds of purification and separation processes.

Beside ATPSs made of PEG and dextran also two other types of two-phase systems have been examined. In case of the water-propylene carbonate two-phase system a strong enrichment of proteins at the phase boundary is achievable. The proteins can be moved towards the phase

boundary within the aqueous lamella they are initially dissolved in. This leads to strong protein enrichments at the interface within a band of approximately 60 µm and less. Accordingly, such a setup opens up possibilities for a continuous enrichment also for other kinds of biomolecules or charged particles by two-phase electrophoresis.

In case of the oil-water two-phase system a channel structure was developed in order to stabilize the phase boundary between water and oil in regard to its position and shape. Since proteins tend to accumulate at the phase boundary in the presence of specific surfactants, such a bilaminated fluidic structure of oil and water in a microchannel offers, for example, possibilities to study the transport of adsorbed proteins along the phase boundary.

## 14.2 Outlook

The results of this work built a solid base for further experiments on two-phase electrophoresis of biomolecules or other types of polymers. After the examination of the transport behavior of proteins and cells, long chain DNA molecules (λ-DNA) will be examined in future transport experiments. In contrast to proteins with their fixed spatial conformation (tertiary structure), λ-DNA does not have a fixed conformation leading to higher degrees of freedom and more possible interactions with the phase boundary. Accordingly, future work will be addressed to the electrophoretic motion of λ-DNA towards and across the phase boundary of ATPSs.

Furthermore, in order to realize systematic studies on the interaction of polymers with fluidic interfaces, the transport behavior of specially designed diblock copolymers will be studied. They allow an easy variation of key parameters such as the hydrophobicity of sub-chains.

Finally, this work demonstrates the huge variety of interesting and challenging scientific issues that are offered by a combination of electrophoresis, biomolecules and two-phase systems in the world of microfluidics.

# *Acknowledgement*

First of all, I want to thank Prof. Dr. Steffen Hardt for his great support, his continuous availability, even over greater distances and for the possibility to pursue my PhD under his direction. The opportunity to work on this exciting and interdisciplinary topic paired with his readiness to share his consolidated knowledge made the last years very valuable to me.

I also gratefully acknowledge Prof. Dr. Jörg P. Kutter of the Department of Micro- and Nanotechnology, Technical University of Denmark, for his helpful support and for kindly agreeing to be the co-examiner of my PhD thesis.

Without financial support, research becomes difficult. Accordingly, thanks to the German Research Foundation (DFG) for supporting this work.

I want to express my gratitude to Dr. Klaus-Stefan Drese for the interesting and regular discussions and for supporting my work whenever it was possible.

Special thanks go to Dr. Friedhelm Schönfeld, my “personal simulator”, not only for his patience in order to introduce me into the mathematical modeling of microfluidics, especially the diffusion part, but also for interesting coffee break discussions.

It was a pleasure to work with Dalibor Dadic on all fabrication issues and further microfluidic challenges. Additionally, I thank him for his moral support and the time sharing my office with him.

Dr. Tobias Baier is gratefully acknowledged for answering all my questions about formulas and the support of the mathematical model of the two-phase flow.

Many thanks to Dr. Frithjof von Germar, Dr. Marion Ritzi and Dr. Tina Röser for fruitful discussions and their competent support in regard to chemical and biological questions.

Many thanks to all members of our lab team, but especially to: Sabine Rink, Carmen Schwind and Sabine Schmahl for their support in various biological and chemical disciplines and also to our laser and mechanical fabrication team at IMM.

I would like to thank Thomas Hahn for his support and the time we spend together in the office and lab. I’m happy about the fact that he will continue the work on this field of research.

And finally, thanks to all members of the IMM for helping me out when necessary.

At this point, I would like to thank my parents for supporting my studies and that they were always there when I needed them.

But for the end, I saved the most important. I’d like to address my special thanks to my wife Antje, the one special person in my life, for her love and her endless support, not only during my PhD thesis. And I also thank our little daughter Marlene Lykka for her lovely and motivating nature.

While writing these last words and finishing my PhD thesis I’m looking forward to spending much time as possible with my little family, back home in the north of Germany.

# List of Abbreviations

| | |
|---|---|
| $\gamma$ | surface tension |
| $\dot{\gamma}$ | shear rate |
| $\varepsilon$ | permittivity |
| $\varepsilon_0$ | dielectric constant |
| $\varepsilon_r$ | vacuum permittivity |
| $\eta$ | dynamic viscosity |
| $\theta$ | contact angle |
| $\theta_a$ | advancing contact angle |
| $\theta_r$ | receding contact angle |
| $\lambda_B$ | Bjerrum length |
| $\lambda_D$ | Debye length |
| $\mu$ | chemical potential |
| $\mu_E$ | electrophoretic mobility |
| $\mu_m$ | mobility |
| $\rho$ | density |
| $\rho_{el}$ | resistivity |
| $\rho_q$ | charge density |
| $\sigma$ | shear stress |
| $\sigma_{ion}$ | ionic conductivity |
| $\sigma_v$ | variance |
| $\phi_0$ | surface potential |
| $\phi_i$ | interface potential |
| $\phi_\zeta$ | zeta potential |
| $\psi_i$ | volume fration |
| a | acceleration |
| A | surface area |
| ATPS | aqueous two-phase system |
| c | concentration |
| Ca | capillary number |
| $c_i$ | ion concentration |
| D | diffusion coefficient |
| E | electric field |
| $e_0$ | elementary charge |
| $E_S$ | surface energy |
| f | body force per unit mass |
| F | Faraday constant |
| $G_{mix}$ | Gibbs free energy of mixing |
| h | channel height |
| $H_{mix}$ | enthalpy of mixing |
| I | current |
| $I_{ion}$ | ionic strength |
| J | flux |
| $J_{diff}$ | flux of diffusion |
| k | partition coefficient |
| $k_b$ | Boltzmann constant |
| L | length |
| $L_c$ | characteristic length |
| $L_{cl}$ | channel length |
| M | degree of polymerization |
| N | number of lattice sites |
| n | number of molecules |
| $N_A$ | Avogadro constant |
| p | pressure |
| PAGE | polyacrylamide gel electrophoresis |
| PEG | poly ethylene glycol |
| pI | isoelectric point |
| P-PEG | PEG-palmitate |
| Q | flow rate |
| $q_0$ | surface charge density |
| r | channel radius |
| R | universal gas constant |
| $r_{0°}$, $r_{45°}$ | sputtering rates |
| Re | Reynolds number |
| $R_{el}$ | electrical resistance |
| $R_f$ | fluidic resistance |

| | |
|---|---|
| SDS | sodium dodecyl sulfate |
| $S_{mix}$ | entropy of mixing |
| T | temperature |
| t | time |
| u | velocity |
| w | channel width |
| W | interchange energy |
| We | Weber number |
| $W_p$ | potential energy |
| z | charge number |

# References


[1] Reyes, D. R., Iossifidis, D., Auroux, P. A., Manz, A. (2002) Micro total analysis systems. 1. Introduction, theory, and technology. *Anal. Chem.* 74(12), 2623-2636.

[2] Auroux, P. A., Iossifidis, D., Reyes, D. R., Manz, A. (2002) Micro total analysis systems. 2. Analytical standard operations and applications. *Anal. Chem.* 74(12), 2637-2652.

[3] Whitesides, G. M. (2006) The origins and the future of microfluidics. *Nature* 442(7101), 368-373.

[4] Hardt, S., Schönfeld, F. (2007) Microfluidic technologies for miniaturized analysis systems, New York: Springer.

[5] Schasfoort, R. B. (2004) Proteomics-on-a-chip: the challenge to couple lab-on-a-chip unit operations. *Expert Rev. Proteomics* 1(1), 123-132.

[6] Figeys, D., Pinto, D. (2001) Proteomics on a chip: promising developments. *Electrophoresis* 22(2), 208-216.

[7] Khandurina, J., Guttman, A. (2002) Bioanalysis in microfluidic devices. *J. Chromatogr. A* 943(2), 159-183.

[8] Pamme, N. (2007) Continuous flow separations in microfluidic devices. *Lab Chip* 7(12), 1644-1659.

[9] Krivankova, L., Bocek, P. (1998) Continuous free-flow electrophoresis. *Electrophoresis* 19(7), 1064-1074.

[10] Shinohara, E., Tajima, N., Suzuki, H., Funazaki, J. (2001) Microfabricated free flow electrophoresis module for sample preparations. *Anal. Sci.* 17, i441-i443.

[11] Loseva, O. I., Gavryushkin, A. V., Osipov, V. V., Vanyakin, E. N. (1998) Application of free-flow electrophoresis for isolation and purification of proteins and peptides. *Electrophoresis* 19(7), 1127-1134.

[12] Kohlheyer, D., Eijkel, J. C., Schlautmann, S., van den Berg, A., Schasfoort, R. B. (2007) Microfluidic high-resolution free-flow isoelectric focusing. *Anal. Chem.* 79(21), 8190-8198.

[13] Kohlheyer, D., Eijkel, J. C., Schlautmann, S., van den Berg, A., Schasfoort, R. B. (2008) Bubble-Free Operation of a Microfluidic Free-Flow Electrophoresis Chip with Integrated Pt Electrodes. *Anal. Chem.*

[14] Zhang, C. X., Manz, A. (2003) High-speed free-flow electrophoresis on chip. *Anal. Chem.* 75(21), 5759-5766.

[15] Effenhauser, C. S., Manz, A., Widmer, H. M. (1993) Glass chips for high-speed capillary electrophoresis separations with submicrometer plate heights. *Anal. Chem.* 65(19), 2637-2642.

[16] Dittrich, P. S., Tachikawa, K., Manz, A. (2006) Micro total analysis systems. Latest advancements and trends. *Anal. Chem.* 78(12), 3887-3908.

[17] Heller, C. (2001) Principles of DNA separation with capillary electrophoresis. *Electrophoresis* 22(4), 629-643.

[18] Gawron, A. J., Martin, R. S., Lunte, S. M. (2001) Microchip electrophoretic separation systems for biomedical and pharmaceutical analysis. *Eur. J. Pharm. Sci.* 14(1), 1-12.

[19] Viovy, J. L. (2000) Electrophoresis of DNA and other polyelectrolytes: Physical mechanisms. *Rev. Mod. Phys.* 72(3), 813-872.

[20] Hofmann, O., Che, D., Cruickshank, K. A., Muller, U. R. (1999) Adaptation of capillary isoelectric focusing to microchannels on a glass chip. *Anal. Chem.* 71(3), 678-686.

[21] Rossier, J., Reymond, F., Michel, P. E. (2002) Polymer microfluidic chips for electrochemical and biochemical analyses. *Electrophoresis* 23(6), 858-867.

[22] Desai, M. J., Armstrong, D. W. (2003) Separation, identification, and characterization of microorganisms by capillary electrophoresis. *Microbiol. Mol. Biol. Rev.* 67(1), 38-51.

[23] Caliper Life Sciences, MA, USA.

[24] Micronit Microfluidics BV, The Netherlands.

[25] Lagally, E. T., Mathies, R. A. (2004) Integrated genetic analysis microsystems. *J. Phys. D: Appl. Phys.* 37(23), R245-R261.

[26] Münchow, G., Dadic, D., Doffing, F., Hardt, S., Drese, K. S. (2005) Automated chip-based device for simple and fast nucleic acid amplification. *Expert Review of Molecular Diagnostics* 5(4), 613-620.

[27] Albertsson, P.-A. (1986) Partition of cell particles and macromolecules. 3 ed., New York: John Wiley & Sons.

[28] Walter, H., Brooks, D. E., Fisher, D. (1985) Partitioning in aqueous two-phase systems, London: Academic Press.

[29] Yamada, M., Kasim, V., Nakashima, M., Edahiro, J., Seki, M. (2004) Continuous cell partitioning using an aqueous two-phase flow system in microfluidic devices. *Biotechnol. Bioeng.* 88(4), 489-494.

[30] Nam, K. H., Chang, W. J., Hong, H., Lim, S. M., Kim, D. I., Koo, Y. M. (2005) Continuous-flow fractionation of animal cells in microfluidic device using aqueous two-phase extraction. *Biomed. Microdevices* 7(3), 189-195.

[31] Hong, Y. K. (2006) Removal of protein using the aqueous two-phase system in the microfluidic device. *Theories and Applications of Chem. Eng.* 12(1), 298.

[32] Santesson, S., Barinaga-Rementeria Ramirez, I., Viberg, P., Jergil, B., Nilsson, S. (2004) Affinity two-phase partitioning in acoustically levitated drops. *Anal. Chem.* 76(2), 303-308.

[33] Meagher, R. J., Light, Y. K., Singh, A. K. (2008) Rapid, continuous purification of proteins in a microfluidic device using genetically-engineered partition tags. *Lab Chip* 8(4), 527-532.

[34] Squires, T. M., Quake, S. R. (2005) Microfluidics: Fluid physics at the nanoliter scale. *Rev. Mod. Phys*. 77(3), 977-950.

[35] Beebe, D. J., Mensing, G. A., Walker, G. M. (2002) Physics and applications of microfluidics in biology. *Annu. Rev. Biomed. Eng.* 4, 261-286.

[36] Pennemann, H., Hardt, S., Hessel, V., Löb, P., Weise, F. (2005) Micromixer based liquid/liquid dispersion. *Chem. Eng. Technol.* 28(4), 501-508.

[37] Hessel, V., Hardt, S., Löwe, H. (1996) Chemical micro process engineering 1: Fundamentals, modelling and reactions, Weinheim: Wiley-VCH.

[38] Branebjerg, J., Gravesen, P., Krog, J. P., Nielsen, C. R. (1996) Fast mixing by lamination. In *Proceedings of Micro Electro Mechanical Systems (MEMS)*, San Diego, CA, USA, 441-446.

[39] Brody, J. P., Yager, P. (1997) Diffusion-based extraction in a microfabricated device. *Sens. Actuators, A* 58(1), 13-18.

[40] Hatch, A., Kamholz, A. E., Hawkins, K. R., Munson, M. S., Schilling, E. A., Weigl, B. H., Yager, P. (2001) A rapid diffusion immunoassay in a T-sensor. *Nat. Biotechnol.* 19(5), 461-465.

[41] Fu, J., Schoch, R. B., Stevens, A. L., Tannenbaum, S. R., Han, J. A patterned anisotropic nanofluidic sieving structure for continuous-flow separation of DNA and proteins. *Nature Nanotech.* 2, 121-128.

[42] Doh, I., Cho, Y.-H. (2005) A continuous cell separation chip using hydrodynamic dielectrophoresis (DEP) process. *Sens. Actuators, A* 121(1), 59-65.

[43] Pamme, N., Wilhelm, C. (2006) Continuous sorting of magnetic cells via on-chip free-flow magnetophoresis. *Lab Chip* 6(8), 974-980.

[44] Xu, Y., Zhang, C. X., Janasek, D., Manz, A. (2003) Sub-second isoelectric focusing in free flow using a microfluidic device. *Lab Chip* 3(4), 224-227.

[45] MacDonald, M. P., Spalding, G. C., Dholakia, K. (2003) Microfluidic sorting in an optical lattice. *Nature* 426(6965), 421-424.

[46] Hannig, K. (1978) Continuous free-flow electrophoresis as an analytical and preparative method in biology. *J. Chromatogr.* 159(1), 183-191.

[47] Kohlheyer, D., Besselink, G. A., Schlautmann, S., Schasfoort, R. B. (2006) Free-flow zone electrophoresis and isoelectric focusing using a microfabricated glass device with ion permeable membranes. *Lab Chip* 6(3), 374-380.

[48] Raymond, D. E., Manz, A., Widmer, H. M. (1994) Continuous sample pretreatment using a free-flow electrophoresis device integrated onto a silicon chip. *Anal. Chem.* 66(18), 2858-2865.

[49] Albrecht, J., Gaudet, S., Jensen, K. F. (2005) Rapid free flow isoelectric focusing via novel electrode structures. In *Proceedings of Micro Total Analysis Systems*, Boston, MA, USA, 1537-1539.

[50] Lu, H., Gaudet, S., Sorger, P. K., Schmidt, M. A., Jensen, K. F. (2003) Micro isoelectric free flow separation of subcellular materials. In *Proceedings of Micro Total Analysis Systems*, Squaw Valley, CA, USA, 915-918.

[51] Song, Y. A., Hsu, S., Stevens, A. L., Han, J. (2006) Continuous-flow pI-based sorting of proteins and peptides in a microfluidic chip using diffusion potential. *Anal. Chem.* 78(11), 3528-3536.

[52] Hoffmann, P., Ji, H., Moritz, R. L., Connolly, L. M., Frecklington, D. F., Layton, M. J., Eddes, J. S., Simpson, R. J. (2001) Continuous free-flow electrophoresis separation of cytosolic proteins from the human colon carcinoma cell line LIM 1215: a non two-dimensional gel electrophoresis-based proteome analysis strategy. *Proteomics* 1(7), 807-818.

[53] Janasek, D., Schilling, M., Franzke, J., Manz, A. (2006) Isotachophoresis in free-flow using a miniaturized device. *Anal. Chem.* 78(11), 3815-3819.

[54] Giddings, J. C. (1985) A system based on split-flow lateral-transport thin (SPLITT) for rapid and continuous particle fractionation. *Sep. Sci. Technol.* 20(9-10), 749-768.

[55] Saldanha, A. D., Gale, B. K. (2002) Viral separations using microfabricated electrical splitt system. In *Proceedings of Micro Total Analysis Systems*, Nara, Japan, 584-586.

[56] Merugu, S., Narayanan, N., Gale, B. K. (2003) High throughput separation using a microfabricated serial electric splitt system. In *Proceedings of Micro Total Analysis Systems*, Squaw Valley, CA, USA, 1191-1194.

[57] Narayanan, N., Saldanha, A., Gale, B. K. (2006) A microfabricated electrical SPLITT system. *Lab Chip* 6(1), 105-114.

[58] Fennah, M., Manz, A. (2002) DNA extraction from bacterial cells by reverse electroporation and SPLITT methods on a microfabricated device. In *Proceedings of Micro Total Analysis Systems*, Nara, Japan, 817-819.

[59] Fuh, C. B., Giddings, J. C. (1997) Isoelectric split-flow thin (SPLITT) fractionation of proteins. *Sep. Sci. Technol.* 32(18), 2945-2967.

[60] Moon, M. H., Kim, H. J., Kwon, S. Y., Lee, S. J., Chang, Y. S., Lim, H. (2004) Pinched inlet split flow thin fractionation for continuous particle fractionation: application to marine sediments for size-dependent analysis of PCDD/Fs and metals. *Anal. Chem.* 76(11), 3236-3243.

[61] Hamann, C. H., Vielstich , W. (2005) Elektrochemie, Weinheim: Wiley-VCH.

[62] Hibara, A., Nonaka, M., Hisamoto, H., Uchiyama, K., Kikutani, Y., Tokeshi, M., Kitamori, T. (2002) Stabilization of liquid interface and control of two-phase confluence and separation in glass microchips by utilizing octadecylsilane modification of microchannels. *Anal. Chem.* 74(7), 1724-1728.

[63] Sato, K., Tokeshi, M., Sawada, T., Kitamori, T. (2000) Molecular transport between two phases in a microchannel. *Anal. Sci.* 16(5), 455-456.

[64] Hibara, A., Tokeshi, M., Uchiyama, K., Hisamoto, H., Kitamori, T. (2001) Integrated multilayer flow system on a microchip. *Anal. Sci.* 17(1), 89-93.

[65] Sato, K., Hibara, A., Tokeshi, M., Hisamoto, H., Kitamori, T. (2003) Microchip-based chemical and biochemical analysis systems. *Adv. Drug Deliv. Rev.* 55(3), 379-391.

[66] Dreyfus, R., Tabeling, P., Willaime, H. (2003) Ordered and disordered patterns in two-phase flows in microchannels. *Phys. Rev. Lett.* 90(14), 144505.

[67] Reddy, V., Zahn, J. D. (2005) Interfacial stabilization of organic-aqueous two-phase microflows for a miniaturized DNA extraction module. *J. Colloid Interface Sci.* 286(1), 158-165.

[68] Zhao, B., Moore, J. S., Beebe, D. J. (2002) Principles of surface-directed liquid flow in microfluidic channels. *Anal. Chem.* 74(16), 4259-4268.

[69] Maruyama, T., Uchida, J., Ohkawa, T., Futami, T., Katayama, K., Nishizawa, K., Sotowa, K., Kubota, F., Kamiya, N., Goto, M. (2003) Enzymatic degradation of p-chlorophenol in a two-phase flow microchannel system. *Lab Chip* 3(4), 308-312.

[70] van der Linden, H. J., Jellema, L. C., Holwerda, M., Verpoorte, E. (2006) Stabilization of two-phase octanol/water flows inside poly (dimethylsiloxane) microchannels using polymer coatings. *Anal. Bioanal. Chem.* 385(8), 1376-1383.

[71] Xiao, H., Liang, D., Liu, G., Guo, M., Xing, W., Cheng, J. (2006) Initial study of two-phase laminar flow extraction chip for sample preparation for gas chromatography. *Lab Chip* 6(8), 1067-1072.

[72] Kralj, J. G., Sahoo, H. R., Jensen, K. F. (2007) Integrated continuous microfluidic liquid-liquid extraction. *Lab Chip* 7(2), 256-263.

[73] Zhao, B., Viernes, N. O., Moore, J. S., Beebe, D. J. (2002) Control and applications of immiscible liquids in microchannels. *J. Am. Chem. Soc.* 124(19), 5284-5285.

[74] Zaslavsky, B. Y. (1995) Aqueous two-phase partitioning, New York: Marcel Dekker.

[75] Walter, H., Johansson, G. (1994) Methods in enzymology - volume 228: Aqueous two-phase systems, San Diego: Academic Press.

[76] Asami, K., Kuwabara, K., Ohtaguchi, K. (2004) Partitioning extraction of fluorescent protein in microchannel. In *Proceedings of Spring National Meeting AIChE*, New Orleans, LA, USA.

[77] Chang, W. J., Park, H. M., Tran, T. H., Koo, Y. M. (2006) Continuous-flow phase-separation of polymer solutions in microfluidic aqueous two-phase extraction system. In *Proceedings of Micro Total Analysis Systems*, Tokyo, Japan, 918-920.

[78] Theos, C. W., Clark, W. M. (1995) Electroextraction - Two-phase electrophoresis. *Applied Biochem. Biotechnol.* 54, 143-157.

[79] Stichlmair, J., Schmidt, J., Proplesch, R. (1992) Electroextraction: a novel separation technique. *Chem. Eng. Sci.* 47(12), 3015-3022.

[80] Levine, M. L., Bier, M. (1990) Electrophoretic transport of solutes in aqueous two-phase systems. *Electrophoresis* 11(8), 605-611.

[81] Oehler, R. D., Clark, W. M. (1996) beta-Lactamase recovery from E. coli cell lysate via two-phase electrophoresis. *Biotechnol. Prog.* 12(6), 873-876.

[82] Clark, W. M. (1992) Electrophoresis-enhanced extractive separation. *Chemtech* 22(7), 425-429.

[83] Marando, M. A., Clark, W. M. (1993) Two-Phase Electrophoresis of Proteins. *Sep. Sci. Technol.* 28(8), 1561-1577.

[84] Zhai, S. L., Luo, G. S., Liu, J. G. (2001) Aqueous two-phase electrophoresis for separation of amino acids. *Sep. Purif. Technol.* 21(3), 197-203.

[85] Zhai, S. L., Luo, G. S., Liu, J. G. (2001) Selective recovery of amino acids by aqueous two-phase electrophoresis. *Chem. Eng. J.* 83(1), 55-59.

[86] Righetti, P. G., Caravaggio, T. (1976) Isoelectric points and molecular weights of proteins. *J. Chromatogr.* 127(11), 1-28.

[87] Malamud, D., Drysdale, J. W. (1978) Isoelectric points of proteins: a table. *Anal. Biochem.* 86(2), 620-647.

[88] Griebel, A., Rund, S., Schonfeld, F., Dorner, W., Konrad, R., Hardt, S. (2004) Integrated polymer chip for two-dimensional capillary gel electrophoresis. *Lab Chip* 4(1), 18-23.

[89] de Mello, A. J., Beard, N. (2003) Dealing with real samples: sample pre-treatment in microfluidic systems. *Lab Chip* 3(1), 11N-19N.

[90] Jung, B., Bharadwaj, R., Santiago, J. G. (2003) Thousandfold signal increase using field-amplified sample stacking for on-chip electrophoresis. *Electrophoresis* 24(19-20), 3476-3483.

[91] Lichtenberg, J., Verpoorte, E., de Rooij, N. F. (2001) Sample preconcentration by field amplification stacking for microchip-based capillary electrophoresis. *Electrophoresis* 22(2), 258-271.

[92] Invitrogen GmbH, Germany.

[93] Camp, J. P., Capitano, A. T. (2005) Size-dependent mobile surface charge model of cell electrophoresis. *Biophys. Chem.* 113(2), 115-122.

[94] Pappas, D., Wang, K. (2007) Cellular separations: a review of new challenges in analytical chemistry. *Anal. Chim. Acta* 601(1), 26-35.

[95] Kang, J. H., Park, J. K. (2005) Technical paper on microfluidic devices - cell separation technology. *APBN* 9(21), 1135-1146.

[96] Herzenberg, L. A., Parks, D., Sahaf, B., Perez, O., Roederer, M., Herzenberg, L. A. (2002) The history and future of the fluorescence activated cell sorter and flow cytometry: a view from Stanford. *Clin. Chem.* 48(10), 1819-1827.

[97] Schönfeld, F., Griebel, A., Karlsen, F., Konrad, R., Rink, S. (2002) Development of a μ-concentrator using dielectrophoretic forces. *JALA* 7(6), 130-134.

[98] Andersson, H., van den Berg, A. (2003) Microfluidic devices for cellomics: a review. *Sens. Actuators, B* 92(3), 315-325.

[99] Fazekas de St Groth, B., Smith, A. L., Koh, W. P., Girgis, L., Cook, M. C., Bertolino, P. (1999) Carboxyfluorescein diacetate succinimidyl ester and the virgin lymphocyte: a marriage made in heaven. *Immunol. Cell Biol.* 77(6), 530-538.

[100] Beijerinck, M. W. (1896) Über eine Eigentümlichkeit der löslichen Stärke. *Zentralbl. Bakteriol.* 2, 698-699.

[101] Scott, R. L. (1949) The thermodynamics of high polymer solutions. V. Phase equilibria in the ternary system: Polymer 1 - Polymer 2 - Solvent. *J. Chem. Phys.* 17(3), 279-284.

[102] Johansson, H. O., Karlstrom, G., Tjerneld, F., Haynes, C. A. (1998) Driving forces for phase separation and partitioning in aqueous two-phase systems. *J. Chromatogr. B* 711(1-2), 3-17.

[103] Cabezas, H., Jr. (1996) Theory of phase formation in aqueous two-phase systems. *J. Chromatogr. B* 680(1-2), 3-30.

[104] Pfennig, A., Schwerin, A., Gaube, J. (1998) Consistent view of electrolytes in aqueous two-phase systems. *J. Chromatogr. B* 711(1-2), 45-52.

[105] Pfennig, A., Schwerin, A. (1995) Analysis of the electrostatic potential difference in aqueous polymer two-phase systems. *Fluid Phase Equilib.* 108(1), 305-315.

[106] Pfennig, A., Schwerin, A. (1998) Influence of electrolytes on liquid-liquid extraction. *Ind. Eng. Chem. Res.* 37(8), 3180-3188.

[107] Brooks, D. E., Sharp, K. A., Bamberger, S., Tamblyn, C. H., Seaman, G. V. F., Walter, H. (1984) Electrostatic and electrokinetic potentials in two polymer aqueous phase systems. *J. Colloid Interface Sci.* 102(1), 1-13.

[108] Haynes, C. A., Carson, J., Blanch, H. W., J.M., P. (1991) Electrostatic potentials and protein partitioning in aqueous two-phase systems. *AIChE J.* 37(9), 1401-1409.

[109] Schluck, A., Maurer, G., Kula, M. R. (1995) Influence of electrostatic interactions on partitioning in aqueous polyethylene glycol/dextran biphasic systems: Part I. *Biotechnol. Bioeng.* 46(5), 443-452.

[110] Schluck, A., Maurer, G., Kula, M. R. (1995) The influence of electrostatic interactions on partition in aqueous polyethylene glycol/dextran biphasic systems: Part II. *Biotechnol. Bioeng.* 47(2), 252-260.

[111] Johansson, G. (1974) Effects of salts on the partition of proteins in aqueous polymeric biphasic systems. *Acta Chem. Scand. B* 28(8), 873-882.

[112] Gupta, R., Bradoo, S., Saxena, R. K. (1999) Aqueous two phase systems: an attractive technology for downstream processing of biomolecules. *Curr. Sci.* 77(4), 520-523.

[113] Shanbhag, V. P., Axelsson, C. G. (1975) Hydrophobic interaction determined by partition in aqueous two-phase systems. Partition of proteins in systems containing fatty-acid esters of poly(ethylene glycol). *Eur. J. Biochem.* 60(1), 17-22.

[114] Shanbhag, V. P., Johansson, G. (1974) Specific extraction of human serum albumin by partition in aqueous biphasic systems containing poly(ethylene glycol) bound ligand. *Biochem. Biophys. Res. Commun.* 61(4), 1141-1146.

[115] Han, J. H., Lee, C. H. (1997) Effects of salts and poly (ethylene glycol)-palmitate on partitioning of proteins and bacillus subtilis neutral protease in aqueous two-phase systems. *Colloids Surf., B* 9, 109-116.

[116] Eriksson, E., Albertsson, P. A., Johansson, G. (1976) Hydrophobic surface properties of erythrocytes studied by affinity partition in aqueous two-phase systems. *Mol. Cell. Biochem.* 10(2), 123-128.

[117] Reuss, F. F. (1809) Charged-induced flow. In *Proceedings of Imperial Society of Naturalists of Moscow*, 327-344.

[118] Sivasankar, S., Subramaniam, S., Leckband, D. (1998) Direct molecular level measurements of the electrostatic properties of a protein surface. *P. Natl. Acad. Sci. USA* 95(22), 12961-12966.

[119] Masliyah, J. H., Bhattacharjee, S. (2006) Electrokinetic and colloid transport phenomena, New York: Wiley-Interscience.

[120] Delgado, A. V., Gonzalez-Caballero, F., Hunter, R. J., Koopal, L. K., Lyklema, J. (2007) Measurement and interpretation of electrokinetic phenomena. *J. Colloid Interface Sci.* 309(2), 194-224.

[121] Mehrishi, J. N., Bauer, J. (2002) Electrophoresis of cells and the biological relevance of surface charge. *Electrophoresis* 23(13), 1984-1994.

[122] Slivinsky, G. G., Hymer, W. C., Bauer, J., Morrison, D. R. (1997) Cellular electrophoretic mobility data: a first approach to a database. *Electrophoresis* 18(7), 1109-1119.

[123] Bauer, J. (1994) Cell electrophoresis, London: CRC Press.

[124] Cook, G. M. (1968) Chemistry of membranes. *Br. med. Bull.* 24(2), 118-123.

[125] Voldman, J. (2006) Electrical forces for microscale cell manipulation. *Annu. Rev. Biomed. Eng.* 8, 425-454.

[126] Baroud, C. N., Willaime, H. (2004) Multiphase flows in microfluidics. *C. R. Physique* 5(5), 547-555.

[127] Zapka, W., Crankshaw, M., Voit, W., Brünahl, J., Herrmann, U., Münchow, G. (2003) Increased inkjet printing frequency from 'offset channel' printheads. In *Proceedings of IS&T's NIP19*, New Orleans, LA, USA, 272-275.

[128] Atencia, J., Beebe, D. J. (2005) Controlled microfluidic interfaces. *Nature* 437(7059), 648-655.

[129] Chung, K. H., Hong, J. W., Lee, D. S., Yoon, H. C. (2007) Microfluidic chip accomplishing self-fluid replacement using only capillary force and its bioanalytical application. *Anal. Chim. Acta* 585(1), 1-10.

[130] Cubaud, T., Ulmanella, U., Ho, C. M. (2004) Two-phase flow in microchannels with surface modifications. In *Proceedings of International Conference on Multiphase Flow*, Yokahama, Japan, PL5.

[131] Günther, A., Jensen, K. F. (2006) Multiphase microfluidics: from flow characteristics to chemical and materials synthesis. *Lab Chip* 6(12), 1487-1503.

[132] Zhao, Y., Chen, G., Yuan, Q. (2006) Liquid-liquid two-phase flow patterns in a rectangular microchannel. *AIChE J.* 52(12), 4052-4060.

[133] Yang, Z. L., Palm, B., Sehgal, B. R. (2002) Numerical simulation of bubbly two-phase flow in a narrow channel. *Int. J. Heat Mass Transfer* 45(3), 631-639.

[134] Guillot, P., Colin, A. (2005) Stability of parallel flows in a microchannel after a T junction. *Phys. Rev. E* 72(6), 066301.

[135] Garstecki, P., Gitlin, I., DiLuzio, W., Whitesides, G. M., Kumacheva, E., Stone, H. A. (2004) Formation of monodisperse bubbles in a microfluidic flow-focusing device. *Appl. Phys. Lett.* 85(13), 2649-2651.

[136] Garstecki, P., Stone, H. A., Whitesides, G. M. (2005) Mechanism for flow-rate controlled breakup in confined geometries: a route to monodisperse emulsions. *Phys. Rev. Lett.* 94(16), 164501.

[137] Hibara, A., Iwayama, S., Matsuoka, S., Ueno, M., Kikutani, Y., Tokeshi, M., Kitamori, T. (2005) Surface modification method of microchannels for gas-liquid two-phase flow in microchips. *Anal. Chem.* 77(3), 943-947.

[138] Sakamoto, K., Nakanishi, H., Tokeshi, M., Yoshida, Y., Kitamori, T. (2004) A stable two phase flow by "sombrero" channel. In *Proceedings of Micro Total Analysis Systems*, Malmö, Sweden, 213-215.

[139] Hibara, A., Nonaka, M., Hisamoto, H., Uchiyama, K., Kikutani, Y., Tokeshi, M., Kitamori, T. (2001) Liquid-liquid two-phase crossing flows in glass microchips by utilizing octadecylsilane modification of microchannels. In *Proceedings of Micro Total Analysis Systems*, Monterey, CA, USA, 549-550.

[140] Rasband, W. S. (1997-2007) ImageJ, U.S. National Institutes of Health, Bethesda, Maryland, USA, http://rsb.info.nih.gov/ij/.

[141] Snakenborg, D., Perozziello, G., Geschke, O., Kutter, J. P. (2007) A fast and reliable way to establish fluidic connections to planar microchips. *J. Micromech. Microeng.* 17(1), 98-103.

[142] Bhagat, A. A. S., Jothimuthu, P., Pais, A., Papautsky, I. (2007) Re-usable quick-release interconnect for characterization of microfluidic systems. *J. Micromech. Microeng.* 17(1), 42-49.

[143] Fredrickson, C. K., Fan, Z. H. (2004) Macro-to-micro interfaces for microfluidic devices. *Lab Chip* 4(6), 526-533.

[144] Upchurch Scientific, Inc., WA, USA.

[145] Gale, B. K., Caldwell, K. D., Frazier, A. B. (1998) A micromachined electrical field-flow fractionation (μ-EFFF) system. *IEEE Trans. Biomed. Eng.* 45(12), 1459-1469.

[146] Gale, B. K., Frazier, A. B., Caldwell, K. D. (1997) Micromachined electrical field-flow fractionation (μEFFF) system. In *Proceedings of Micro Electro Mechanical Systems*, Nagoya, Japan, 193-194.

[147] Gale, B. K., Caldwell, K. D., Frazier, A. B. (1998) Characterization of a micromachined electrical field-flow fractionation (μEFFF) system. In *Proceedings of Solid-State Sensor and Actuator Workshop*, Hilton Head, SC, USA, 342-345.

[148] Gale, B. K., Frazier, A. B. (1999) Scaling Effects in a micromachined electrical field-flow fractionation (μ-EFFF) system with integrated detector. In *Proceedings of BMES/EMBS Conference*, Atlanta, GA, USA, 842.

[149] Gale, B. K., Caldwell, K. D., Frazier, A. B. (2002) Geometric scaling effects in electrical field flow fractionation. 2. Experimental results. *Anal. Chem.* 74(5), 1024-1030.

[150] Gale, B. K., Caldwell, K. D., Frazier, A. B. (2001) Geometric scaling effects in electrical field flow fractionation. 1. Theoretical analysis. *Anal. Chem.* 73(10), 2345-2352.

[151] Palkar, S. A., Schure, M. R. (1997) Mechanistic study of electrical field flow fractionation. 1. Nature of the internal field. *Anal. Chem.* 69(16), 3223-3229.

[152] Palkar, S. A., Schure, M. R. (1997) Mechanistic study of electrical field flow fractionation. 2. Effect of sample conductivity on retention. *Anal. Chem.* 69(16), 3230-3238.

[153] Kantak, A. S., Merugu, S., Gale, B. K. (2003) Microfabricated cyclical electrical field flow fractionation. In *Proceedings of Micro Total Analysis Systems*, Squaw Valley, CA, USA, 1199-1202.

[154] Lao, A. I., Trau, D., Hsing, I. M. (2002) Miniaturized flow fractionation device assisted by a pulsed electric field for nanoparticle separation. *Anal. Chem.* 74(20), 5364-5369.

[155] Brask, A., Kutter, J. P., Bruus, H. (2005) Long-term stable electroosmotic pump with ion exchange membranes. *Lab Chip* 5(7), 730-738.

[156] de Jong, J., Lammertink, R. G., Wessling, M. (2006) Membranes and microfluidics: a review. *Lab Chip* 6(9), 1125-1139.

[157] Takamura, Y., Onoda, H., Inokuchi, H., Adachi, S., Oki, A., Horiike, Y. (2001) Low-voltage electroosmosis pump and its application to on-chip linear stepping pneumatic pressure source. In *Proceedings of Micro Total Analysis Systems*, Monterey, CA, USA, 230-232.

[158] Dhopeshwarkar, R., Sun, L., Crooks, R. M. (2005) Electrokinetic concentration enrichment within a microfluidic device using a hydrogel microplug. *Lab Chip* 5(10), 1148-1154.

[159] Brask, A., Goranovic, G., Bruus, H. (2002) The low-voltage cascade EOF pump: comparing theory with published data. In *Proceedings of Micro Total Analysis Systems*, Nara, Japan, 79-81.

[160] Mutlu, S., Svec, F., Mastrangelo, C. H., Fréchet, J. M. J., Gianchandani, Y. B. (2004) Enhanced electro-osmotic pumping with liquid bridge and field effect flow rectification. In *Proceedings of Micro Electro Mechanical Systems (MEMS)*, Maastricht, The Netherlands, 850–853.

[161] Takamura, Y., Onoda, H., Inokuchi, H., Adachi, S., Oki, A., Horiike, Y. (2003) Low-voltage electroosmosis pump for stand-alone microfluidics devices. *Electrophoresis* 24(1-2), 185-192.

[162] Caballero, J. P. (2008) Aufbau einer Roboterplattform zum vollautomatisierten Zusammenbau und zur Oberflächenoptimierung von mikrofluidischen Polymerchips. Frankfurt am Main, Germany: University of Applied Science.

[163] Lin, H., Storey, B. D., Oddy, M. H., Chen, C.-H., Santiago, J. G. (2004) Instabilities of electrokinetic microchannel flows with conductivity gradients. *Phys. Fluids* 16(6), 1922-1935.

[164] Jeffrey, D. Z., Reddy, V. (2006) Two phase micromixing and analysis using electrohydrodynamic instabilities. *Microfluid. Nanofluid.* 2(5), 399-415.

[165] Boy, D. A., Storey, B. D. (2007) Electrohydrodynamic instabilities in microchannels with time periodic forcing. *Phys. Rev. E* 76, 026304.

[166] Goranovic, G. (2003) Electrohydrodynamic aspects of two-fluid microfluidic systems: theory and simulation. Lyngby, Denmark: Technical University of Denmark.

[167] Sundaram, N., Tafti, D. K. (2004) Evaluation of microchamber geometries and surface conditions for electrokinetic driven mixing. *Anal. Chem.* 76(13), 3785-3793.

[168] Shin, S. M., Kang, I. S., Cho, Y. K. (2005) Mixing enhancement by using electrokinetic instability under time-periodic electric field. *J. Micromech. Microeng.* 15(3), 455-462.

[169] El Moctar, A. O., Aubry, N., Batton, J. (2003) Electro-hydrodynamic micro-fluidic mixer. *Lab Chip* 3(4), 273-280.

[170] Cho, H., Kim, H.-Y., Kang, J. Y., Kim, T. S. (2007) How the capillary burst microvalve works. *J. Colloid Interface Sci.* 306(2), 379-385.

[171] Lee, S.-H., Lee, C.-S., Kim, B.-G., Kim, Y.-K. (2003) Quantitatively controlled nanoliter liquid manipulation using hydrophobic valving and control of surface wettability. *J. Micromech. Microeng.* 13(1), 89-97.

[172] Furuberg, L., Mielnik, M., Gulliksen, A., Solli, L., Johansen, R., Voitel, J., Baier, T., Riegger, L., Karlsen, F. (2008) RNA amplification chip with parallel microchannels and droplet positioning using capillary valves. *Microsyst. Technol.* 14(4-5), 673-681.

[173] Brown, L., Koerner, T., Horton, J. H., Oleschuk, R. D. (2006) Fabrication and characterization of poly(methylmethacrylate) microfluidic devices bonded using surface modifications and solvents. *Lab Chip* 6(1), 66-73.

[174] Spritzendorfer, M., Steger, R., Waibel, G. (2003) Entwicklung neuer Verbindungstechniken für Komponenten miniaturisierter Mikrosysteme aus Kunststoff. Stuttgart, Germany: Hahn-Schickard Gesellschaft.

[175] Bundgaard, F., Nielsen, T., Nilsson, D., Shi, P., Perozziello, G., Kristensen, A., Geschke, O. (2004) Cyclic olefin copolymer (COC/Topas) - an exceptional material for exceptional lab-on-a-chip systems. In *Proceedings of Micro Total Analysis Systems*, Malmö, Sweden, 372-374.

[176] Steigert, J., Haeberle, S., Brenner, T., Müller, C., Steinert, C. P., Koltay, P., Gottschlich, N., Reinecke, H., Rühe, J., Zengerle, R., Ducrée, J. (2007) Rapid prototyping of microfluidic chips in COC. *J. Micromech. Microeng.* 17(2), 333-341.

[177] Shinohara, H., Mizuno, J., Shoji, S. (2007) Low-temperature direct bonding of poly(methyl methacrylate) for polymer microchips. *IEEJ Trans.* 2(3), 301-306.

[178] Bhattacharyya, A., Klapperich, C. M. (2007) Mechanical and chemical analysis of plasma and ultraviolet-ozone surface treatments for thermal bonding of polymeric microfluidic devices. *Lab Chip* 7(7), 876-882.

[179] Tsao, C. W., Hromada, L., Liu, J., Kumar, P., DeVoe, D. L. (2007) Low temperature bonding of PMMA and COC microfluidic substrates using UV/ozone surface treatment. *Lab Chip* 7(4), 499-505.

[180] Zuniga, A. D. G., Minim, L. A. R., Coimbra, J. S. R., Arquete, D. A. R., da Silva, L. H. M., Maffia, M. C. (2006) Interfacial tension and viscosity for poly(ethylene glycol) + maltodextrin aqueous two-phase systems. *J. Chem. Eng. Data* 51(3), 1144-1147.

[181] Bruus, H. (2007) Theoretical microfluidics, New York, NY, USA: Oxford University Press.

[182] Mathematica - Wolfram Research.

[183] Anna, S. L., Bontoux, N., Stone, H. A. (2003) Formation of dispersions using "flow focusing" in microchannels. *Appl. Phys. Lett.* 82(3), 364-366.

[184] Davidson, M. R., Harvie, D. J. E., Cooper-White, J. J. (2005) Flow focusing in microchannels. *ANZIAM J.* 46(E), C47-C58.

[185] Shibusawa, Y., Takeuchi, N., Sugawara, K., Yanagida, A., Shindo, H., Ito, Y. (2006) Aqueous-aqueous two-phase systems composed of low molecular weight of polyethylene glycols and dextrans for counter-current chromatographic purification of proteins. *J. Chromatogr. B* 844(2), 217-222.

[186] Guillot, P., Panizza, P., Salmon, J. B., Joanicot, M., Colin, A., Bruneau, C. H., Colin, T. (2006) Viscosimeter on a microfluidic chip. *Langmuir* 22(14), 6438-6445.

[187] Galambos, P., Forster, F. (1998) An optical micro-fluidic viscometer. In *Proceedings of Micro Electro Mechanical Systems (MEMS)*, Anaheim, CA, USA, 187-191.

[188] Baek, J. Y., Park, J. Y., Ju, J. I., Lee, T. S., Lee, S. H. (2005) A pneumatically controllable flexible and polymeric microfluidic valve fabricated via in situ development. *J. Micromech. Microeng.* 15(5), 1015-1020.

[189] Studer, V., Hang, G., Pandolfi, A., Ortiz, M., Anderson, W. F., Quake, S. R. (2004) Scaling properties of a low-actuation pressure microfluidic valve. *J. Appl. Phys.* 95(1), 393-398.

[190] Ayala, V. C., Michalzik, M., Harling, S., Menzel, H., Guarnieri, F. A., Büttgenbach, S. (2007) Design, construction and testing of a monolithic pH-sensitive hydrogel-valve for biochemical and medical application. *J. Phys.: Conf. Ser.* 90, 012025.

[191] Edahiro, J., Nakashima, M., Kasim, V., Yamada, M., Seki, M. (2002) Continuous Cell Partitioning in Two-Phase Flow System. In *Proceedings of Micro Total Analysis Systems*, Nara, Japan, 569-571.

[192] Kantak, A., Srinivas, M., Gale, B. (2006) Characterization of a microscale cyclical electrical field flow fractionation system. *Lab Chip* 6(5), 645-654.

[193] Mutlu, S., Yu, C., Selvaganapathy, P., Svec, F., Mastrangelo, C. H., Frechet, J. M. J. (2002) Micromachined porous polymer for bubble free electro-osmotic pump. In *Proceedings of Micro Electro Mechanical Systems (MEMS)*, Las Vegas, NV, USA, 19-24.

[194] Selvaganapathy, P., Leung Ki, Y.-S., Renaud, P., Mastrangelo, C. H. (2002) Bubble-free electrokinetic pumping. *J. Microelectromech. S.* 11(5), 448-453.

[195] Erickson, D., Li, D. (2003) Analysis of alternating current electroosmotic flows in a rectangular microchannel. *Langmuir* 19(13), 5421-5430.

[196] Storey, B. D., Tilley, B. S., Lin, H., Santiago, J. G. (2005) Electrokinetic instabilities in thin microchannels. *Phys. Fluids* 17, 018103.

[197] Melcher, J. R., Taylor, G. I. (1969) Electrodynamics: a review of the role of interfacial shear stresses. *Ann. Rev. Fluid Mech.* 1, 111-146.

[198] Persat, A., Zangle, T., Posner, J., Santiago, J. (2007) Chips & Tips: On-chip electrophoresis devices: Do's, don'ts and dooms. *Lab Chip*.

[199] Binks, B. P., Lumsdon, S. O. (2000) Influence of particle wettability on the type and stability of surfactant-free emulsions. *Langmuir* 16(23), 8622-8631.

[200] Lin, Y., Skaff, H., Emrick, T., Dinsmore, A. D., Russell, T. P. (2003) Nanoparticle assembly and transport at liquid-liquid interfaces. *Science* 299(5604), 226-229.

[201] Xu, H., Yan, F., Tierno, P., Marczewski, D., Goedel, W. A. (2005) Particle-assisted wetting. *J. Phys.: Condens. Matter* 17(9), S465-S476.

[202] Kramers, H. A. (1940) Brownian motion in a field of force and the diffusion model of chemical reactions. *Physica* 7(4), 284-304.

[203] Shulgin, I. L., Ruckenstein, E. (2006) Preferential hydration and solubility of proteins in aqueous solutions of polyethylene glycol. *Biophys. Chem.* 120(3), 188-198.

[204] Atha, D. H., Ingham, K. C. (1981) Mechanism of precipitation of proteins by polyethylene glycols. Analysis in terms of excluded volume. *J. Biol. Chem.* 256(23), 12108-12117.

[205] Stiles, P. J., Fletcher, D. F. (2004) Hydrodynamic control of the interface between two liquids flowing through a horizontal or vertical microchannel. *Lab Chip* 4(2), 121-124.

[206] Cussler, E. L. (1997) Diffusion: Mass transfer in fluid systems. 2 ed., London: Cambridge University Press.

[207] Crank, E. L. (1975) Mathematics of diffusion, Oxford: Clarendon Press.

[208] Comsol Multiphysics - www.comsol.de.

[209] Matlab - www.mathworks.com - Documentation.

[210] Forsythe, G. E., Malcolm, M. A., Moler, C. B. (1976) Computer methods for mathematical computations, New Jersey: Prentice Hall.

[211] Baumann, K.-H., Mühlfriedel, K. (2002) Mass transfer studies with laser-induced fluorescence across liquid/liquid phase boundaries. *Chem. Eng. Technol.* 25(7), 697-700.

[212] Farruggia, B., Nerli, B., Pico, G. (2003) Study of the serum albumin-polyethyleneglycol interaction to predict the protein partitioning in aqueous two-phase systems. *J. Chromatogr. B* 798(1), 25-33.

[213] Fuh, B. C., Levin, S., Giddings, J. C. (1993) Rapid diffusion coefficient measurements using analytical SPLITT fractionation: application to proteins. *Anal. Biochem.* 208(1), 80-87.

[214] Papadopoulos, S., Endeward, V., Revesz-Walker, B., Jurgens, K. D., Gros, G. (2001) Radial and longitudinal diffusion of myoglobin in single living heart and skeletal muscle cells. *P. Natl. Acad. Sci. USA* 98(10), 5904-5909.

[215] Lavalette, D., Hink, M. A., Tourbez, M., Tetreau, C., Visser, A. J. (2006) Proteins as micro viscosimeters: Brownian motion revisited. *Eur. Biophys. J.* 35(6), 517-522.

[216] Lavalette, D., Tetreau, C., Tourbez, M., Blouquit, Y. (1999) Microscopic viscosity and rotational diffusion of proteins in a macromolecular environment. *Biophys. J.* 76(5), 2744-2751.

[217] Mattison, K. W., Kaszuba, M. (2004) Automated Protein Characterization. *American Biotechnology Laboratory*, 8-11.

[218] Peters, T. J. (1996) All about albumin: biochemistry, genetics, and medical applications, San Diego: Academic Press.

[219] NCIB Entrez Structure - www.ncbi.nlm.nih.gov/sites/entrez.

[220] Origin (OriginLab Corporation US) - Documentation.

[221] Henning, M., Braun, D. (2005) Convective polymerase chain reaction around micro immersion heater. *Appl. Phys. Lett.* 87, 183901.

[222] Baskir, J. N., Hatton, T. A., Suter, U. W. (1989) Protein partitioning in two-phase aqueous polymer systems. *Biotechnol. Bioeng.* 34(4), 541-558.

[223] Levine, M. L., Cabezas, H., Jr., Bier, M. (1992) Transport of solutes across aqueous phase interfaces by electrophoresis. Mathematical modeling. *J. Chromatogr.* 607(1), 113-118.

[224] Uselova-Vcelakova, K., Zuskova, I., Gas, B. (2007) Stability constants of amino acids, peptides, proteins, and other biomolecules determined by CE and related methods: recapitulation of published data. *Electrophoresis* 28(13), 2145-2152.

[225] Hasl, G., Pauly, H. (1973) Schmelzverhalten und kalorische Eigenschaften einer Mischung von Rinderserumalbumin, Kochsalz und Wasser. *Biophysik* 10(2), 125-136.

[226] Huber, C., Niederwieser, D., G., G., Zier, K., Braunsteiner, H. (1982) Dichteverteilung menschlicher Lymphozyten. *Ann. Hematol.* 45(6), 375-383.

[227] Boyum, A., Brincker Fjerdingstad, H., Martinsen, I., Lea, T., Lovhaug, D. (2002) Separation of human lymphocytes from citrated blood by density gradient (NycoPrep) centrifugation: monocyte depletion depending upon activation of membrane potassium channels. *Scand. J. Immunol.* 56(1), 76-84.

[228] Miller, R., Fainerman, V. B., Makievski, A. V., Kragel, J., Grigoriev, D. O., Kazakov, V. N., Sinyachenko, O. V. (2000) Dynamics of protein and mixed protein/surfactant adsorption layers at the water/fluid interface. *Adv. Colloid Interface Sci.* 86(1-2), 39-82.

# Publications

Parts of the thesis have been published by the author in the following Journals and Conferences:

**Journal Papers**


[P1] Münchow, G., Schönfeld, F., Hardt, S., Graf. K. (2008) Protein diffusion across the interface in aqueous two-phase systems. *Langmuir* 24 (16), 8547-8553.

[P2] Münchow, G., Hardt, S., Kutter, J. P., Drese, K. S. (2007) Electrophoretic partitioning of proteins in two-phase microflows. *Lab Chip* 7(1), 98-102.

[P3] Münchow, G., Hardt, S., Kutter, J. P., Drese, K. S. (2006) Protein transport and concentration by electrophoresis in two-phase microflows. *JALA* 11(6), 368-373.


**Conferences**


[P4] Münchow, G., Hardt, S., Kutter, J. P., Drese, K. S. (2007) Continuous Separation of proteins and cells by two phase electrophoresis in microchannels. In *Proceedings of Micro Total Analysis Systems*, Paris, France, 808-810.

[P5] Münchow, G., Hardt, S., Kutter, J. P., Drese, K. S. (2007) Two-Phase Electreophoresis in Microchannels. In *Proceedings of DFG Workshop Micro- and Nanofluidics*, Bad Honnef, Germany, Best Talk Award.

[P6] Münchow, G., Hardt, S., Kutter, J. P., Drese, K. S. (2006) Electrophoretic partitioning of proteins in two-phase microflows. In *Proceedings of LabAutomation*, Palm Springs, CA, USA, Candidate of 10 finalists for ALA Innovation Award.

[P7] Münchow, G., Hardt, S., Kutter, J. P., Drese, K. S. (2006) Electrophoretic partitioning of proteins in two-phase microflows. In *Proceedings of DFG Workshop Micro- and Nanofluidics*, Bad Honnef, Germany.

[P8] Münchow, G., Hardt, S., Kutter, J. P., Drese, K. S. (2006) Protein manipulation by two-phase electrophoresis. In *Proceedings of MipTec*, Basel, Switzerland.

[P9] Münchow, G., Hardt, S., Drese, K. S., Kutter, J. P. (2006) Electrophoretic transport of proteins in microchannels filled with immiscible aqueous phases. In *Proceedings of Nanotech*, Boston, MA, USA.

[P10] Münchow, G., Drese, K. S., Hardt, S., Kutter, J. P. (2005) Towards two-phase electrophoresis in microchannels. In *Proceedings of Micro Total Analysis Systems*, Boston, MA, USA, 850-852.

[P11] Münchow, G., Hardt, S., Kutter, J. P., Drese, K. S. (2005) Biomolecule Separation by Electrophoresis in Two-Phase Systems. In *Proceedings of DFG Workshop Micro- and Nanofluidics*, Bad Honnef, Germany.

**Publications not related to this thesis**


[P12] Münchow, G., Drese, K. S. (2007) Nucleic acid amplification in microsystems. In *Microfluidic Technologies for Miaturized Analysis Systems*, New York: Springer, 523-567.

[P13] v. Germar, F., Münchow, G., Drese, K. S. (2007) Rapid prototyping process for lab-on-a-chip systems offered in the europractice project INTEGRAMplus. *MST News* 1, 24.

[P14] Drese, K. S., Münchow, G., Ritzi, M. (2006) Fast development strategy: one-week-to-chip. In *Proceedings of LabAutomation*, Palm Springs, CA, USA.

[P15] Münchow, G., Dadic, D., Doffing, F., Hardt, S., Drese, K. S. (2005) Automated chip-based device for simple and fast nucleic acid amplification. *Expert Rev. Mol. Diagn.* 5(4), 613-620.

[P16] Doffing, F., Herrmann, M., Münchow, G., Drese, K. S. (2005) On-chip blood sample preparation for subsequent PCR. In *Proceedings of Micro Total Analysis Systems*, Boston, MA, USA, 811-813.

[P17] Münchow, G., Drese, K. S., Dadic, D., Doffing, F., Hardt, S. (2005) Rapid polymerase chain reaction in polymeric microchannels. In *Proceedings of LabAutomation*, San Jose, CA, USA.

[P18] Dadic, D., Münchow, G., Doffing, F., Drese, K. S. (2005) Modular lab-on-a-chip platform. In *Proceedings of LabAutomation*, San Jose, CA, USA.

[P19] Baier, T., Herrmann, M., Doffing, F., Münchow, G., Dadic, D., Drese, K. S. (2005) Design-rules of a ferrofluidic actuator for lab-on-a-chip applications. In *Proceedings of LabAutomation*, San Jose, CA, USA.

[P20] Münchow, G., Dadic, D., Drese, K. S. (2005) Metering and merging of liquid microdrops. In *Proceedings of LabAutomation*, San Jose, CA, USA.

[P21] Münchow, G., Doffing, F., Dadic, D., Drese, K. S. (2005) Microfluidic modular lab-on-a-chip platform enables rapid PCR. In *Proceedings of MipTec*, Basel, Switzerland, Basel Miptec Award Winner.

[P22] Drese, K. S., Münchow, G., von Germar, F., Frese, I., Schönfeld, F., Ritzi, M. (2005) How to get a reading from a lab-on-a-chip-system. In *Proceedings of Dresdner Sensor Symposium*, Dresden, Germany, 49-56.

[P23] Münchow, G., Drese, K. S. (2004) Modulares Chipsystem für rasante PCR-Analysen mit integrierter Probenpräparation. *Laborwelt* 5, 4-6.

[P24] Drese, K. S., Münchow, G., D., D., Doffing, F., Hardt, S., Sörensen, O., Müller, T., Klein-Vehne, A. (2004) Rapid polymerase chain reaction in polymeric microchips driven by ferrofluids. In *Proceedings of Micro Total Analysis Systems*, Malmö, Sweden, 811-813.

[P25] Zapka, W., Crankshaw, M., Voit, W., Brünahl, J., Herrmann, U., Münchow, G. (2003) Increased inkjet printing frequency from ‘offset channel’ printheads. In *Proceedings of IS&T's NIP19*, New Orleans, LA, USA, 272-275.

**Awards**

Best Talk Award at DFG Workshop Micro- and Nanofluidics, sponsored by DFG
Münchow, G., Hardt, S., Kutter, J. P., Drese, K. S. (2007) Two-Phase Electreophoresis in Microchannels. In *Proceedings of DFG Workshop Micro- and Nanofluidics*, Bad Honnef, Germany.

Basel Award at Miptec 2005, sponsored by Basel Convention Center:
Münchow, G., Doffing, F., Dadic, D., Drese, K. S. (2005) Microfluidic modular lab-on-a-chip platform enables rapid PCR. In *Proceedings of MipTec*, Basel, Switzerland.

# *Curriculum Vitae*

| | |
|---|---|
| **Name** | **MÜNCHOW, Götz** |
| Birth | 30.03.1977 in Reinbek, Germany |
| **Education** | |
| 1987 - 1996 | **Gymnasium Schwarzenbek** |
| 1997 - 2003 | **Albert-Ludwigs-Universität Freiburg i.Br.,** Germany<br>Diplom-Ingenieur of Microsystem Technology |
| 2009 | **Technische Universität Darmstadt,** Germany<br>PhD in Engineering |
| **Employment** | |
| 2002 | **XaarJet AB,** Järfälla, Schweden<br>Graduand |
| 2003 - 2004 | **Institut für Mikrotechnik Mainz GmbH,** Mainz, Germany<br>Development Engineer |
| 2004 - 2008 | **Institut für Mikrotechnik Mainz GmbH,** Mainz, Germany<br>PhD Studies |
| since 2008 | **Dräger Medical AG & Co. KG,** Lübeck, Germany<br>Project Manager, R&D |